"BACE1 dependent function of Neuregulin1 in peripheral nervous system myelination"

Dissertation

for the award of the degree
"Doctor rerum naturalium" (Dr. rer. Nat)
Division of Mathematics and Natural Sciences
of the Georg-August-Universität Göttingen

submitted by

Viktorija Velanac

from Belgrade (Serbia)

Göttingen 30.11.2009

Prof. Klaus-Armin Nave Ph.D. (Reviewer)

Department of Neurogenetics / Max Planck Institute of Experimental Medicine

Prof. Dr. Wolfgang Brück (Reviewer)

Deptartment of Neuropathology / Georg August University Goettingen

Prof. Dr. Hannelore Ehrenreich

Department of Clinical Neurosciences/ Max Planck Institute of Experimental Medicine

Date of the oral examination: 15th of January 2010

Declaration

I hereby declare that the PhD thesis entitled, **"BACE1 dependent function of Neuregulin1 in peripheral nervous system myelination"**, has been written independently and with no other sources and aids than quoted. I would like to acknowledge Dr. Michael Wehr (for Split-Tev assay), Dr. Carla Taveggia (for viral infection of DRG culture) and Mostafa Bakhti (for CNS neuron-oligodendrocyte co-culture)

30.11.2009   Viktorija Velanac

To my sister

Acknowledgments

List of figures

Abbreviations

ADAMs	A disintegrin and metalloproteases
AD	Alzheimer's disease
APS	Ammonium persulphate
BACE1	β-site amyloid precursor protein cleaving enzyme 1
BBB	Blood brain barrier
bp	Base pairs
BSA	Bovine serum albumin
ºC	Degree Celsius
cDNA	Complementary DNA
CMT	Charcot-Marie-Tooth disease
CNS	Central nervous system
CRD	Cystein rich domain
CTD	C-terminal domain
DAB	3,3'-Diaminobenzidine
DAPI	4'-6-Diamidino-2-phenylindole
ddH2O	Double distilled water
DMEM	Dulbecco's Modified Eagle Medium
DMSO	Dimethyl sulfoxide
DNA	Deoxyribonucleic acid
DNase	Deoxyribonuclease
dATP	2'-deoxyadenosine 5'-triphosphate
dCTP	2'-deoxycytidine 5'-triphosphate
dGTP	2'-deoxyguanosine 5'-triphosphate
dTTP	2'-deoxythymidine 5'-triphosphate
DRG	Dorsal root ganglion
E	Embryonic day
EAE	Experimental autoimmune encephalomyelitis
FBS	Fetal bovine serum
EDTA	Ethylendiamin-tetraacetat
EGF	Epidermal growth factor
EGFP	Enhanced green fluorescent protein
ELISA	Enzyme-linked immunosorbent assay
EM	Electron microscopy
ER	Endoplasmatic reticulum
FCS	Fetal calf serum
g	Gravity
GAD65	Glutamic acid decarboxylase 65
GFAP	Glial fibrillary acidic protein
GS	Goat serum
HA	Hemagglutinin
HEK293T	Human embryonic kidney 293T cell line
HRP	Horse radish peroxidase
HS	Horse serum
ICC	Immunocytochemistry
IB	Immunoblotting
Ig	Immunoglobulin
IHC	Immunohistochemistry

kD	Kilo Dalton
LB	Luria-Bertani medium
M	Molar
MAPK	Mitogen-activated protein kinase
MBP	Myelin basic protein
mg	Milligram
µg	Microgram
MGB	Modified Gitschier buffer
min	MInutes
ml	Milliliter
µl	Microliter
mM	Millimolar
MMP	Matrix metalloproteases
mRNA	Messenger ribonucleic acid
MS	Multiple sclerosis
mSc	Myelinating Schwann cell
NGF	Nerve growth factor
ng	Nanogram
nmSc	Non myelinating Schwann cell
NRG1	Neuregulin1
OD	Optical density
ON	Over night
OPCs	Oligodendrocyte precursor cells
P	Postnatal day
PAGE	Polyacrylamide gel electrophoresis
PBS	Phosphate buffer saline
PCR	Polymerase chain reaction
PC12	Pheochromocytoma cell line
Pen/Strep	Penicillin/Streptomycin
PFA	Paraformaldehyde
PI3K	Phosphatidylinositol-3-kinase
PLL	Poly-L-Lysin
PNS	Peripheral nervous system
PSD-95	Postsynaptic density protein 95
PTEN	Phosphatase and tensin homolog
RE	Recycling endosome
rHIgM	Recombinant Human immunoglobulin M
RLUs	Relative luminescence units
RNA	Ribonucleic acid
rpm	Rotations per minute
RT	Room temperature
RT-PCR	Reverse transcriptase polymerase chain reaction
sec	Seconds
SEM	Standard error of mean
Sc	Schwann cell
SDS	Sodium dodecyl sulphate
STDEV	Standard deviation
sHIgM	Serum human immunoglobulin M
TACE	Tumor necrosis factor-α converting enzyme
TBS	Tris buffer saline
tg	Transgenic

TEMED	Tetramethylethylendiamin
TEV	Tobacco etch virus
tg	Transgenic
TGN	Trans-Golgi network
TMEV	Theiler's murine encephalomyelitis virus
TM	Transmembrane
VGLUT	Vesicular glutamate transporter
WB	Western blot
wt	Wild type

1   ABSTRACT

The neuronal epidermal growth factor (EGF)-like growth factor NRG1 type III serves as a master regulator of myelination in the peripheral nervous system (PNS). It has been proposed that NRG1 type III is proteolytically cleaved to become fully active, but the identity of the protease(s) as well as the number and order of cleavage events have been elusive. Peripheral myelination is strongly impaired in BACE1 (β-site amyloid precursor protein-cleaving enzyme 1) null mutants, very similar to NRG1 type III heterozygous mouse mutants, suggesting that BACE1-processing is required for the myelinating activity of NRG1 type III. However, a functional interaction between NRG1 type III and BACE1 *in vivo* has not been demonstrated.

In this study, we have used transgenic mouse lines that neuronally overexpress N-terminally epitope-tagged full length NRG1 type III and a C-terminally shortened NRG1 type III-variant that mimics BACE1 processing in the stalk region ('GIEF') to further explore NRG1 processing and a functional interaction between BACE1 and NRG1 type III in myelination *in vivo*. Neuronal overexpression of the 'GIEF'-variant induces sciatic nerve hypermyelination, very similar to full length NRG1 type III. This demonstrates that the product of BACE1-mediated cleavage in the stalk region is myelination competent, whereas back signalling by the cytoplasmic tail of NRG1 type III is dispensable for myelination. Unexpectedly, overexpression of NRG1 type III retains the potential to promote myelination in BACE1 null mutants, albeit at reduced capacity. These findings identify a functional interaction of BACE1 and NRG1 in peripheral myelination *in vivo*, but also point to more complex processing mechanisms involving other proteases.

We also took advantage of the *in vivo*-expression of epitope-tagged NRG1-variants to study the subcellular localization and transport of NRG1-variants in spinal cord motor neurons. Histological and biochemical analysis strongly suggest that subsequently to cleavage in the stalk region, N- and C-terminal NRG1 type III-fragments are sorted to distinct membrane domains and that vesicular transport of the N-terminal fragment (harboring the EGF-like domain) into the axonal compartment is rate-limiting. Finally, we observed an additional smaller-sized N-terminal product in sciatic nerve, compatible with EGF-like domain shedding from the axonal surface. Thus, our data strongly suggest an orderly array of proteolytic processing as a critical component of NRG1 type III-mediated peripheral myelination.

2 INTRODUCTION

2.1 Myelination in the peripheral nervous system

2.1.1 Function of the myelin sheath

Formation of a myelin sheath around axons enabled fast nerve impulse propagation and fulfilled one of the crucial conditions for the evolution of a complex nervous system in vertebrates. By insulating axons, the myelin sheath increases resistance and decreases the capacitance of the axonal membrane. Together with clustering of voltage gated sodium channels at the node of Ranvier, myelin creates fast saltatory conduction of action potentials. Myelination thereby improves the propagation speed of electrical pulses along axons by 10 fold, excluding the necessity for an enlargement of the axonal diameter to achieve the same goal (Garbay et al., 2000; Hartline and Colman, 2007). Fast conducting myelinated fibers of a few µm in diameter represent an evolutionary advantage if we consider the space constrains of the central nervous system (CNS) and the requirement for high speed information processing. Vertebrate body size would not be imaginable without fast propagation of nerve impulses. For instance, the magnitude of conduction velocity for sensory information and motor reactions along the correspondingly increased length of peripheral nervous system (PNS) axons would not satisfy functional criteria without the existence of myelin. Although myelin serves similar functions in the PNS and CNS, it is formed by two distinct types of glial cells and the myelination process is differentially regulated (Sherman and Brophy, 2005). In the PNS, the myelin sheath is formed by Schwann cells (Sc) that spirally elongate their membranes to wrap the axon and from one myelin segment surrounded by the basal lamina. In the CNS oligodendrocytes extend processes to form multiple myelin segments around multiple axons of variable diameter. The function of myelin forming glial cells extends beyond providing electrical isolation for axons. Sc and oligodendrocytes also have an important role in maintaining axonal integrity (Nave and Trapp, 2008). Secondary axonal loss occurs, for instance after demyelination in the CNS as a part of neuropathology of multiple sclerosis (Trapp and Nave, 2008). Type1 Charcot-Marie-Tooth (CMT) disease, an inherited peripheral neuropathy, is also characterized by primary demyelination followed by the loss of axonal integrity with a severe clinical outcome (Nave et al., 2007). It is not clear to which extent myelin formation per se contributes to this support. Mutations in oligodendrocyte proteins are found to affect axon integrity without change in the myelin compartment (Lappe-Siefke et al., 2003). Similarly, an experimental therapy in a rat animal model of CMT1 improved axonal function without a corresponding improvement

in myelination (Meyer zu Horste et al., 2007). The process of development and differentiation of myelinating glia has been extensively studied in efforts to understand the basis of their functional mechanisms and molecular players of myelin formation. (Jessen and Mirsky, 2005; Poliak and Peles, 2003; Sherman and Brophy, 2005). A detailed insight in to these mechanisms will hopefully contribute to the development of successful strategies to restore lost functions of glial cells in demyelinating diseases and peripheral neuropathies.

2.1.2 Structure and composition of the peripheral nervous system myelin

The myelin sheath represents a highly specialized cellular compartment of myelinating Sc which is formed by tightly packed Sc membranes. The myelin membrane has a specific lipid-protein composition. It is enriched in lipids, which comprise 70-80% of the myelin membrane. Main lipid classes are cholesterol, phospholipids and glycosphingolipids, which assemble to form membrane lipid microdomains (Stoffel and Bosio, 1997). Proteins constitute 20-30% of the myelin dry mass. Myelin proteins are highly specific for the myelin membrane and unlike myelin lipids are normally not found as constituents of any other cell membrane. The majority of the proteins found in the myelin membrane are proteins of compacted myelin, such as myelin protein zero (PO), peripheral myelin protein 22 (PMP22) and myelin basic protein (MBP) (Arroyo and Scherer, 2000). Compacted myelin is a structure with characteristic radial periodicity resulting from tightly apposed membranes. Compaction is achieved by homophilic interactions of the extracellular domains of P0 tetramers on opposing membranes, that bring together extracellular sides of the membranes forming the intraperiod lines (Shapiro et al., 1996). Importance of the P0 protein in compaction, has been shown in P0 null mutants which fail to form compact myelin (Giese et al., 1992). The intracellular compartments in the myelin sheath with the cytoplasmic domain of P0 and MBP form the major dense lines. Compact myelin is interrupted by non-compacted regions of cytoplasm filled spiral channels, called Schmidt-Lantermann incisures, which are important for the transport of molecules through the myelin sheath (Balice-Gordon et al., 1998). Myelin associated protein (MAG), E-cadherin, and connexin32 (cx32) are proteins found within non-compacted myelin. Action potentials along myelinated fibers are formed at the node of Ranvier, a small patch of naked axonal membrane with highly concentrated voltage gated sodium channels. This local depolarization of the membrane is transmited along the myelin internode to the next node of Ranvier in a so called saltatory fashion (Poliak and Peles, 2003). Myelin segments confer lateral polarity between two nodes of Ranvier, with structurally specialized domains to provide the functional conditions for saltatory conduction of nerve impulses. One can

3

distinguish nodal, paranodal, juxtaparanodal and internodal domain (Salzer et al., 2008). Sc microvilli make contact with the nodal region. Paranodal regions are flanking the node of Ranvier on both sides where Sc membranes protrude to form uncompacted paranodal myelin loops, which are connected to the axon by septate junctions. Axo-glial contacts at the paranode are established through the interaction between glial neurofascin 155 (Nf-155) and axonal contactin associated protein (Caspr) and contactin (Charles et al., 2002). It is believed that the paranode is the initial site of myelin attachment to the axon, that secures separation of the electrical activity in the axonal region from the internode. The juxtaparanode is a region where shaker like potassium channels are accumulated, and it is maintained through interaction between axonal transient axonal glycoprotein1 (Tag1)/Caspr2 heterodimer and juxtaparanodal glial Tag1 (Traka et al., 2003). Finally, the Internodal region is a region of compacted myelin in a close apposition to the axonal membrane. Recently, it has been shown that the contact between the internode and axonal membrane is maintained by the Necl protein family, specifically axonal Necl1 and glial Necl4, which are crucial for myelin formation (Maurel et al., 2007; Spiegel et al., 2007).

2.1.3 Schwann cells: myelinating glia of the PNS

Mature myelinating Sc (mSc) are generated in the course of regulated, gradual differentiation from pluripotent neural crest progenitor cells, which are the source of all components of the PNS (Le Douarin, 1986). Two cell types with distinct morphological characteristics and cell specific markers can be identified during embryonic development of the Sc lineage, before final differentiation into mature Sc (Jessen and Mirsky, 2005). Schwann cell precursors (SCP) develop first in the Sc lineage around embryonal day 12 (E12) from neural crest cells migrating into developing nerves. These cells associate with multiple axons, and undergo proliferation and differentiation, largely dependent on neighboring axonal signals (Salzer et al., 1980). Axon derived NRG1 growth factor has been found to be critical for SCP survival, proliferation and development (Birchmeier and Nave, 2008). Formation of immature proliferating Sc can be detected in the nerve at E14 and these cells remain the nerve resident Sc until the time of birth. These cells are characterized by the presence of a basal lamina and autocrine survival mechanisms which make them less dependent on axonal contact compared to SCP (Meier et al., 1999). *In vitro,* it was shown that autocrine survival factors include insulin-like growth factor 2 (IGF2), neurotrophin 3 (NT3), platelet derived growth factor-β (PDGFβ), leukemia inhibitory factor (LIF) and lysophosphatidic acid (LPA) (Dowsing et al., 1999; Meier et al., 1999; Weiner and Chun, 1999). This characteristic of immature Sc is the base for Sc plasticity observed after PNS injury

which is critical for axonal outgrowth and nerve regeneration (Chen et al., 2007) In the postnatal phase, immature Sc exit the cell cycle and adopt either a myelinating or a non myelinating phenotype. During the process of radial axon sorting each mSc segregates axon in a 1:1 ratio and extends myelin membrane to create a multilamellar compact myelin sheath of one myelin segment (Sherman and Brophy, 2005). Non myelinating Sc (nmSc) ensheath multiple small axons, thus forming Remak bundles in which individual small caliber axons are segregated into pockets by a nmSc cytoplasm (Jessen and Mirsky, 1998). Axonal diameter appears to be critical for the Sc fate decision. Only axons larger than ~1 µm in diameter acquire a compact myelin sheath (Friede, 1972; Voyvodic, 1989). Additionally, the number of spiral myelin wraps formed around the axon is also regulated and proportional to axon diameter (Smith et al., 1982). This ratio has a constant value and is expressed as the g-ratio (ratio between inner and outer axonal diameter). The development of Sc is directed and regulated to achieve adequate myelin formation, which ensures optimal functional properties of myelinated fibers. Sc numbers are adjusted to form appropriate number of myelin segments along the axons and the myelin sheath thickens is adjusted to the axon diameter.

2.2 The Neuregulin1 family of growth factors

2.2.1 Neuregulin1 isoforms

Neuregulins (NRG) 1-4 are a family of growth and differentiation factors with multiple functions in the nervous system development (Falls, 2003). NRG1 is best characterized. It is encoded by one of the largest mammalian genes which results in multiple transcripts due to differential promoter usage and alternative splicing (Steinthorsdottir et al., 2004). NRG1 isoforms comprise a repertoire of more than 30 different soluble and membrane-bound proteins, at least in humans (Mei and Xiong, 2008). All isoforms contain an EGF like signalling domain, which alone is sufficient to induce ErbB receptor activation and downstream signalling. Based on their distinct N-terminal structure NRG1 isoforms can be classified into six main groups (Mei and Xiong, 2008). As groups IV-VI have not been extensively characterized they will not be discussed further. The N-terminus of type I isoforms is characterized by an immunoglobulin (Ig) like domain (Fig. 1A). Members of this group were independently identified and named heregulin (Holmes et al., 1992), acetylcholine receptor-inducing activity ARIA (Falls et al., 1993) and neu-differentiation factor (Wen et al., 1992). The type II variants, also known as glial growth factor (GGF) (Marchionni et al., 1993) harbor a "kringle" domain N- terminal to the Ig-like domain (Fig. 1A). NRG1 type III isofoms, one of which is also known as sensory and motor neuron derived factor

(SMDF) (Ho et al., 1995), are lacking an Ig domain and harbor a cystein-rich domain (CRD). The CRD-domain serves as a second transmembrane domain, thus type III variants are supposed to be tightly associated with the cell surface (Fig. 1A). An additional isoform variability is created by alternative splicing in the EGF-like domain (α versus β) with the β variant being more potent in signalling (Jones et al., 1999) (Fig. 1A). Cytoplasmic tail is also a source of structural variability, as different variants (a, b, c) exist (Wen et al., 1994 485) (Fig. 1A). Most of the NRG1 isoforms are synthesized as a transmembrane proproteins. *In vitro* studies showed that proproteins are proteolyticaly processed by proteases of the ADAMs family (ADAMS17 and ADAMS19) (Horiuchi et al., 2005; Yokozeki et al., 2007) and BACE1 (Hu et al., 2008; Hu et al., 2006; Willem et al., 2006). After processing, the extracellular parts of type I and type II isoforms are released from the cell surface for paracrine signaling (Fig. 1B).
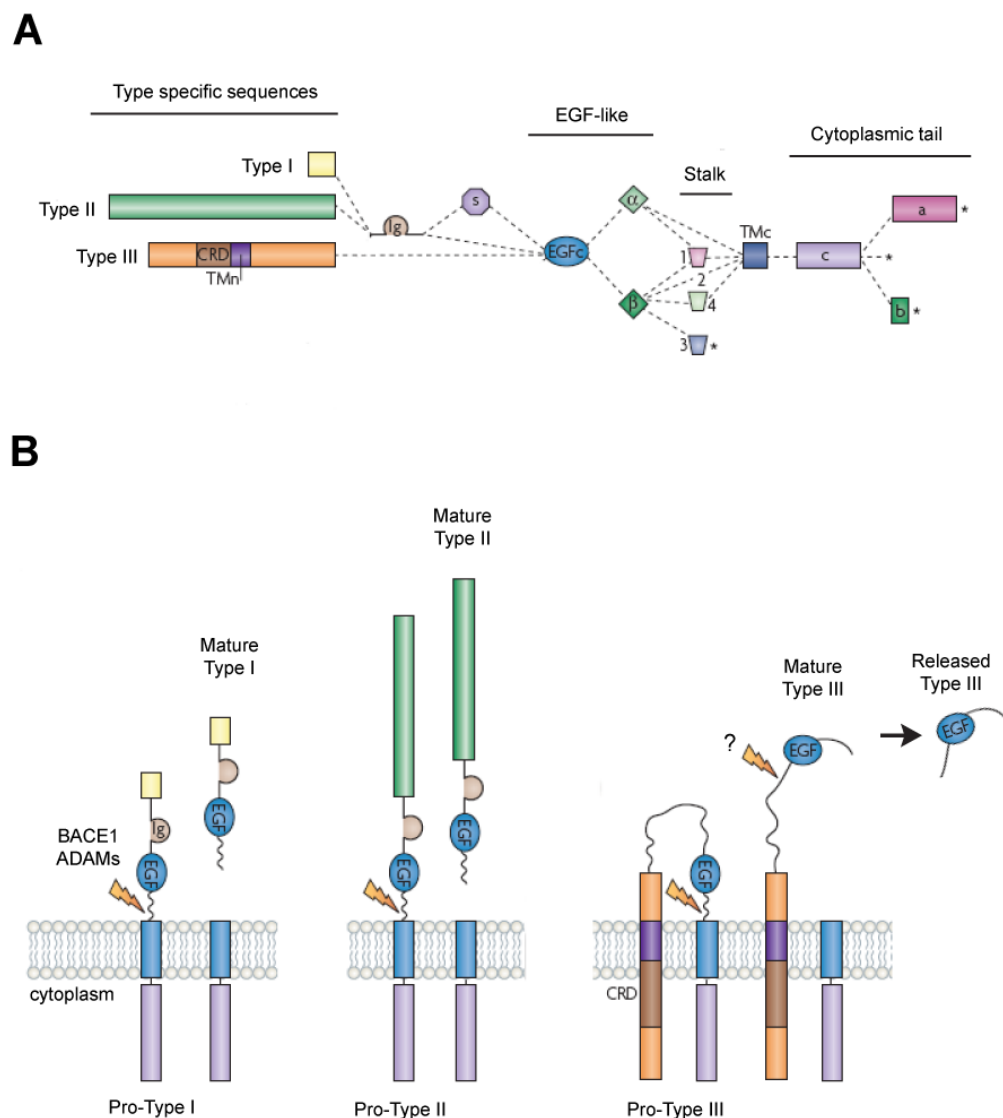
Fig. 1 NRG1 protein isoforms

6

(A) According to their distinct N-terminal region sequences NRG1 isoforms are classified into three main groups. Isoform specific region in Type III isoforms contains cysteine rich domain (CRD) with an N-terminal transmembrane domain (TMn). Types I and II have an immunoglobulin (Ig)-like domain and can obtain additional variability by differentially spliced spacer (S) region. Epidermal growth factor (EGF)-like signalling domain is present in all isoforms with alternative α or β type. Variability is also generated by splicing in the stalk region (1-4) and splice variant 3 does not contain C-terminal transmembrane domain (TMc). Splicing in the cytoplasmic tail region produces a, b or c variant. (*)- STOP codon.
(B) NRG1 isoforms are mainly produced as transmembrane proproteins with the EGF-like domain facing the extracellular space. Proproteins are processed by proteases BACE1 and/or ADAMs (lightning arrow) to generate mature signalling fragments. Mature Type I and Type II fragments are shed after processing for paracrine signalling. Mature Type III fragment is membrane bound due to presence of hydrophobic sequence in CRD domain. Potential second cut might occur (labeled with the question mark) to release EGF-like domain of Type III isform. (Adapted from Mei, 2008)

The EGF-like domain of NRG1 type III even after processing in the stalk region stays attached to the cell membrane due to the presence of the CRD-domain to mediate juxtacrine signalling (Wang et al., 2001) (Fig. 1B). Recently, it has been speculated that further processing of NRG1 type III and a release of the EFG-like domain might occur (Birchmeier and Nave, 2008; Willem et al., 2009) (Fig. 1B). Studies with isoform-specific null mutants revealed that the immense structural variability of NRG1 isoforms and pattern of expression indeed translates into differential functions (Meyer et al., 1997; Wolpowitz et al., 2000). Ig-domain containing isoforms were found to be important for heart, cranial sensory neurons and sympathetic development. In contrast, CRD-domain containing isoforms were indispensable for normal development of SCP and the neuromuscular junction, but developed no heart abnormalities. Neuronal overexpression of different NRG1 isoforms in transgenic mice also revealed distinct phenotypes in the PNS (Gomez-Sanchez et al., 2009; Michailov et al., 2004). Only the type III-β_1 isoform induced hypermyelination in the PNS, supporting isoform specific function. Distinct functions of NRG1-isoforms likely reside in structural differences and expression patterns. Paracrine signalling mediated by type I and type II and juxtacrine type III signalling specify distinct cell signalling paradigms. Even if the release of the type III isoform occurs different signalling microenvironments are plausible due to the distinct N-terminal structure compared to the NRG1 type I and type II. Soluble signalling fragments of the type I and type II isoforms contain Ig-like domain that interacts with the extracellular matrix heparin sulphate proteoglycans (Loeb and Fischbach, 1995) and can potentiate signalling by concentrating ligand at the site of action as shown for ARIA at the neuromuscular junction (Li and Loeb, 2001).

2.2.2 ErbB receptor and signaling pathways

NRG1 function is mediated by the EGF-like effector domain through activation of single-transmembrane receptor tyrosine kinases of the ErbB family (Mei and Xiong, 2008). The ErbB family comprises 4 members, ErbB 1-4 (Citri and Yarden, 2006).

NRG1 does not appear to be a ligand for the ErbB1 (epidermal growth factor receptor EGFR), but only binds to the extracellular domains of ErbB3 and ErbB4 receptors. ErbB2 has an impaired ligand binding domain and functions only as a coreceptor (Klapper et al., 1999). Upon binding, NRG1 induces conformational changes that allow receptor homo- or heterodimerization, which in turn activates the intracellular tyrosine kinase domain and auto-phosphorylation of tyrosine residues at the C-terminus. Auto-phosphorylation of the cytoplasmic tail induces subsequent binding of adaptor proteins that stimulate downstream signalling cascades. To convey signals the ErbB3 receptor is compelled to form heterodimers as it is devoid of an active kinase domain (Guy et al., 1994). As ErbB2 is impaired in ligand binding, only the ErbB4 receptor can form functional homodimers. Nevertheless, the ErbB2 receptor serves as a preferential dimerization partner due to the structure of the extracellular domain that contains a constitutively exposed dimerization arm (Garrett et al., 2003). Analysis of ErbB expression and NRG1-induced receptor heterodimerization revealed that NRG1 signals in oligodendrocytes through ErbB2/ErbB4 and in Sc through ErbB2/ErbB3 receptor heterodimers (Deadwyler et al., 2000; Vartanian et al., 1997). Analysis of the ErbB-specific mutants confirmed ErbB2/ErbB3 mediated NRG1 signalling in Sc development (Garratt et al., 2000b; Morris et al., 1999; Riethmacher et al., 1997). The mitogen-activated protein (MAP) kinase (Raf-MEK-ERK) and phosphatidylinositol-3-kinase (PI3K-Akt) pathways are two major signalling pathways activated by NRG1-mediated stimulation of ErbB receptors in the cultured Sc (Li et al., 2001). The regulated and balanced activation of these two signalling pathways by NRG1 evokes differential responses in Schwann cells during development. Sc proliferation, survival and myelination are dependent on PI3K activation (Maurel and Salzer, 2000) whereas the MAPK pathway was shown to inhibit Sc differentiation (Harrisingh et al., 2004; Ogata et al., 2004). Besides forward signalling to ErbB receptors by the EGF domain, unconventional back signalling of the C-terminal domain (CTD) of NRG1 has been reported in neurons *in vitro* (Bao et al., 2003). Soluble ErbB dimers and depolarization induce γ-secretase mediated release of CTD from the membrane, which than translocates into the nucleus to promote transcription and neuronal survival. Another study showed that NRG1-CTD binds to zinc-finger transcription factor Eos to enhance transcriptional activity of PSD-95 promoter after stimulation of synaptic activity in mouse cohlea (Bao et al., 2004). NRG1 binding to the ErbB4 receptor can induce γ-secretase mediated release of the receptor intracellular domain which also translocates to the nucleus to regulate transcription (Ni et al., 2001; Sardi et al., 2006).

2.2.3 Regulation of Sc development by NRG1

Motor and sensory neurons of the PNS predominantly express type III isoforms of NRG1 (Bermingham-McDonogh et al., 1997; Ho et al., 1995; Meyer et al., 1997) (Fig. 2; 2-5), Axonal NRG1 affects Sc development on many different levels (Garratt et al., 2000a) (Fig. 2; 1-4). A critical role of NRG1-ErbB signalling in Sc development was demonstrated by studies using both ligand and receptor knock out mutants. Mice deficient in Nrg1 type III display a substantial reduction of the Sc precursor pool (Wolpowitz et al., 2000). These mutants fail to form functional neuromuscular junctions and experience perinatal death due to the inability to breathe. Consequently, studies of postnatal differentiation and myelination are not possible in these mutants. Correspondingly, inactivation of ErbB2 and ErbB3 receptors leads to an even more severe Sc phenotype, namely having a complete lack of Sc precursors and Sc in peripheral nerves (Morris et al., 1999; Riethmacher et al., 1997; Wolpowitz et al., 2000). Already on the level of neural crest cells, stimulation by NRG1 defines the glial fate of these multipotent progenitors and induces differentiation towards the Schwann cell lineage *in vitro* (Shah et al., 1994). Additional *in vitro* experiments with cultured Sc from embryonic and postnatal nerves showed that NRG1 promoted proliferation, survival and differentiation of Sc precursors and immature Sc (Dong et al., 1995; Morrissey et al., 1995). NRG1 also regulates apoptosis in the Sc lineage. Apoptotic death in the Sc lineage is a mechanism to match the number of Sc to the number of myelin segments formed along the axon. Apoptosis of immature Sc in culture could be blocked by NRG1 (Syroid et al., 1996). Furthermore developmental and axotomy induced apoptosis of immature Sc *in vivo* is prevented by the addition of NRG1 (Grinspan et al., 1996).
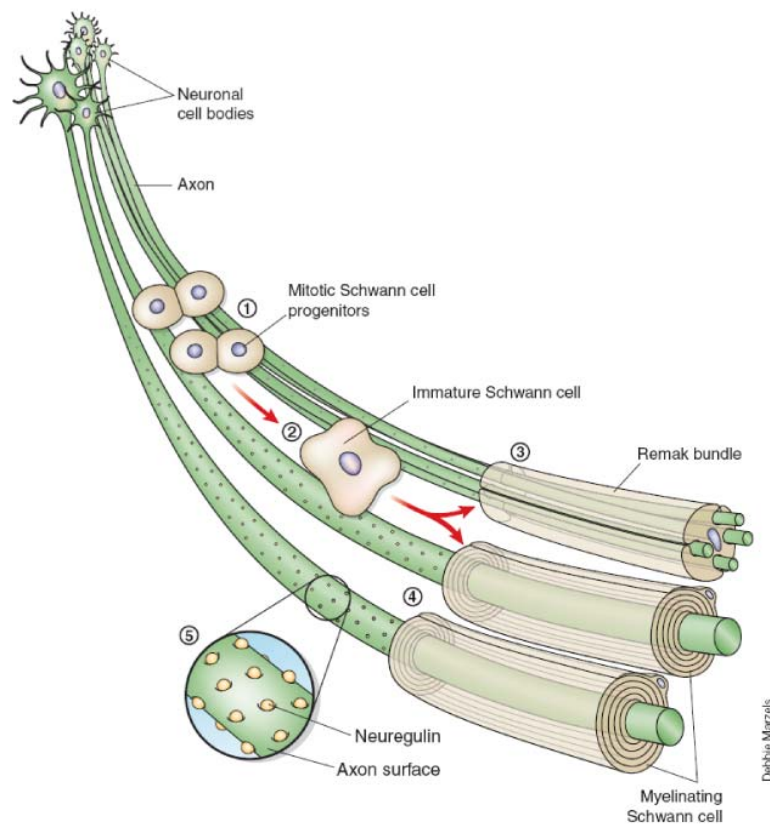
Fig. 2 Regulation of Sc development by NRG1

Sc are derived from proliferating neural crest progenitors (1) which migrate into developing nerves early in development. Under the influence of axonal signals they later develop into immature Sc (2). In the phase of final differentiation immature Sc associated with small caliber axons from Remak bundle (3). Sc associated with axons typically larger than 1 μm differentiate into mSc (4). All the phases of Sc development are controlled by NRG1 expressed on the axonal surface (5) (Adapted from Nave and Schwab, 2005)

2.2.4 The role of NRG1 type III-β_1 in myelination

NRG1 type III-β_1 has emerged as a master regulator of PNS myelination. The fate of immature Sc associated with multiple axons in the peripheral nerves is defined by the level of NRG1 on the axonal surface (Nave and Salzer, 2006). High levels of NRG1 on the axons larger than ~1 μm in diameter, will induce development of immature Sc into mSc resulting in formation of compact myelin sheath around single axons (Fig. 2; 2-4). Low levels of NRG1 on axons smaller than ~1 μm in diameter, will direct immature Sc towards a non myelinating phenotype. The nmSc ensheathe multiple small diameter axons in a Remak bundle (Fig. 2; 2-3). DRG neurons prepared from embryos of NRG1 type III knock out mice are not myelinated in DRG-Sc co-cultures. Conversely, increase of NRG1 type III-β_1 protein levels by viral overexpression is sufficient to induce myelination of normally unmyelinated sympathetic postganglionic fibers, when cultured in the presence of Sc (Taveggia et al., 2005). Additionally, it was found that

10

overexpression of type III isoform in transgenic mice induces ectopic myelination of small diameter c-fibers normally found in Remak bundles (Humml and Schwab unpublished). These observations unquestionably show that Sc perceive levels of NRG1 as a biochemical measure of axon caliber and define the further course of differentiation (Taveggia et al., 2005). Furthermore, levels of NRG1 type III-β_1 control myelin sheath thickness, such that axons with a wide range of diameter, maintain a constant g-ratio values (Michailov et al., 2004). Overexpression of the NRG1 type III isoform in neurons induces formation of thicker myelin sheath when compared to wt animals. Haploinsuficiency of the same isoform correspondingly leads to the formation of thinner myelin sheath. Inactivation of ErbB signaling in myelinating Schwann cells leads to the same hypomyelinating phenotype (Garratt et al., 2000b). Specificity of the type III isoform of NRG1 in myelin thickness regulation was confirmed as no similar effect was achieved by neuronal overexpression of the NRG1 type I isoform (Michailov et al., 2004). This finding suggested the importance of a directional presentation of NRG1 and juxtacrine signalling for the function in myelination mediated only by the type III-β_1 isoform. This is in line with the finding that incorrect presentation of NRG1 to the mSc in culture after addition of soluble NRG1 inhibited formation of myelin and even resulted in dedifferentiation of myelin forming Sc and demyelination (Zanazzi et al., 2001). Surprisingly neuronal overexpression of the NRG1 type III-β_3 failed to increase myelin thickness (Gomez-Sanchez et al., 2009). Thus, it seems that protein structure plays a major role in defining specific signalling patterns, which are beyond simple paracrine versus juxtacrine signalling mechanisms in order to induce proper myelin formation.

2.3 Proteolytic processing and activation of NRG1 type III

Proteolytic processing of membrane proteins is known to regulate signaling processes (Hooper et al., 1997). Both ligand and receptors can be activated or inactivated after ectodomain shedding. As previously mentioned, NRG1 type III is synthesized as a proprotein that is proteolytically cleaved to be engaged in signaling (Wang et al., 2001). In the following chapter proteases that have been reported to play a role in NRG1 processing will be discussed in more details.

2.3.1 Role of BACE1 in NRG1 processing and myelination

β-site amyloid precursor protein cleaving enzyme 1 (BACE1) is a β-secretase with aspartyl protease activity, which is well known for the release of amyloid-β-peptide (Aβ), the constituent of amyloid plaques in Alzheimer's disease (AD) (Zacchetti et al., 2007). BACE1 is highly expressed in neurons (Laird et al., 2005) where it mediates

cleavage and release of multiple substrates. Since its discovery 10 years ago (Vassar et al., 1999) numerous studies revealed BACE1 substrates other than APP, such as low-density lipoprotein receptor related protein (LPR) (von Arnim et al., 2005), amyloid-β precursor-like proteins (APLP1/2) (Li and Sudhof, 2004), sialyltransferase ST6Gal-I (Kitazume et al., 2001), β-subunit of the voltage gated sodium channel (Wong et al., 2005) and P-selectin glycoprotein ligand1 (PSLG1) (Lichtenthaler et al., 2003). Until recently, the physiological role of BACE1 has been elusive as phenotype analysis of BACE1-/- mutants showed only moderate hyperactivity in behavioral assays (Dominguez et al., 2005). More detailed analysis revealed that BACE1 null mutants have impaired myelination in PNS and CNS suggesting a role of BACE1 in myelination (Hu et al., 2006; Willem et al., 2006). Sciatic nerve remyelination after nerve crush is also delayed in BACE1-/- mutants (Hu et al., 2008). Thus, side effects of AD treatment by blocking BACE1 activity require serious consideration. PNS axons of BACE1 null mutants exhibit significant hypomyelination similar to NRG1 type III heterozygous mutants (Hu et al., 2006; Michailov et al., 2004; Willem et al., 2006). Strong expression of BACE1 in CNS during active myelination and accumulation of unprocessed NRG1 in the BACE1-/- mutant brains strongly suggested NRG1 as a new physiological substrate of BACE1 and attributed the myelination phenotype of BACE1-/- mice to inefficient NRG1 processing. Even though processing of the NRG1 III-β_1 by BACE1 in the stalk region has been shown *in vitro* and the BACE1 cleavage site in NRG1 protein sequence GIEF/MEAE has been identified (Hu et al., 2008; Willem et al., 2004) there is no evidence of NRG1 type III-β_1 processing in PNS *in vivo*. Another open question is whether additional cleavage by BACE1 or other proteases occurs to release the EGF domain of NRG1 type III from the membrane. This proteolytic event repeatedly suggested in the literature remains to be proven (Birchmeier and Nave, 2008; Hu et al., 2008; Wang et al., 2001; Willem et al., 2004; Willem et al., 2009)

2.3.2 NRG1 processing by the metalloproteases of ADAMs family

ADAMs (a disintegrin and metalloproteases) constitute a family of more than 30 membrane anchored proteins with a role in protein ectodomain shedding mediated by the metalloprotease catalytic domain (Blobel, 2005). Not all ADAM proteins posses a catalytically active protease domain that classifies them as a subgroup of the matrix metalloproteases (MMP) family (Schlondorff and Blobel, 1999). Only about half of them are proteolytically active and the presence of the integrin binding (disintegrin) domain distinguishes them from other MMPs. The disintegrin domain by which ADAMs mediate cell-cell and cell-matrix interactions is specifically important for the cell adhesion function of proteolytic inactive ADAMs (White, 2003). Other ADAMs, especially

ADAM17 (TACE-tumor necrosis factor-α converting enzyme), are known to participate in cleavage dependent activation and release of various transmembrane protein ligands, such as tumor necrosis factor α (TNFα) (Black et al., 1997; Moss et al., 1997) and EGFR ligands (Sahin et al., 2004), thereby modulating signalling events. Therefore, the role of ADAMs processing of NRG1 has been addressed by numerous studies. Two members of the ADAMs family expressed in neurons (Yang et al., 2006) ADAM17 (TACE) and ADAM19 (meltrin β) have been identified to cleave NRG1 proteins in various *in vitro* assays. Absence of ADAM17 in cells has been shown to abolish cleavage of the transfected NRG1 type I isoforms with EGF-α (Montero et al., 2000) and EGF-β domains (Horiuchi et al., 2005). *In vivo*, the contribution of ADAM17 processing to NRG1 function remains unknown due to the perinatal death of ADAM17 -/- mice mutants induced by hart abnormalities (Jackson et al., 2003) and defects in epithelial structures such as skin, intestine, and lung (Peschon et al., 1998; Zhao et al., 2001). Processing of NRG1 type I-β isoforms was not affected after transfection of ADAM19-deficient cells (Horiuchi et al., 2005; Zhou et al., 2004). Independent studies however revealed the role of ADAM19 in intracellular processing of NRG1 type I-β (Shirakabe et al., 2001; Yokozeki et al., 2007). Recently, the role of ADAM19 in Sc development and nerve regeneration has been addressed.(Wakatsuki et al., 2009). In this study the observed delay in remyelination in ADAM19 null mice, was explained by impaired intracellular processing activity by ADAM19, which normally inactivates NRG1 type I to prevent MAPK pathway stimulation in Sc and enables activation of the promyelinating Akt pathway by axonal NRG1 type III. Contribution of ADAM10 (kuzbanian) to the NRG1 processing has been evaluated because of the known function in cleavage of APP substrate (Kojro et al., 2001; Lammich et al., 1999) and especially after BACE1 has been identified to process NRG1. However, NRG1 processing was shown to be insensitive to ADAM10 both in cell culture and *in vivo* (Freese et al., 2009). In all studies of NRG1 processing by ADAM17 and 19, the NRG1 type I-β isoform was used. Even though processing of NRG1 type III-β$_1$ could be blocked by inhibition of ADAMs in cell culture (Hu et al., 2008) using broad spectrum ADAMs inhibitor, it is remains unclear if a functional interaction exists between ADAMs and the NRG1 type III-β$_1$ isoform. Recently metalloendoprotease nardilysin (Nrd1/NRDc) has been found to play a role in myelination and indirectly in NRG1 processing (Ohno et al., 2009). Nrd1-/- mice have hypomyelination in PNS. Correspondingly, neuron specific overexpression of Nrd1 promotes myelination showing that NRDc levels regulate myelin sheath thickness. Moreover, it was shown that NRDc indirectly enhances NRG1 shedding by activating BACE1 and TACE.

2.4 Aim of the study

Previous studies have revealed a critical role of NRG1 type III-β_1 in formation of peripheral myelin. Membrane bound NRG1 type III-β_1 is an instructive myelination signal and its level determines myelin sheath thickness (Michailov et al., 2004; Taveggia et al., 2005). Recently, it has been shown that BACE1 inactivation leads to hypomyelination similar to haploinsufficiency of NRG1 type III-β_1 (Willem et al., 2006). This finding suggested BACE1-mediated NRG1 type III-β_1 activation for myelination, but a direct evidence for this interaction in PNS *in vivo* has not been presented. The goal of this study was to further explore BACE1 mediated activation of NRG1 for PNS myelination *in vivo*. For that purpose, we have generated a transgenic mouse line with neuronal overexpression of a tagged NRG1 type III-β_1 variant "GIEF" mimicking BACE1 processing, and analyzed the effect on myelination. We also compared the "GIEF" line myelination phenotype with that of tagged full length NRG1 type III-β_1 "HANI". Further, we wanted to address NRG1 processing *in vivo* and the structure of the active NRG1 type III-β_1 fragment by biochemical analysis of transgenic full length and processed NRG1 type III-β_1 in wt and BACE1 null background. Finally, we took advantage of transgenic mouse lines overexpressing tagged NRG1 variants to investigate trafficking and subcellular localization of NRG1 in neurons.

3 MATERIALS AND METHODS

3.1 Materials

3.1.1 Kits Chemicals and protocol source

The Chemicals used in experiments were purchased from Sigma-Aldrich and Merck unless stated otherwise. All molecular biology kits were purchased from Qiagen, Invitek, Promega, Stratagene, Sigma-Aldrich and Macherey-Nagel. General laboratory plastic ware was purchased from Gilson, Falcon and Eppendorf.

Websites referred for online protocols
Neuroscience:
http://mrw.interscience.wiley.com/emrw/9780471142300/home/
Molecular biology
http://mrw.interscience.wiley.com/emrw/9780471142720/home/
Protein
http://mrw.interscience.wiley.com/emrw/9780471140863/home/

3.1.2 Molecular biology buffers

50x Trisacetate EDTA (TAE) buffer
2 M   Trisacetate, pH 8.0
50 mM   EDTA
57.1 ml   glacial acetic acid
Adjust to the 1000 ml volume with ddH2O

1x Tris-EDTA (TE) buffer
10 mM   Tris-HCl, pH 8.0
1 mM   EDTA

10x modified Gitschier buffer (MGB)
6.7 ml   1M Tris-HCl, pH 8.8
1.66 ml   1M (NH4)2SO4
650 µl   1M MgCl2
Add ddH2O the a final volume of 10ml

1x MGB buffer (Working solution)
1 ml   10x MGB
500 µl   10% Triton X-100
8.5 ml   ddH2O

Injection buffer for transgene constructs
5 mM Tris   pH 7.5
0.1 mM   EDTA

1% Ethidiumbromide in ddH2O (10 mg/ml)
Final concentration in a gel 1 µg/ml

10x DNA sample buffer

25 mg	Xilene cyanol
25 mg	Bromophenol Blue
1.25 ml	10% SDS
12.5 ml	100% Glycerol
10 ml	500 mM EDTA pH 8

Add ddH2O to the final volume of 25 ml

10mM dNTP (50x stock)

2 mM each nucleotide (dATP, dCTP, dGTP, dTTP) (Boehringer)
200 µM final concentration in a PCR reaction (50 µM each nucleotide)

3.1.3 Protein biochemistry buffers

10x Phosphate buffered saline (PBS)

1.7 M	NaCl
34 mM	KCl
40 mM	Na2HPO4 x 2H2O
18 mM	K2HPO4

Adjust pH 7.2 with 1N NaOH.

Modified RIPA buffer (protein lysis buffer)

50 mM	Tris-HCl, pH 7.4
150 mM	NaCl
1 mM	EDTA
0.1%	SDS
1.0%	sodium deoxycholate
1.0%	TritonX-100

Phosphatase inhibitors

1 mM	sodium orthovanadate
0.5 mM	zinc chloride
4 mM	sodium pyrophosphate
1 mM	sodium fluoride

Complete Mini protease inhibitors (Roche) 1 tablet/10 ml of RIPA buffer

Phosphatase and protease inhibitors are added freshly to the RIPA buffer before use.

3.1.4 SDS PAGE and Western blotting solutions

4x Tris-HCl (Separating gel buffer)

1.5 M	Tris-HCl, pH 8.8

4x Tris-HCl (Stacking gel buffer)

1 M	Tris-HCl, pH 6.8

8 % Polyacrylamide separating gel (4 gels of 0.75 mm thickness)

9.3 ml	H2O
5.3 ml	30% acrylamide/bis-acrylamide (29:1)

4.0 ml   4x Tris-HCl
0.2 ml   10% SDS
60 µl   10% APS
12 µl   TEMED

12% Polyacrylamide separating gel (4 gels of 0.75 mm thickness)
6.6 ml   H2O
8 ml   30% acrylamide/bis-acrylamide (29:1)
5 ml   4x Tris-HCl
0.2ml   10% SDS
60 µl   10% APS
8 µl   TEMED

0.13% Polyacrylamide stacking gel (4 gels of 0.75 mm thickness)
5.5 ml   H2O
1.3 ml   30% acrylamide/bis-acrylamide (29:1)
1 ml   4x Tris-HCl
80 µl   10% SDS
80 µl   10% APS
8 µl   TEMED

5x SDS sample buffer
100 mM   Tris, pH 6.8
5% (w/v)   SDS
10% (v/v)   0.4% Bromphenolblue (in EtOH)
50% (v/v)   Glycerol

5x Trisglycine electophoresis buffer
125 mM   Tris base
1.25 M   Glycine
0.5%   SDS
pH ~ 6.8 no adjustment necessary

10x Trisglycine transfer buffer
250 mM   Tris base
1.92 M   Glycine

1x Transfer buffer
25 mM   Tris base
192 mM   Glycine
20%   Methanol

Coomassie blue (Staining solution)
2 g   Coomassie brilliant blue (R-250)
1 L   Methanol
200 ml   Acetic acid
800 ml   ddH2O
Stir overnight and filter through a Whatman paper.

20x Tris buffered saline (TBS)
1 M   Tris base

3 M   NaCl
Adjust pH to 7.4 with fuming HCl.

1x TBS with Tween-20 (TBST)
50 mM   Tris-HCl (pH 7.4-7.6)
150 mM   NaCl
0.05%   Tween-20

Western blot stripping buffer
0.2 M   Glycine-HCl, pH 2.5
0.1%   Tween-20

Western blot blocking buffer
5% non-fat dry Milk powder in 1x TBST

Enhanced Chemiluminescence (ECL) Western-blot detection kit
Western Lightning™ Plus-ECL, Enhanced luminol reagent plus (Perkin Elmer Life Sciences, Inc.).

ECL-Hyperfilms (Amersham Biosciences)

PVDF membrane -Hybond P pore size 0.45 µm (Amersham)

3.1.5 DNA and protein markers

DNA-marker Lambda/HindIII   Promega
GeneRuler 1 kb DNA ladder   Fermentas
GeneRuler 100 bp DNA ladder   Fermentas
Precision Plus prestained protein standard   BioRad

3.1.6 Immunocytochemystry buffers

1x Phosphate buffered saline (PBS)
117 mM   NaCl
3.4 mM   KCl
4 mM Na_2HPO_4 x $2H_2O$
1.8 mM KH_2PO_4
Adjust to pH 7.2 with 1N NaOH

4 % Paraformaldehyde in Phosphate buffer
10 ml   0.2 M NaH_2PO_4 x H_2O
40 ml   0.2 M Na_2HPO_4 x $2H_2O$
25 ml   16% Formaldehyde
25 ml ddH_2O

Blocking Buffer
2%   BSA (Fraction V)
2%   Horse serum
0.02%   Biotin
0.1%   Porcine skin gelatine
0.025%   Saponin

Dissolved in PBS

Permealisation buffer
0.1% Saponine in PBS

Mounting Media
Aqua polymount (Polysciences)

3.1.7 Histology buffers and solutions

Phosphate buffer (Stock Solutions)
0.2 M   NaH2PO4 x H2O
0.2 M   Na2HPO4 x 2H2O

Phosphate buffer working solution (pH 7.4)
20 ml   0.2M NaH2PO4
80 ml   0.2M Na2HPO4
100 ml   ddH2O

Perfusion fixative for immunostainings:
4% Paraformaldehyde in Phosphate buffer

Karlsson-Schultz (fixative solution for electron microscopy)
10 ml   0.2 M NaH2PO4 x H2O
40 ml   0.2 M Na2HPO4 x 2H2O
0.5 g   NaCl (0.5% final concentration)
25 ml   16% PFA (4% final concentration)
10 ml   25% Glutaraldehyde (2.5% final concentration)
Add ddH2O to a final volume of 100 ml

Citrate Buffer (stock solution)
0.1 M   Citric acid
0.1 M   Sodium citrate dihydrate
Stored at 4°C

Citrate Buffer (working solution, 0.01 M, pH 6.0)
9 ml   0.1 M Citric acid
41 ml   0.1 M Sodium citrate dihydrate
450 ml   ddH2O
Always freshly prepared

Tris Buffer (stock solution)
0.5 M   Tris base
Adjust to pH 7.6 with HCl
Stored at 4°C

Tris Buffer (working solution)
100 ml   0.5 M Tris base (pH 7.6)
9 g   NaCl
Add up to 1000 ml with ddH2O
Always freshly prepared

Washing buffer (2% milk powder in Tris Buffer)
20 g of non-fat milk powder
Add Tris buffer up to 1000 ml

Bovine Serum Albumin in PBS (PBS/BSA)
20 ml   0.2 M NaH_2PO_4
80 ml   0.2 M Na_2HPO_4
1.8 g   NaCl
1 g   BSA
100 ml   ddH2O

Blocking buffer
20% Goat serum in PBS/BSA

Ca^{+2}/Mg^{+2}- free HEPES buffered Earles balanced salt solution (E/H)
120 mM   NaCl
10 mM   NaHCO3
1 mM $NaH_2PO_4xH_2O$
2.5 mM   KCl
20 mM   Glucose
20 mM   HEPES
0.3%   BSA
0.0005%   Phenol Red
Adjust pH to 7.4 and filter through 0.22 µm pore size filters to sterilize. Store frozen or on 4 ºC in sterile bottles.

Mounting media
Eukit   (Kindler)
Aqua polymount   (Polysciences)
Shandon Cryomatrix   (Thermo Scientifics)

3.1.8 Histology staining solutions and reagents

Mayer's Haematoxylin solution
Dissolve 1 g Haematoxylin in 1000 ml dH2O
Add 0.2 g sodium iodate and 50 g of potassium aluminium sulphate under constant shaking.
Add 50 g chloralhydrate and 1 g citric acid
Filter the solution before use.

Eosin solution
Stock solution (10x)
10 g of Eosin were dissolved in 100 ml of ddH2O and left to mature.

Eosin working solution
Add 2.5 ml of stock solution to 250 ml ddH2O and finish by adding 12 drops of glacial acetic acid

Scott's solution
2 g   KHCO3
20 g   MgSO4

Add ddH20 to the final volume of 1l

HCl-Alcohol

1.25 ml	HCl
350 ml	Ethanol
150 ml	ddH2O

Reagents for Gallyas silver impregnation of myelin

Incubation solution

1 g	Ammonium nitrate
1 g	Silver nitrate

Dissolve in 1000 ml ddH2O
Add 3 ml 4% Sodium hydroxide (pH 7.4-7.6)
Brown precipitate formed can be dissolved by shaking. Solution can be used for 8-10 weeks.

Physical developer

Solution A

5%	Sodium carbonate (dehydrated) in ddH2O

Solution B

2 g	Ammonium nitrate
2 g	Silver nitrate
10 g	Wolframosilicic acid (silicotungstic acid)

Dissolve in 1000 ml ddH2O

Solution C

2 g	Ammonium nitrate
2 g	Silver nitrate
10 g	Wolframosilicic acid (silicotungstic acid)
7 ml	Formalin (37% paraformaldehyde)

Dissolve in 1000 ml ddH2O

To make the physical developer, add gently first 70 ml of solution B and than 30 ml of solution C, gently with constant shaking to 100 ml of solution A.

Fixing solution
2% sodium thiosulphate

Methylenblue Stock solution

1 g	Na-tetraborat (Borax)
1 g	Methylenblau

Add H2O to the final volume of 100ml
The solution is stable for a month

Azur II stock solution
1 g Azur II in 100 ml ddH2O
The solution is stable for a month

Methylenblue-Azur II working solution
Mix both staining solutions in a 1:1 ratio and filter through a syringe filter tip when applying to the sections.

Chemicals for EM contrasting
4% Uranyl acetate
Reynolds lead citrate
1M HCl

3.1.9 Bacteria and bacterial culture media

Bacterial strains
Escherichia coli XL1-Blue   (Stratagene)

TB jap
10 mM PIPES
15 mM   CaCl2
250 mM   KCl
Adjust pH to 6.7 with KOH
55mM   MnCl2x2H2O
Sterilize by filtrating (0.22 µm filter pore size)

LB medium (Luria and Bertani medium)
1 %   Bacto-Pepton
0.5 %   Yeast extract
1 %   NaCl
 Media pH was set to 7.5 with 10 N NaOH and autoclaved.

Selective LB media was supplemented with following antibiotics:
100 µg/ml   Ampicillin
50 µg/ml   Kanamycin

LB-Agar plates
1 %   Bacto-Pepton
0.5 %   Yeast extract
1 %   NaCl
1.2%   Bacto-agar
Mix with adjusted pH7.5 is autoclaved and left to cool to 55°C when desired antibiotics are added.

For blue-white selection LB-agar is further supplemented with
35 µg/ml   X-Gal (5-bromo-4-chloro-3-indolyl-β-D-galactopyranoside)
15 µg/ml   IPTG (Isopropyl-β-D-thiogalactopyranosid)

Plates are stored at 4°C.

Bacterial glycerol stock (1ml)
80%   fresh overnight bacterial culture in LB media with antibiotic
20%   100% glycerol

3.1.10   Cell lines and cell culture media

All the media and the cell culture chemicals were purchased from GIBCO or LONZA unless stated otherwise

3.1.10.1 Mammalian cell lines and media

PC12: Rat adrenal pheochromocytoma cell line (Greene and Tischler, 1976)
Medium:
DMEM   (1g/l glucose)
10%   HS
10%   FBS (heat inactivated)
1%   Pen/Strep
1%   L-Glutamin

COS7: African green monkey kidney immortalized cell line (Jensen et al., 1964)
Medium:
DMEM   (1g/l Glucose)
10%   FBS (heat inactivated)
1%   Pen/Strep
1%   L-Glutamin

HEK293T: Human embryonic kidney immortalized cell line (Graham et al., 1977)
Medium:
DMEM   (4.5 g/L Glucose)
10%   FBS (heat inactivated)
1%   Pen/Strep
1%   L-Glutamin

2x Freezing medium for eukaryotic cell lines:
40%   DMEM
20%   DMSO
40%   FBS

3.1.10.2 Chemicals and media for primary cell culture

DRG-Schwann cell co-culture general chemicals:

Leibovitz's L-15 medium
Ascorbic acid (Sigma)
0.25%   Trypsin solution
10 µg/ml stock   2,5S NGF in DMEM (Alomone lab)
10 mM   GM6001 ADAMS protease inhibitor (Calbiochem)
1mM stock   ßsecretase inhibiotor IV in DMSO (Calbiochem)

Maintainance medium:
MEM (Earles salts and L-Glut)
10%   FBS
1%   Pen/Strep
50ng/ml   NGF

Myelinating media:
MEM (Earles salts and L-Glut) (Gibco)
10%   FBS (Gibco)
1%   Pen/Strep (Lonza)
50ng/ml   NGF
50µg/ml   Ascorbic acid

3.1.11   Oligonucleotides

All oligonucleotides (primers) were synthesized at "Oligo Syntesys Lab" of the Max Planck Institute of Experimental Medicine. They are provided at 50pM concentration. In house identification numbers are displayed in brackets.

3.1.11.1 Genotyping primers

Nrg1 TypeIII transgenic
Forward: 5'-GGCTTTCTCTGAGTGGCAAAGGACC -3'   (6467)
Reverse: 5'-GTCCACAAATACCCACTTTAGGCCAGC -3'   (11980)
Amplification product: 552bp

BACE knock out
Forward: 5'-CGGGAAATGGAAAGGCTACTCC -3'   (12889)
Reverse WT: 5'-AGGCAGCTTTGTGGAGATGGTG -3'   (12888)
Reverse KO: 5'-TGGATGTGGAATGTGTGCGAG -3'   (12890)
Amplification products: WT 272bp band and mutant 157bp band

BACE1 transgenic
Forward: 5'-GGCTACAACATTCCACAGACA -3'   (11784)
Reverse: 5'-GTTCTGAGATATTTGAAGGAC -3'   (11785)
Amplification product: 300bp

3.1.11.2 Quantitative real time PCR primers

β-actin
Forward: 5'-CTTCCTCCCTGGAGAAGAGC-3'   (9146)
Reverse: 5'-ATGCCACAGGATTCCATACC-3'   (9147)

Neuregulin1 type III
Forward: 5'-TGAGAACACCCAAGTCAGGA -3'   (9156)
Reverse: 5'-CCCAGTCGTGGATGTAGATGT-3'   (9157)

3.1.11.3 RT-PCR primers

Neuregulin1 type III transgene
Forward: 5'-GGTGCAGCAACTGGAGGCGTTG -3'   (5648)
Reverse: 5'-GTCCACAAATACCCACTTTAGGCCAGC -3'   (11980)
Amplification product: 450bp from cDNA template

β-actin
Forward: 5'-GATATCGCTGCGCTGGTCGTC -3'   (4262)
Reverse: 5'-CATGGCTGGGGTGTTGAAGGTC -3'   (4264)
Amplification product: 300bp from cDNA template, 800bp from genomic DNA template

3.1.11.4 Cloning primers

GIEF construct cloning:
Forward: 5'-ATATGAATTCCTCGAGGCCACCATGTACCCATACGATGTTCCAG
ATTACGCTCTTTACCCATACG-3'   (10948)
Reverse: 5'-TACTCGAGGCTAAAATTCAATCCCAAGATGCT -3'   (10851)

Cloning of GIEF into the pLenti6/V5-DEST
Forward: 5'GGGGACAAGTTTGTACAAAAAAGCAGGCTCTACCATGTACCCATA
CGATGTTCCAGATTAC -3'   (13578)
Reverse:5'-GGGGACCACTTTGTACAAGAAAGCTGGGTCCTAAAATTCAATCC
CAAGATGCTTGTAGAAGC -3'   (13760)

Cloning of HANI into the pLenti6/V5-DEST
Forward: 5'-GGGGACAAGTTTGTACAAAAAAGCAGGCTCTACCATGTACCCAT
ACGATGTTCCAGATTAC -3'   (13578)
Reverse: 5'-GGGGACCACTTTGTACAAGAAAGCTGGGTCTTATACAGCAATA
GGGTCTTGGTTAGCG -3'   (13761)

3.1.12   Plasmids

Vector	Resistance	Source
pGEM-T	Amp	Promega
pCMV2-GIEF	Kan	
pCMV2-HANI	Kan	
pcDNA3.1-BACE1	Amp	
pEGFP-N1	Kan	Clontech
pTSC-Thy1.2	Amp	(Caroni, 1997)
pTSC-Thy1.2 GIEF	Amp	
pDONR207	Gent	
pLenti6/V5-DEST	Amp	Invitrogen

3.1.13   Enzymes

Restriction enzymes	New England Biolabs
REDTaq DNA polymerase	Sigma-Aldrich
HotStarTaq DNA polymerase	Qiagen
GoTaq polymerase	Promega
Easy-A HiFi PCR cloning enzyme	Stratagene
Superscript III Reverese Transcriptase	Invitrogen
CIP (alkaline phosphatase)	Roche
T4 DNA ligase	Promega
Gateway BP Clonase II	Invitrogen
Gateway LR Clonase II Plus	Invitrogen
CIP (Calf intestine alkaline phosphatase)	Roche
Power SYBR Green PCR master mix	Applied Biosystems
ProteinaseK	Roth
DNase	Qiagen

25

3.1.14   Antibodies

Primary antibodies

Antibody	Species	Dilution	Application	Company
GAPDH	Mouse	1:1000	IB	Stressgen
GFAP	Rabbit	1:200	IHC	DAKO
HA	Mouse	1:250	IHC	Covance
HA	Rat	1:1000	IB	Roche
Krox20	Rabbit	1:400	IHC	Dies Meijer
Mac3	Rat	1:500	IHC	Pharmingen
MBP	Rabbit	1:200	ICC	DAKO
NF200	Rabbit	1:200	IHC	Sigma
Necl1	Rabbit	1:000	ICH/IB	Elior Peles
NRG1	Rabbit	1:100 /1:500	ICC/IB	Santa Cruz
Oct6	Rabbit	1:200	IHC	Dies Meijer
P0	Mouse	1:000	IHC	J.J Archelos
pAkt (ser473)	Rabbit	1:1000	IB	Cell signalling
Peripherin	Rabbit	1:500	IHC	Chemicon
pMAPK	Rabbit	1:1000	IB	Cell signalling
α-tubulin	Mouse	1:2000	IB	Sigma
Tuj1	Mouse	1:250/1:500	IHC/ICC	Covance
rHIgM22	Human	10µg/ml	IHC	Mayo clinic, MN
sHigM42	Human	10µg/ml	IHC	Mayo clinic, MN
sHIgM39	Human	10µg/ml	IHC	Mayo clinic, MN
sHIgM79.08	Mouse	10µg/ml	IHC	Mayo clinic, MN
CB2BG8	Human	10µg/ml	IHC	Mayo clinic, MN

Secondary antibodies

Antibody	Species	Dilution	Application	Company
α-rabbit-cy2	Goat	1:100	IHC	Dianova
α-rabbit-cy3	Goat	1:1000	IHC	Dianova
α-rabbit-Alexa488	Goat	1:400	ICC	Dianova
α-rabbit-HRP	Goat	1:5000	IB	Dianova
α-mouse-cy2	Goat	1:100	IHC	Dianova
α-mouse-cy3	Goat	1:1000	IHC	Dianova
α-mouse-HRP	Goat	1:5000	IB	Dianova
α-Rat-HRP	Goat	1:5000	IB	Dianova
α-Human-FITC	Goat	1:100	IHC	Jackson

3.1.15   Mouse lines

HANI   NRG1 typeIII HA tagged on the N terminus (Gummert unpublished)

GIEF. BACE1 processed NRG1typeIII HA tagged on the N terminus

BACE1 knock out   (Cai et al., 2001)

BACE1 transgenic   (Willem et al., 2004)

3.2 Methods

3.2.1 Molecular cloning

3.2.1.1 Generation of chemical competent *E. coli* (XL-1 blue)

E. coli XL-1 blue culture was grown in 4 ml LB-tetracycline (10 µg/ml) medium ON at 37ºC with gentle shaking. On a next day bacterial culture was inoculated into 200 ml LB-tetracycline media and left to grow at 37ºC with gentle shaking until OD600 ~0.5. The culture was then centrifuged on 4ºC at 5000g for 10 min. After careful removal of the supernatant, bacterial pellet was washed with 80 ml "TB jap" containing 2% DMSO. After another centrifugation for 10 min at 5000g on 4ºC pellet was resuspended in 18 ml of "TB jap" containing 7% DMSO and incubated on ice for 10 min. Bacterial cells in 100µl aliquots were snap frozen and stored at -80ºC. The competence of the cells was ($4x10^7 – 1x10^8$ /µg pUC18 DNA),

3.2.1.2 Transformation of XL1 blue

Chemical competent *E.coli* (100 µl) where thawed on ice and transferred into pre cooled 2 ml safe lock tubes. 50-150 ng of plasmid DNA or typically half of the ligation mix was added without mixing in to the bacterial suspension and left on ice for 30 min. Bacteria where heat shocked for 40 sec on 42ºC and than incubated on ice for 2 min. 800µl of LB medium was added to the bacteria and they where left to shake for 45 min in the 37ºC incubator in order to develop enough antibiotic resistance. 200 µl of the bacterial suspension was plated onto the LB plates supplemented with appropriate antibiotic. Plates were incubated ON at 37ºC to grow colonies. Propagation of single bacterial clones was carried out by inoculation into 4 ml of LB medium and ON incubation at 37°C with gentle shaking.

3.2.1.3 Storage and revival of glycerol stocks

Genetically modified *E. coli* were stored as glycerol stocks (20 % glycerol (v/v)) at -80°C. For revival of the culture, 4-5 ml of LB medium with appropriate antibiotic was inoculated by bacteria from a glycerol stock picked with an autoclaved toothpick. The inoculated LB medium was incubated ON at 37°C with gentle shaking.

3.2.2 DNA isolation and purification

3.2.2.1 Small scale DNA purification "mini prep"

The small scale amounts of plasmid DNA were purified using Qiagen's "QIAprep 8 Miniprep kit" or Macherey-Nagel's "NucleoSpin Plasmid QuickPure kit". The DNA preparation is carried out by a modified 'alkaline lysis' protocol (Birnboim and Doly, 1979) followed by binding of the DNA to an anion-exchange resin under the appropriate pH and low-salt conditions and subsequent wash and elution steps.
Briefly, ON cultures in 4 ml of LB media with antibiotics were transferred into the 2 ml safe lock tubes and bacteria were pelleted by centrifugation at 8200 rpm for 5 min at RT. Plasmids were isolated from this bacterial pellet following the manufacturer's protocol. The bound plasmid DNA was eluted from the columns with 50 µl of prewarmed (50°C) ddH20.

3.2.2.2 Large scale DNA purification "maxi/midi prep"

Large scale amounts of plasmid DNA were purified using Qiagen's 'Plasmid midi kit' or Macherey-Nagel's "NucleoBond PC500 EF Maxi kit" that are based on an 'alkaline lysis' procedure (Birnboim and Doly, 1979) coupled to an anion exchange resin purification under appropriate low-salt and pH conditions. The contaminating RNAs and low-molecular weight impurities are removed by medium salt washes. The plasmid DNA is then eluted from the resin by a high-salt buffer and precipitated with isopropanol followed by several washes to remove residual salt from the elution buffer. Briefly, 1 ml of fresh ON 4 ml Bacterial culture was used to inoculate 200 ml of LB medium (with antibiotic) which was than incubated at 37°C with gentle shaking ON. Bacteria were pelleted by centrifugation at 6,000g for 20 min at 4°C (SLA-1500 rotor). Plasmids were isolated from the bacterial pellet following the manufacturer's protocol. Finally, the plasmid pellet was resuspended in ~500 µl endotoxin free ddH2O.

3.2.2.3 Preparation of mouse genomic DNA

Standard method

Mouse genomic DNA for genotyping was prepared from 5mm pieces of tail biopsy. For lysis each tail was placed in tightly closed tube with 200 µl of lysis buffer containing 180 µl of 1X MGB and 20 µl of proteinase K (10 mg/ml). Lysis was carried out ON at 52°C with vigorous shaking. Digested tails where centrifuged 5 min at 5000 rpm and proteinase K was heat inactivated by 10 min incubation at 95°C. Lysate was then centrifuged at 5000 rpm for 10 min. 1 µl of the supernatant was used in genotyping PCR reactions. Alternatively surface phase of the supernatant was diluted with ddH20 (1:5) and 1.5-2 µl of this diluted DNA was used in the genotyping PCR reaction.

Preparation of a highly clean mouse genomic DNA

To obtain higher purity of the genomic DNA, preparation was done with Invitek's "Invisorb Spin Tissue Mini Kit", combining cell lysis with column purification. Briefly, mouse tail or brain tissue was digested with proteinase K in lysis buffer G ON at 52°C. DNA was then purified following the manufacturer's protocol. After purification genomic DNA was eluted from the column with 100 µl pre-warmed elution buffer.

3.2.2.4 DNA extraction from agarose gels

DNA extraction from agarose gels was performed using Qiagen's"QIAquick Gel Extraction kit" or Macherey-Nagel's "NucleoSpin Extract II kit". The principle of the gel extraction kit is based on the ability of DNA fragments to bind to silica-membranes under high-salt conditions at pH 7.5. Briefly, the desired DNA fragment visualized by UV light was cut out of the agarose gel and placed into a safe lock tube. DNA fragments were isolated from agarose by following the manufacturer's protocol. Finally, the DNA was eluted in 50 µl of prewarmed (50 °C) ddH2O.

3.2.2.5 DNA precipitation

To concentrate and purify the DNA sample in solution a precipitation was performed. 3M sodium acetate pH 5.2 (1/10 of the final volume) was first added to a DNA sample. After extensive mixing 2.5-3 volumes of 100% ethanol were added and the solution was mixed well once again. After incubation of 1 hour at -20 ºC precipitate was pelleted by 10 min centrifugation step at maximum speed. Pellet was washed once with 70%

ethanol and after 2 min centrifugation at maximum speed, the supernatant was removed and the pellet was left to air dry to remove any residual ethanol. Dry pellet was then resuspended in an adequate volume of ddH2O. For precipitation of small amounts of DNA a carrier substance (glycogen) was added to the DNA sample at the beginning to increase the efficiency and enable the visualization of the pellet.

3.2.2.6 Transgene DNA purification for microinjection

70 µg of pTSC vector containing the Thy1 cassette with GIEF were digested with PvuI and NotI ezymes in the appropriate NEB buffer 3 to remove the vector backbone. A small aliquot of the restriction reaction was analyzed by gel electophoresis to verify the fragment size and efficiency of the digestion. The digested transgene vector was than loaded onto a gel without ethidium bromide for elecrophoresis. After separation the transgene containing DNA fragment was cut out and extracted from the agarose gel using Qiagen's"QIAquick Gel Extraction kit". DNA was eluted of the gel extraction column with Tris- EDTA injection buffer. For further purification DNA for the injection was ethanol precipitated. After precipitation the DNA pellet was resuspended in the Tris- EDTA injection buffer to the final concentration of 30 ng/µl. 200 µl of the DNA sample together with a gel photo proof of the 40 ng of DNA fragment next to the Lambda/HindIII DNA-marker were submitted to the transgenic facility for pronuclear microinjection.

3.2.3 DNA modification and analysis

3.2.3.1 DNA amplification *in vitro* by polymerase chain reaction (PCR)

The polymerase chain reaction PCR (Mullis et al., 1986) is a method that enables *in vitro* enzymatic amplification of selected DNA sequence. The reaction is catalyzed by the DNA polymerase from the termophilic bacterium *Thermus aquaticus* (Taq Polymerase) which is stable at the melting temperature of the double stranded DNA and has an optimal activity at 72 ºC. Template sequence for amplification is defined with primers, single stranded oligonucleotides that complementary bind to the sense and antisense strand on the opposite ends of the template. A PCR amplification is performed in a thermocycler (Thermocycler T3, Biometra) through multiple repetitions of the three step PCR cycle. In the first phase of PCR double stranded DNA template is denatured at 95ºC. In the second step (variable temperature) primers anneal to the complementary sequences of the template DNA. Finally each strand of the template is replicated by elongation of the primer sequence by the Taq Polymarse which adds nucleotides complemetary to the template.

Standard PCR reaction mix for the RedTaq polymerase (Sigma):
1 µl   DNA (100 pg-100 ng)
1 µ   sense primer (10 pM)
1 µl   antisense primer (10 pM)
2 µl   dNTP mix (2 mM)
2 µl   10x RedTaq buffer
1 µl   RedTaq polymerase (1 U/µl)
1 2µl   ddH2O

Taq Polymerase introduces about 0.8 mismatches per 1 kb per amplification cycle. To avoid a PCR induced mutagenesis, genetic constructs were amplified with the DNA

proofreading EasyA high fidelity polymerase with 3'-5' exonuclease activity. Additionally number of cycles in PCR reaction was lowered.

3.2.3.2 DNA restriction

Restriction digest of DNA is carried out by the restriction endonucleases. These enzymes recognize specific, mostly palindromic sequences of dsDNA, 4-8 bp long and cut dsDNA leaving sticky or blunt ends. The dsDNA with 5' and 3' sticky ends can be ligated to another DNA fragment cut by the same or compatible restriction enzymes. This feature makes them a powerful cloning tool. Moreover, DNA sequence identity can be determined by the specific pattern of endonuclease fragmentation. For analytical digests, in typically 20 µl digestion reaction, ~500ng of DNA was incubated at 3 ºC with 1-10 units of an enzyme in optimal buffer condition and addition of BSA. Preparative digests for cloning were scaled up proportionally. Restriction enzymes can be inactivated by incubation at 65°C for 20 min. Gel extraction of the digested fragments normally removes enzymes from the final DNA sample.

3.2.3.3 Dephosphorilation of the restriction digested plasmid DNA

To prevent the re-ligation of restriction digested vector DNA prepared for cloning, 5'-phosphoryl groups where removed by calf intestinal alkaline phosphatase (CIP). To remove phosphoryl groups 1-2 U of CIP were added to a restriction digested DNA and the reaction volume was adjusted to obtain a 1 time concentration of dephosphorilation buffer (provided as 10x concentrate). Reaction mix was incubated at 37ºC for 30min. CIP was eliminated from the sample by subsequent gel extraction.

3.2.3.4 DNA ligation

The bacteriophage T4 'DNA ligase' was used to catalyze the formation of phosphodiester bonds between 3'-hydroxyl and 5'-phosphoryl groups of the two restriction digested DNA fragments. Ligation reaction was set in the final volume of 10-15 µl and it contained 3U of T4 ligase, optimal buffer conditions and vector-insert DNA in a 1 to 3 ratio. The ligation is carried out ON at 4°C and typically half of the ligation reaction volume was used for transformation.

3.2.3.5 Gateway cloning

Gateway® Cloning Technology (Invitrogen) is based on site-specific recombination between chromosomes of Bacteriophage λ and *E. coli* catalyzed by Int (integrase) and IHF (Integration Host Factor). Detailed description of the system can be found online in the Invitrogen's product manual book. Tagged NRG1 constructs were efficiently cloned into the vector for Lentiviral expression using this method. PCR amplified NRG1 constructs flanked by attB1 and attB2 sites were cloned into the pDONR vector carrying attP1 and attP2 sites in a so called "BP reaction" as follows:

3 µl   attB-PCR product (PEG precipitated 10-100 ng)
1 µl   pDONR207 (100 ng)
1 µl   BP clonase II

After 2 hours of incubation on RT 5 µl of the reaction were used to transform XL1 blue competent cells.

Selected pDONR207 clones with integrated NRG1 constructs now flanked by attL sites were sequenced and used as an "entry clones" (pENTR) to integrate NRG1 constructs in to the final Lentiviral expression vector containing attR sites in so called "LR reaction":

1 μl pENTR   (~100 ng/μl) 1 μl
1 μl pLenti6.2/V5DEST   (60ng/μl) 1 μl
0.5 μl   LR clonase II

The reaction was incubated ON at RT and on the next day enzymes were inactivated with 1 μl Proteinase K 10 min at 37ºC followed by 5 min inactivation at 95ºC.

2.5 μl reaction were used for transformation and positive clones were inoculated into the LB medium with ampicillin for ON cultures.

3.2.3.6 Agarose gel electorphoresis for the size separation of DNA fragments

For the separation of DNA fragments 1% to 2% agarose gels with ethidiumbromide were used. Gels were placed into the electrophoresis chambers filled with 1xTAE buffer so that the gel surface was covered by buffer and wells were filled. Standard DNA marker (100bp or 1kb ladder) and DNA samples in sample buffer were loaded into the wells. After loading, the chamber was connected to a power supply and gel was run until the desired fragment separation was achieved. For documentation, snapshots of UV-trans-illuminated gels were taken.

3.2.3.7 Measurement of the DNA concentration and purity

DNA concentration and purity was determined with UV spectrophotometer (Biophotometer, Ependorf). Concentration of a substance in aqueous solution is proportional to its absorption according to the Lambert-Beer law. Concentration of DNA in a solution can be determined by absorbance at 260 nm and 320 nm. DNA has absorption maximum at 260nm so the absorbance at 260 nm (A_{260}) corresponds to the amount of DNA in the solution. Absorbance measurement at 320 nm (A_{320}) provides a general measurement of the turbidity of the sample and is normally substracted from the A_{260} value as a background reading for the calculation of DNA concentration. To determine a protein contamination of the sample absorbance is measured at 280 nm (A_{280}). Phenol and guanidium salts contaminations are detected by absorbance measurement at 230 nm (A_{230}).

To determine the concentration of the DNA in the solution, DNA was diluted 1:50 in 100 μl final volume and the absorbance was measured at 230 nm, 260 nm, 280 nm and 320 nm. DNA concentration was calculated from the formula

$$(μg/ml) = (A_{260} - A_{320}) × F × V$$

F- multiplication factor (50 for DNA)
V- dilution factor

Purity of a sample was estimated from a ratios A_{260}/A_{280} and A_{260}/A_{230}. A good quality DNA sample should have an A_{260}/A_{280} ratio of 1.7–2.0 and an A_{260}/A_{230} ratio of greater than 1.5. For an accurate measurement, the A_{260} value must lie between 0.1 and 1.

3.2.3.8 DNA sequencing

DNA samples were sequenced at the sequencing facility of the Max Planck Institute of Experimental Medicine. 16 μl of DNA samples (100 ng/μl) diluted in ddH2O and sequencing primer information were submitted for sequencing and obtained sequencing data was analyzed using DNAStar (Edit Seq) software package and BLAST at 'National Centre for Biotechnology Information' (NCBI) (http://www.ncbi.nlm.nih.gov/blast/Blast.cgi). Sequences were also verified on public domain databases such as ENSEMBL (http://www.ensembl.org).

3.2.3.9   Primer design

All primers are designed manually based on the template sequence information using the DNAStar (EditSeq) software, pDRAW 32 software, BLAST at NCBI, and oligocalculator (http://www.pitt.edu/~rsup/OligoCalc.html). They where designed to have at least 20 bp overlap with the template sequence, and the melting temperature ~60ºC.

3.2.4   RNA isolation and analysis

3.2.4.1   RNA isolation ('RNeasy mini prep')

Small scale RNA isolation from animal tissue was performed using "Qiagen's RNeasy Mini Prep" kit. The kit is based on a selective binding of RNAs bigger than 200 bases to a silica-gel based membrane under high-salt conditions, which excludes binding of 5S, 5.8S and tRNAs. RNA isolation and purification was carried out following the manufacturer's instructions.

Briefly, frozen (-80ºC) spinal cord or brain tissue was transferred into the RLT buffer and immediately homogenized with a Ultra-Turrax T8 for 30 sec. After addition of ethanol for optimal binding, the homogenate was applied to the RNeasy mini column where the RNA sample was treated with DNase, washed from the contaminants and finally eluted with 2 times 50 μl RNase free ddH2O.

3.2.4.2   RNA precipitation

To concentrate RNA sample a precipitation was performed. 1 μl of glycogen carrier was added to the RNA sample and mixed. In the following step 3 M sodium acetate pH 5.2 (1/10 of the final volume) was added to the sample. After mixing by pipeting, 3 volumes of 100% ethanol were added and the solution was mixed well once again. After incubation of 1 hour at -20ºC precipitate was pelleted by 10 min centrifugation step at maximum speed. The pellet was washed once with 200 μl of 80% ethanol and after 2 min centrifugation at maximum speed, the supernatant was removed and the pellet was left to air dry to remove any residual ethanol. A dry pellet was then resuspended in an adequate volume of RNase free ddH2O.

3.2.4.3   cDNA synthesis

In order to analyze specific RNA expression profile, the RNA repertoire isolated from mouse tissue was converted into the more stable complementary single stranded DNA (cDNA) library. First-strand cDNA is synthesized in a reverse transcription reaction catalyzed by RNA dependent DNA polymerase SuperScript III at 55ºC.

cDNA synthesis protocol:

X μl   RNA (500ng total)
4 μl   primers (random nonamers 25pmol/μl)
Add RNAse free ddH2O to a final volume of 13μl

To co-precipitate RNA and primers, the mixture was incubated for 10 min at 70ºC and 2 min on ice.

Afterwards the following premix was added to the reaction:

4 μl   5x first strand buffer
1 μl   dNTP's (10 mM)
1 μl   DDT (100 mM)
1 μl   SuperScript III reverse transcriptase (200 U/μl)

The final 20µl reaction mixture was incubated in a thermocycler under following settings:

25 ℃   10 min
50 ℃   30 min
55 ℃   30 min
70 ℃   15 min
4 ℃   1 min

Synthesized cDNA was diluted 5 times with ddH2O.

3.2.4.4   Quantitative real time PCR (qRT-PCR)

QRT-PCR was performed using Light Cycler 480 (Roche) and SYBR Green Master Mix according to the Manufacturer (Applied Biosystems). Assay for the gene expression analysis contained 5 µl of SYBR Green Master Mix, 2 ng of cDNA, 1 pM of primer pairs and ddH20 to the final volume of 10.2 µl. All reactions were performed in quadruplicates. PCR reaction was carried out under following temperature conditions 60 for 1 min, 95 for 15 sec [45 cycles]. Analysis of the measurements was done with LC480 software. Results were displayed as histograms of relative gene expression with respect to the β-actin housekeeping gene.

3.2.5 Protein biochemistry methods

3.2.5.1   Preparation of protein lysates from cell cultures

To acquire protein material for the subsequent WB analysis DRG-Schwann cells co-cultures were lysed in RIPA buffer. Briefly, 12-well plates with cultures were transferred onto ice. Coverslips with cells were washed 2 times with PBS, 50 µl of RIPA buffer was applied and cells were scraped from the coverslips with the pipette tip. Scraped cells from 6-8 coverslips were pooled into a safe lock tube and homogenized for 1 min with the Ultra-Turrax T8. The homogenized material was left on ice for 15 min to lyse. To pellet the undigested material, cell lysates were centrifuged for 20 min on 4ºC at maximum speed. The supernatant containing the soluble proteins was transferred into a new tube and kept at –20ºC until use. The pellet containing the cell debris and unsolubilised material was also kept and stored at –20ºC.

Protein lysates from transfected cells were prepared from 90% confluent 6 cm plates 24 hours post transfection. Briefly, cells were washed on ice 2 times with PBS, 150 to 250 µl of RIPA buffer was added and the cells were scraped with a rubber cell scraper. After transfer into a safe lock tube cells were left to lyse on ice for 15 min. Following this step protocol does not differ from the DRG culture protein lysates preparation.

3.2.5.2   Preparation of protein lysates from animal tissue

To prepare proteins out of frozen mouse nervous system tissue (-80ºC) spinal cords and sciatic nerves were homogenized in 600 µl and 200 µl RIPA buffer, respectively. Homogenization was carried on for 1 min with the Ultra-Turrax T8 or with the Precylis homogenizer (5000rpm 1x10sec). The homogenized material was than lysed on ice for 20 min. Lysed tissue was then centrifuged at 4ºC for 30 min at maximum speed. The supernatant containing the soluble proteins was transferred into a new tube and kept at –20ºC until use. Pellets were also kept and stored at –20ºC.

3.2.5.3 Protein concentration measurement by the Lowry assay

The protein concentration was measured using the Bio-Rad DC Protein Assay kit. The assay was performed in a 96-well plate (flat bottom) according to the manufacturer's "micro plate" assay protocol and absorbance was measured at 650 nm with a microtitre plate reader. The working principal of the kit is similar to the Lowry assay (Lowry et al., 1951). The two step assay is based on the reaction between protein and copper in an alkaline medium, followed by the reduction of the Folin reagent that produces several reduced species of a characteristic blue color with a maximum absorbance at 750 nm. The color development is primarily due to the oxidation of the amino acids tyrosine and tryptophan, and to a lesser extent, cystine, cysteine, and histidine.

3.2.5.4 Preparation of the protein samples for SDS electrophoresis

For the separation by SDS polyacrilamide electrophoresis protein samples were denatured. Portions of the protein lysates containing 15-40 μg of protein were mixed with 5x sample buffer and 1% ß-mercaptoethanol in a 1.5 ml safe lock tube. Volumes of the samples were equalized with RIPA buffer and samples were than incubated at 95ºC for 10 min.

3.2.5.5 Discontinuous SDS polyacrilamide electrophoresis

The size separation of the proteins from a sample was performed using the discontinuous SDS polyacrylamide gel electrophoresis (SDS-PAGE) described by Laemmli (Laemmli, 1970). The glass plates and the 0.75 mm or 1.75 mm spacer plates were assembled according to the Bio-Rad instructions. The separating acrylamid gel solution of the desired percentage was poured between the glass plates and separated from the air by a layer of ddH20 saturated with isobutyl alcohol. The gel was left to polymerize for 30 min at room temperature. After rinsing the isobutyl alcohol twice with ddH2O, the stacking gel solution was added. A Teflon comb (10 or 15 teeth) was immediately inserted into the stacking gel solution and the gel was left to polymerize for 45 min. Polymerized gels were kept up to a week at 4ºC. The chamber for electrophoresis (mini protean 3) was assembled according to the the Bio-Rad directions and filled with the electrophoresis buffer. The comb was carefully removed and the wells were washed with electrophoresis buffer. 10-40 μg of denatured protein samples and 10 μl of prestained protein marker were loaded onto the gel. The chamber was connected to a power supply and the gel was run under a constant current protocol (10 mA/0.75 mm gel) until the tracking dye reached the end of the gel. The gel was than carefully removed and it was proceeded with Coomasie staining or Western Blotting.

3.2.5.6 Coomassie staining

To verify the protein transfer, the SDS-PAGE gels were stained with Comassie solution. Briefly, the gel covered with Coomassie solution was coocked in a microwave for 30 sec. Than the gel was washed with ddH2O at room temperature with gentle shaking until the protein bands were clearly visible.

3.2.5.7 Western Blotting

Electrophoretic transfer

For the immunodetection proteins resolved by size on SDS-gel were transferred onto a PVDF membrane by electrophoresis, as originally described with modification (Towbin et al., 1979). PVDF membranes were activated for 15 sec in 100% methanol and placed into transfer buffer. Blotting pads, and the Whatman paper were pre-soaked in transfer buffer and the blotting sandwich was assembled as on the following scheme.
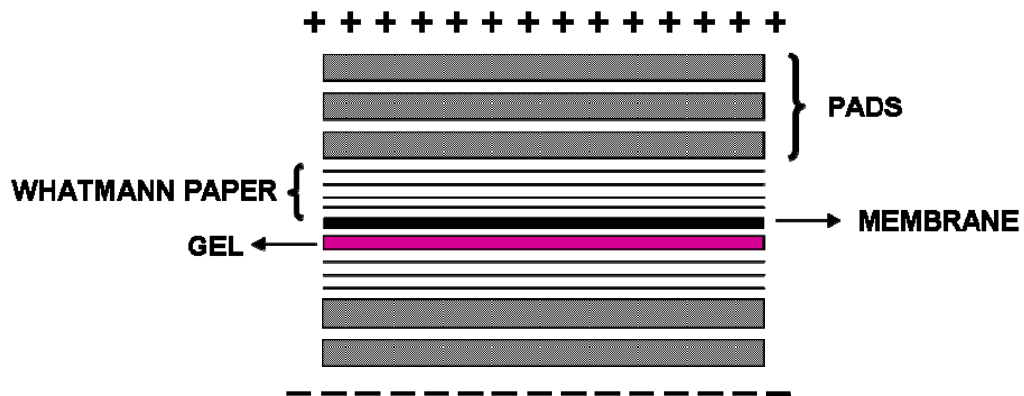
The protein transfer was performed using Invitrogen's chamber system(Western Blot chamber XCell II, Invitrogen) under a constant voltage of 38 V and a maximum current of 275 mA for a 1.5 mm gel and for 70 min at 4ºC.

Immunological detection of proteins on PVDF membranes

Membranes were first blocked for 30 min at room temperature in blocking buffer and than placed into a 50 ml falcon with 3 ml of the primary antibody diluted in blocking buffer. Incubation was carried out ON at 4ºC with constant rotation. After four 10 min washes in TBST, the membrane was incubated with the HRP-conjugated secondary antibody diluted in blocking buffer for 1 hr at RT. The membrane was again washed with TBST four times 10 min, followed by 1 min incubation with the Enhanced Chemiluminescence Detection (ECL) solution. The membrane was than placed into a plastic transparent foil brief and the ECL photographic film was exposed to the membrane to visualize the labeled proteins. The exposure time varied between 5 sec and 10 min depending on the signal intensity. The films were then developed in a KODAK X-OMAT developer.

To reprobe the same membrane with a different antibody, the membrane was incubated in a stripping buffer for 1 hr at 60°C with vigorous shaking. After washing in TBST and blocking, the membrane was ready for the antibody incubation.

3.2.6 Cell cultures

Handling of the cell culture material and preparation of the media and solutions were performed under sterile conditions in the laminar flow tissue culture hood.

3.2.6.1 Maintenance of the cell lines

All eukaryotic cell lines were grown on 10 -15 cm cell culture dishes with an appropriate medium in a humidified incubator (Hera Cell 150, Thermo Scientific) at 37°C and 5% CO2.

Poly-L-Lysin (PLL) coating of cell culture dishes

Cell lines adhere better when grown on Poly-L-Lysin (Invitrogen) substrate. The surface of the cell culture dish was covered with a thin layer of PLL in ddH2O (0.02 mg/ml) and left for 20 min at room temperature. Dishes were washed twice with the sterile ddH2O and left to dry. Dry PLL coated dishes were kept at 4ºC up to one month. PC12 cells were always plated onto PLL coated dishes. HEK 293T cells were plated on PLL for the transfection assays.

Passaging of the cell lines

After reaching 90% of confluence cells were trypsinized and transferred onto the new culture dish. Briefly, confluent cells were washed with sterile PBS and 1 ml of 0.25% Trypsin-EDTA was applied to detach the cells. After 1-2 min incubation, the trypsin was inactivated by the addition of 10 ml of full cell culture medium. Trypsinized cells were washed off the dish surface by pipetting and transferred than into a 50 ml falcon tube. Cells were pelleted by a 5 min centrifugation at 800g and the supernatant was discarded. The cell pellet was than resuspended in 5 ml of medium and triturated with a 1 ml pipette to achieve a better single cell separation. Variable amounts of cell suspension were than plated onto the new dish with medium.

Determination of the cell number in a cell suspension

To determine cell number in a cell suspension 10 µl of the cell suspension was pipetted on to a Neubauer counting chamber. Cells from the one quadrant of 4 different fields were counted. Number of cells was determined according to the formula: cells/ml = cells counted in 4 quadrants x 4 x 10000

Generation of frozen eukaryotic cell lines stocks

Cells were grown until a 90% confluence on a 15 cm dish (approximately $20x10^6$ cells). After trypsinization cells were resuspended in 5 ml of ice cold growth medium. Than 500 µl of cell suspension were transferred into a previously prepared and labeled cryovial with 500 µl of 2x ice cold freezing media. To mix the cells, the cryovial was gently inverted a couple of times. Cells were frozen on –20ºC for two hours. They were kept at –80ºC for 6 to 12 hours before placing into liquid nitrogen for long term storage. Typically cells before passage 10 were used to make frozen stocks.

Revival of frozen eukaryotic cell lines stocks

A cell culture dish (10 cm) with warm growth medium was prepared. The frozen stock of cells was taken out of the liquid nitrogen and placed onto dry ice. The cryovial with cells was placed into a 37ºC water bath to heat and loosen the frozen stock from the cryovial walls. Still frozen cells were quickly released from the cryovial into the previously prepared plate. After two passages the cell were ready for experiments.

3.2.6.2 Cell lines transfections

Transfection by lipofection method was used to introduce plasmid DNA in to the mammalian cells. For the transfections cells were plated in a chosen setting depending on the experimental purpose:

Cell line	ICC/24 well plate	WB/6 cm culture dish
PC12	250 000	800 000
HEK 293T	100 000	500 000
COS7	250 000	600 000

Cells were left to grow until a 50-70% confluence and transfected using Lipofectamine 2000 Transfection Reagent (Invitrogen) according to the adjusted manufacturer recommendations. For the 24 well plate 50 µl of OptiMEM medium were mixed with 500 ng of plasmid DNA. 1 µl of Lipofectamine was mixed with another 50 µl of OptiMEM. The OptiMEM with diluted DNA and Lipofectamine were than mixed and left for 20 min to form complexes. Growth medium on cells was replaced with 400 µl fresh medium and 100 µl of OptiMEM with formed DNA- Lipofectamine complexes were added. For 6 cm dishes volumes were scaled up to 500 µl OptiMEM, 2 µg DNA and 4 µl of Lipofectamine. 1 ml of OptiMEM with formed DNA-Lipofectamin complexes was - in this case- added to the cells with 1 ml of freshly changed full growth medium.

3.2.6.3 Split Tev assay

Two cell Split Tev assay was performed as described in (Wehr et al., 2006; Wehr et al., 2008). Briefly, NRG1 constructs were transfected into PC12 cells. This transfected cell population was mixed with the PC12 cell population expressing ErbB2 receptor and PI3 kinase proteins coupled to the components of the Split Tev system. NRG1 mediated ErbB receptor dimerization and recruitment of PI3 kinase was detected by measurement of the luciferease reporter gene activation. The results were displayed in relative luminescence units (RLUs).

3.2.6.4 Dorsal Root Ganglion (DRG) neuron-Schwann cell co-culture

Dorsal Root Ganglion (DRG) neurons-Schwann cells co-culture was used to study myelination *in vitro*.

3.2.6.4.1 Preparation of the culture

DRG neurons-Schwann cells co-culture is prepared from dissected E13 mouse embryos DRG's. Thirteen days pregnant mouse (the plug day is counted as E0) is sacrificed and the uterus with embryos was carefully removed from the abdomen and put into a 10 cm dish with L15 medium. Embryos were taken out of the uterus and transferred into the new 10 cm dish with cold L15. Embryos were kept on ice until the end of the preparation. One by one, embryos were dissected under the binocular in a 6 cm dish using sterilized #5 Dumont medical biology forceps. After decapitation and removal of the abdominal organs, the ventral side of the spinal column was exposed. DRG's were extracted attached to the spinal cord by carefully pulling the spinal cord out of the ventrally open spinal column. All the spinal cords with attached DRG's were collected into a 6 cm dish with L15 medium and kept on ice. DRG's were than plucked of the spinal cord and spinal cords were discarded. Extracted DRG's in L15 medium were transferred into a 15 ml Falcon tube with a disposable plastic pipette. DRG's were

pelleted by a 5 min centrifugation at 700 g and the medium was discarded. After addition of 1 ml of 0.25% trypsin, DRG's were placed in a water bath at 37ºC and digested for 45 min. Trypsinization was stopped by adding 1.5 ml FBS and 3 ml L15 medium. To obtain a single cell suspension, DRG's were triturated with a 5 ml pipette and subsequently with a glass Pasteur pipette (tip reduced by flame polishing). The single cell suspension was centrifuged for 10 min at 800 g, the supernatant removed and cells resuspended in ~ 1 ml of growth medium. Cells number was determined by pipetting 10 µl of the cell suspension into a Neubauer counting chamber, and 75000 cells in 50 µl medium were gently placed in the middle of collagen coated coverslip (18 mm) in a 12 well plate. In this way a small cell culture island containing neurons, Schwann cells and fibroblast is formed on each coverslip. Cultures were placed into the incubator over night to settle. On the next day, after cells had attached, wells were carefully filled with 1 ml of DRG growth medium. Cultures were kept in the incubator without changing the medium for a week. During this week period DRG neurons processes extend to form a network. Proliferated Schwann cells aligning the processes are visible and ready to myelinate once permissive conditions are provided.

3.2.6.4.2 Myelination induction of the culture

Myelination of the DRG neurons by Schwann cells was achieved by addition of ascorbic acid (50 ng/ml final concentration) to the full growth medium. Under these conditions, Schwann cells can form a basal lamina and myelin segments around extended axons of DRG neurons. Ascorbic acid powder is diluted in ddH2O to a 1000x (5 mg/ml) stock. Aliquots of ascorbic acid stocks were frozen and freshly added to the growth medium that is now changed every second day. The extent of *in vitro* myelination was analyzed 7 or 14 days post myelination.

3.2.6.4.3 Treatment of the culture with proteases inhibitors

DRG cultures were treated with 0.5-2 µM ß secretase inhibitor IV and 1 µM ADAM's protease inhibitor GM6001. Proteases inhibitors treatment started on the day 5 post preparation. The inhibitors were added freshly, every time myelinating media has been changed. Effects of the inhibitors on mmyelination were analyzed 7 or 14 days post myelination induction.

3.2.6.4.4 Viral infection of the DRG neurons

DRG neurons were prepared from E14 mouse embryos as described previously and selected by cycles of treatment with FUDR as described previously (Taveggia et al., 2005). Lentivirus expressing HANI and GIEF NRG1 variants was generated using ViraPower Lentiviral Expression System (Invitrogen) according to manufacturer's protocol. For infection DRG neurons cultures were incubated with viral supernatants in DRG culture media for 16 hours. Infection was confirmed by HA staining 11 days post-infection. Rat Sc were prepared as described (Taveggia et al., 2005) and added to the established DRG neuron culture. Myelination was initiated by addition of ascorbic acid to the media.

3.2.6.4.5 CNS neurons-oligodendrocytes co-culture

Primary cultures of rat oligodendrocytes were prepared as described previously (Simons et al., 2000). After shaking, cells were plated in DMEM containing B27 supplement, 1% horse serum, L-thyroxine, tri-iodothyronine, glutamine, pen/strep, pyruvate, and bicarbonate. For neuronal culture, the mixed brain cultures were

prepared from E16 mice and cultivated for 2 weeks at a density of 50000 cells/cm^2 on poly-L-lysine–coated glass coverslips. Co-cultures of neurons and oligodendrocytes were prepared by adding primary oligodendrocytes to already 2 week cultivated mixed brain cultures. After 5 days, the cocultures were fixed and stained to monitor the myelination process.

3.2.7 Immunocytochemistry

3.2.7.1 Immunostaining of transfected cell lines

Before fixing the cells for immunostaining, the medium was removed and cells were washed once with PBS. For fixation, cells were incubated with 4% PFA for 10 min at room temperature. Cells were than washed 3x with PBS and permeablized for 1 min in permeabilization buffer followed by a incubation with blocking buffer for 1 hour at RT. Coverslips were than transferred in to a box with parafilm and 100 µl of primary antibody dilution in blocking buffer was applied onto a coverslip. The incubation was carried on in a humidified chamber at 4ºC ON. On the next day, coverslips were washed three times with PBS, and 100 µl of the fluorescent secondary antibody in blocking buffer were applied. After an incubation period of 1 hour at RT, the coverslips were washed three times with PBS and the nuclear dye DAPI diluted in PBS was applied for 10 min. Coverslips were washed again 2x with PBS, dipped shortly into ddH2O and mounted with AquaPolymount.

To stain the extracellular surface epitopes and prevent the antibody from entering intracellular spaces a "Live staining" protocol was applied. The plate with cells was placed on ice, medium was removed and ice cold DMEM was added for 3 min to further cool the cells. Primary antibody dissolved in cold 3% HS in DMEM was gently added and incubated for 15 min on ice. Cells were extremely carefully washed once with PBS and finally fixed with 4% PFA for 10 min. Coverslips were washed 3x with PBS and fluorescent secondary antibody diluted in PBS was applied for 45 min on RT. After 3x washing with PBS, DAPI nuclear dye diluted in PBS was applied for 10 min. Coverslips were washed again 2x with PBS dipped shortly into ddH2O and mounted with AquaPolymount

3.2.7.2 Immunostaining of DRG neurons-Schwann cells co-culture

To fix the cells for immunostaining, medium was removed, wells were washed once with PBS and the cells were incubated with 4% PFA for 10 min at RT. Cells were washed 3x with PBS and permeablized for 5 min at -20ºC with precooled methanol. Cells were washed 3x with PBS and blocked in 3% BSA in PBS for 1 hour at RT. Coverslips were than transferred into a box with parafilm and 150 µl of primary antibody in blocking buffer were applied onto the coverslip. The incubation was carried on in a humidified chamber ON at RT. Following steps do not differ from the protocol for immunostaining of the cell lines.

3.2.8 Histology and immunohistochemistry

3.2.8.1 Perfusion fixation of mouse tissue for histology

To anesthetize mice 2.5% Avertine with a dose of 0.2 ml per 10 g of body weight were injected intraperitonealy. Once the mouse was anestesized it was fixed onto a Styrofoam board ventral side up and a piece of the tail was taken for the confirmation

of the genotype. The abdomen was opened and the cuts were made through the diaphragm and laterally of the rib cage to expose the heart. A 27 gauge needle butterfly connected to a peristaltic pump was inserted into the left ventricle and the right atrium was open by a small cut to ensure the perfusion flow. With help of the peristaltic pump, the mouse was first perfused with warm HBSS to clear the blood out of the circulatory system. The mouse was than perfused with 20-40 ml of the appropriate cold fixative, depending on the type of subsequent histological analysis (see histology fixatives in the material section). After the perfusion, fixed spinal cord, dorsal root ganglia and sciatic nerves were dissected and placed in cold perfusion fixative for post fixation. Tissue was kept in fixative at 4ºC until embedding. Tissue for paraffin embedding was further processed after the ON postfixation. Tissue intended for epon embedding and EM analysis can be kept longer in perfusion fixative but for very long storage should be transferred into 1% PFA. Tissue for immuno-EM should be transferred from the perfusion fixative into 1% PFA after no longer than 4 hours for ON postfixation.

3.2.8.2 Procedures for tissue embedding

Paraffin embedding

Before the embedding process, the tissue was washed with PBS. Spinal cords were cut into 5 - 6 pieces and put into the plastic perforated chambers. Sciatic nerves and DRG's were embedded in 2% agar blocks and also placed in plastic perforated chambers. Chambers with tissue were properly labeled and placed into the automated system (HMP 110, MICROM) for dehydration and paraplast impregnation.
The tissue was dehydrated by an incubation in an ascending row of ethanol dilutions at room temperature:

50% Ethanol	1 hour
70% Ethanol	2x 1 hour
96% Ethanol	2x 1 hour
100% Ethanol	2x 1 hour
Isopropanol	1 hour
Xylene	2x 2 hours

After dehydration, the tissue was impregnated with paraffin by a 2x 2 hours incubation at 60ºC. The tissue was than placed in the molds with hot paraffin and filled molds were left to firm on a cold plate. Labeled paraffin blocks were kept at room temperature until cutting.

Cryoembedding

Perfusion fixed tissue was placed into a block of Shandon cryomatrix embedding medium and immediately frozen on dry ice until the block turned white. Frozen blocks were kept at – 80ºC until use.

Agarose embedding

Fresh spinal cord tissue was embedded in 3% low melting point agarose on the surface of filter paper.

Epon embedding

Tissue for subsequent EM imaging was embedded using an automated system (EM-TP, Leica) in a multi step process involving osmification, dehydration and epon impregnation.
Epon mix was prepared 30 min before embedding in the following way:

171.3 g   Glycidether 100
115 g   DDSA (Dodecenyl succinic anhydride)
89 g   MNA (Methyl nadic anhydride)
Mix using magnet stirrer for 10 min and than add
6.5 ml   DMP-30
Mix using magnet stirrer for 20 min

Before the embedding, tissue was washed from the fixative with 0.1 M phosphate buffer and placed into the plastic chambers. Chambers were than placed into the machine for embedding and tissue was processed using following set up:

Solution	Incubation time	Temperature
Phosphate buffer	3 times 10 min	4ºC
2% OsO4	4 hours	4ºC
ddH20	3 times 10 min	4ºC
30% Ethanol	20 min	4ºC
50% Ethanol	20 min	4ºC
70% Ethanol	20 min	4ºC
90% Ethanol	20 min	4ºC
100% Ethanol	4 times 10 min	4ºC
Propylenoxid	3 times10 min	RT
Propylenoxid/Epon 2:1	2 hours	RT
Propylenoxid/Epon 1:1	2 hours	RT
Propylenoxid/Epon 1:2	4 hours	RT
Epon	4 hours	RT

Tissue was than placed into the labeled Epon filled molds and left ON at 60ºC for Epon polymerization.

3.2.8.3 Tissue sectioning

Paraffin embedded tissue was cut using a microtome (HM 400, MICROM). A cooled paraffin block was cut into 5 µm thick sections. Sections were placed into the 42ºC water bath to flatten the tissue. Floating sections were picked with positively charged glass slides and left to dry over night at 37ºC.

Epon embedded tissue was cut using a microtome (Ultracut S, Leica). Semi-thin sections 0.5 µm were cut with a diamante knife (Diatome Histo 45º) and ultra-thin sections of 50 nm for electron microscopy with (Diatome Ultra 45º). Each cut sections was released from the block into a water filled pool on a knife holder. For light microscopy, floating 0.5 µm sections were picked with a glass stick, into the water puddle on a glass slide, dried on a hot plate at 60ºC and stained. For electron

microscopy 50 nm sections were placed on a double sized slot grid (2mm-1mm, AGAR) coated with Formvar polyvinyl and contrasted.

Cryo sections were made using a cryostat (Leica). Shandon Cryomatrix embedded tissue was transferred from – 80ºC in to the cryostat (-18ºC to -20ºC) and after 5 min of temperature equilibration cut into 10-15 µm sections. Sections were put on super frost glass slides and allowed to dry on RT for at least 30 min. Sections were stored at – 80ºC until use.

For floating tissue slices staining 225 µm thick cross or sagital sections were cut out of the agarose embedded spinal cord using the McIlwain tissue chopper. Individual tissue slices were separated immediately under the binocular and transferred into a 24 well plate containing cold E/H for staining.

3.2.8.4 Hematoxylin- Eosin (HE) staining

Hematoxylin-Eosin (HE) staining is a widely used histological staining method that gives information of the overall tissue structure. Cells are easily differentiated with this type of staining as hematoxylin stains basophilic nuclei in dark purple and eosin stains eosinophilic cytoplasm pink. For HE staining, paraffin sections were first deparaffinised by incubation of the slides two times for 10 min in Xylol and 1x 10 min in Xylol/Isopropanol (1:1), followed by a rehydratation with 5 min incubation steps in the descending ethanol dilutions (100%, 90%, 70%, and 50%). After 5 min wash in ddH2O, sections were stained with 0.1% Haematoxylin for 5 min and washed with ddH2O.The dark purple color was differentiated by a quick dipp in HCl-Alcohol solution. To stop the differentiation process and properly develop the color, sections were incubated for 5 min in Scott's solution. After a short rinse in ddH2O they were counterstained with 0.1% Eosin for 3-5 min. The excess dye was washed of with ddH2O. Sections were dehydrated in the ascending row of ethanol dilution (50%, 70%, 90%, and 100%) by short incubations (10-30 sec) depending on the stability of the Eosin stain. Sections were then incubated for 10 min in Xylol/Isopropanol (1:1) and 2x 10 min in Xylol. Sections were mounted with the Xylol based mounting medium Eukitt.

3.2.8.5 Gallyas staining of myelin on paraffin sections

This myelin staining technique developed by Gallyas (Gallyas, 1979) is based on the binding of colloidal silver to myelin that can be than visualized by light microscopy after a particular process of physical development. Paraffin sections were deparaffinised and rehydrated as for HE stainig. After 5 min incubation in ddH2O sections were incubated with 2:1 mixture of pyridine (200 ml) and acetic acid anhydride (100 ml) for 30 min. Sections were washed three times for 10 min in ddH2O and incubated for 10 min at room temperature in the preheated (1 min in microwave at 150 W) incubation solution. Afterwards they were washed three times for 5 min in 0.5% acetic acid. Sections were then developed by incubation in a developer solution for 3-15 min and the extent of developed color was controlled under the microscope. Color development was stopped with 1% acetic acid with three incubation steps of 5 min. Finally, slides were washed properly in ddH2O. To stabilize the silver staining, slides were incubated in 2% sodium thiosulfate solution for 5 min. After two 5 min washings in ddH2O sections were dehydrated in as for HE staining (alchohol row incubations for 5 min) and mounted with Eukitt.

3.2.8.6 DAB immunostaining of the paraffin sections

DAB immunostaining is based on the enzymatic reaction of Horseradish Peroxidase (HRP) attached to a secondary antibody and the DAB substrate, which forms a stable brown precipitate that can be visualized with light microscope (Harlow and Lane, 1988). Paraffin sections with 5 µm of thickness were incubated at 60ºC for 10 min and than deparaffinized and dehydrated as for the HE staining. Sections were than incubated for 5 min in ddH2O and citrate buffer. For antigen retrieval sections were cooked for 10 min in boiling citrate buffer at 650 W in a microwave oven. During the cooking process, evaporated H2O was replenished to maintain the buffer molarity. After cooking, sections in citrate buffer were left on RT for 20 min or longer to cool down, followed by a 5 min washing step in Tris buffer with 2% milk powder. Slides with sections were mounted with plastic cover-plates for following steps of the protocol. They were first washed with Tris buffer with 2% milk powder to test if the slides were mounted properly and the pace of the flow is optimal. Endogenous peroxidases were inactivated by incubation with 100 µl of 3% hydrogen peroxide for 5 min followed by a blocking step for 20 min at RT with 100 µl of blocking buffer. Then 100 µl of the primary antibody in PBS/BSA were applied onto a slide and incubated ON at 4°C. Sections were then washed with 2% milk-powder in Tris buffer followed by an incubation with 100 µl of the biotinylated secondary antibody (Dako LSAB2, yellow bottle solution A) for 10 min at RT. After washing with 2% milk-powder in Tris buffer, 100 µl of Steptavidine conjugated to Horseradish Peroxidase (Dako LSAB2, red bottle solution B) were added and the sections were incubated for 10 min at RT. Finally sections were washed with Tris buffer. Slides were than mounted of the plastic cover slides and placed into a box for staining by 10 min incubation with 100 µl of DAB substrate solution (1ml Dako Substrate buffer with two drops of DAB). Sections were then washed with ddH2O twice for 5 min. Sections were counterstained with Haematoxylin for 30 sec and after washing once in ddH2O for 5 min, the sections were rehydrated and mounted as for the HE staining.

3.2.8.7 Fluorescent immunostaining of paraffin sections

The protocol for fluorescent immunostainig of paraffin sections does not differ from the DAB staining protocol until the steps after the antigen retrieval. After cooling down, the sections were washed 3x for 5 min with 2% milk-powder in Tris buffer. Slides were than placed into a humidified box and blocked with 150 µl of blocking buffer for 20 min at RT. After the blocking buffer was applied onto a section, the slide was covered with a piece of parafilm to equally distribute the blocking solution over the slide surface. This procedure allows application of low (as low as 100 µl) volumes of the solutions onto a slide. 100 -120 µl of primary antibody were applied after blocking, slides were covered with paraffin and incubated ON at 4°C in a humidified chamber. On the next day slides were washed with 3x for 5 min with 2% milk-powder in Tris buffer and 120 µl of the fluorescent secondary antibody and DAPI in PBS/BSA were applied. After parafilm was placed onto a slide, the incubation took place at RT for 1 hour. Sections were then washed 3 times for 5 min in Tris buffer and mounted with AquaPolymount.

3.2.8.8 Fluorescent staining of cryo sections

Slides were taken from – 80ºC and a ring with an immupen was marked around the tissue slice to allow the solution to form a puddle. Slices were than rehydrated with PBS for 5 min and permeabilised for 10 min with 0.05% saponine in PBS. Tissue was blocked with 10% GS in PBS for 20 min followed by an incubation with the primary

antibody diluted in 5% GS in PBS for 2 hours on RT. After 3x for 5 min washing with PBS, the fluorescent secondary antibody diluted in 5% GS in PBS was applied and incubated for 1 hour at RT in darkness. Slices were than washed 3x for 5 min with PBS and mounted with Vectashield containing DAPI.

3.2.8.9 Fluorescent staining of tissue slices

All incubation steps were done at 4ºC with gentle rocking to minimize the volumes required. Tissue slices were placed in a 24-well plate filled with E/H solution on ice. The tissue was incubated in 4% BSA in E/H for 30 min to 1 hour. Primary antibody diluted in 1% BSA in E/H was incubated over night. Slices were than washed with large volumes of E/H three times for 5 min. Afterwards slices were fixed with 4% PFA for 30 min and washed with PBS twice. Fluorescent secondary antibody diluted in 1% BSA in E/H was applied and incubated for 1 hour in darkness. After three washes of 5 min in PBS, slides were mounted with Vectashield containing DAPI to visualize the nuclei. Slides were imaged immediately for the best results and stored at 4ºC for several weeks.

3.2.8.10 Methylenblue-Azur II staining of semithin sections

To stain myelin on semi-sections, freshly prepared Methylenblue-Azur II working solution was applied through the syringe filter tip onto the dry slides with semi-sections on a hot plate at 60ºC. After 1 min of incubation, the Methylenblue-Azur II was washed with ddH2O and slides were left to dry. Dry slides were finally mounted with Eukit.

3.2.8.11 Tissue contrasting for electron microscopy

Grids were placed with the shiny side up on the drops and incubated in a following way
30 min   Uranyl acetate (light sensitive)
3x 1 min   ddH2O
6 min   Reynolds lead citrate
4x 1 min   ddH2O
Grids were carefully dried with a stripe of filter paper

3.2.9 Imaging

To image the processed tissue and cell culture material following microscopy equipment was utilized:

Epifluorescence upright microscope: DMRXA (Leica) with Kappa DX20 H-FW digital camera

Confocal microscope: SP2-AOBS Leica

Electon microscope: LEO EM912 Omega (Zeiss) with on-axis 2048x2048-CCD camera (Proscan)

3.2.10   Animal maintenance and handling

All mouse mutants used in this study were maintained and bred in the animal facility of the Max-Planck-Institute of Experimental Medicine. Animals were kept and handled in

compliance with animal policies of the Max-Planck-Institute of Experimental Medicine and approved by the German Federal State of Lower Saxony.

3.2.10.1 Generation of transgenic GIEF mouse

To generate GIEF transgenic mouse mutant, transgene DNA was purified as described in the methods section 3.2.2.6. DNA microinjection into mouse pronuclei (C57/Bl6N) and embryo transfer were performed at the transgenic facility of the Max -Planck-Institute of Experimental Medicine. Born animals were ear marked and tail biopsy for DNA preparation and genotyping of potential founders were taken at the age of 3-4 weeks.

3.2.10.2 Breeding of the mouse mutants

All mice mutants were bred at 8 weeks of age. To maintain and expand the mutant lines, mutant mice were bred to wt mice of the C57/Bl6N strain.

3.2.10.3 Genotyping of the mouse mutants

At the 3 weeks of age mice tail biopsy was taken. DNA for genotyping was prepared with the standard procedure. DNA of potential founders was prepared with the "Invisorb Spin Tissue Mini Kit" kit. Genotype was determined by performing genotyping PCRs with mutant specific genotyping primers described in material section 3.1.11.1.

20 µl genotyping PCR reaction:
1 µl	tail DNA
1 µ	genotyping forward primer (10 pM)
1 µl	genotyping reverse primer (10 pM)
2 µl	dNTP mix (2mM)
2 µl	10x RedTaq buffer
1 µl	RedTaq polymerase (1U/µl)
12 µl	ddH2O

PCR programs:

HANI/GIEF
1. 95ºC	3 min
2. 95ºC	45 sec
3. 58ºC	30 sec
4. 72ºC	1 min
2 to 4	35 cycles
5. 72ºC	10 min
6. 4ºC	pause

BACE ko
1. 95ºC	3 min
2. 95ºC	45 sec
3. 58ºC	1 min
4. 72ºC	1 min
2 to 4	35 cycles
5. 72ºC	10 min
6. 4ºC	pause

BACE1 tg

1. 95ºC   3 min
2. 95ºC   30 sec
3. 56ºC   30 sec
4. 72ºC   1 min
2 to 4   35 cycles
5. 72ºC   10 min
6. 4ºC   pause

3.2.10.4 Theiler's murine encephalomyelitis virus (TMEV) mediated model of MS

TMEV induced demyelinating disease is a relevant mouse model of MS because of pathological similarities including inflammation, demyelination and axonal loss (Rodriguez et al., 1987). After intracerebral injection of Daniel's strain TMEV into the susceptible SJL/J strain, mice within two weeks develop acute encephalitis followed by a progressive chronic demyelinating disease and axonal loss in the spinal cord (McGavern et al., 2000). The TMEV induced demyelination model used in this study was generated at the Mayo Clinic (Rochester, MN) animal facility, in accordance with the guidelines for use of experimental animals by the Mayo Clinic and the National Institutes of Health. SJL/J mice were infected with 200000 plaque forming units of Daniel`s strain of TMEV by a 10 μl volume intracerebral injection. Animals were used 4 months post infection.

4 RESULTS

4.1 Generation of the HA tagged NRG1 variant mimicking the BACE1 processed NRG1 type III-β1

NRG1 type III-β1 proprotein is being processed in stalk region *in vitro* by BACE1 and possibly other proteases to generate a mature membrane bound N-terminal signalling fragment containing EGF like domain (Falls, 2003; Wang et al., 2001). However detection of the N-terminal fragment of the NRG1 has been hampered due to the lack of available antibodies. The only commercial antibody (sc-348, Santa Cruise) that gives satisfactory and reliable results recognizes the cytoplasmic tail of NRG1 type III. Thus, after proteolytic cleavage of the NRG1 proproteins in the stalk region it is not possible to follow the localization and transport of N-terminal fragment. In order to perform comprehensive studies of the mature signalling fragments, detection of both fragments resulting after processing is required. In our study we have therefore used NRG1 type III-β1 termed "HANI" which is full length NRG1 modified by addition of 2 HA tags (IDYPYDVPDYASL) at the N-terminus (Fig. 3A). Introduced tag enables immunodetection of the N-terminus and creates the possibilities to study cellular localization of N-terminal NRG1 fragment as well as processing by WB. Recently BACE1 protease was implicated in processing and activation of NRG1 for the function in myelination (Willem et al., 2006). To further investigate the role of the BACE1 in activation of NRG1 we have generated the construct representing BACE1 processed NRG1 type III-β1 termed "GIEF". This construct represents N-terminal fragment of NRG1 type III-β1 resulting after cleavage by BACE1. In order to detect GIEF protein for histological and biochemical analysis it was necessary to introduce a tag. Therefore, HA tagged BACE1 processed NRG1 type III-β1, flanked by XhoI sites was PCR amplified from HANI cDNA sequence. Resulting GIEF protein is a truncated HANI protein ending with EGF-like domain flanked by GIEF amino acid sequence at the C-terminus (Hu et al., 2008) mimicking BACE1 cleavage (Fig. 3A).
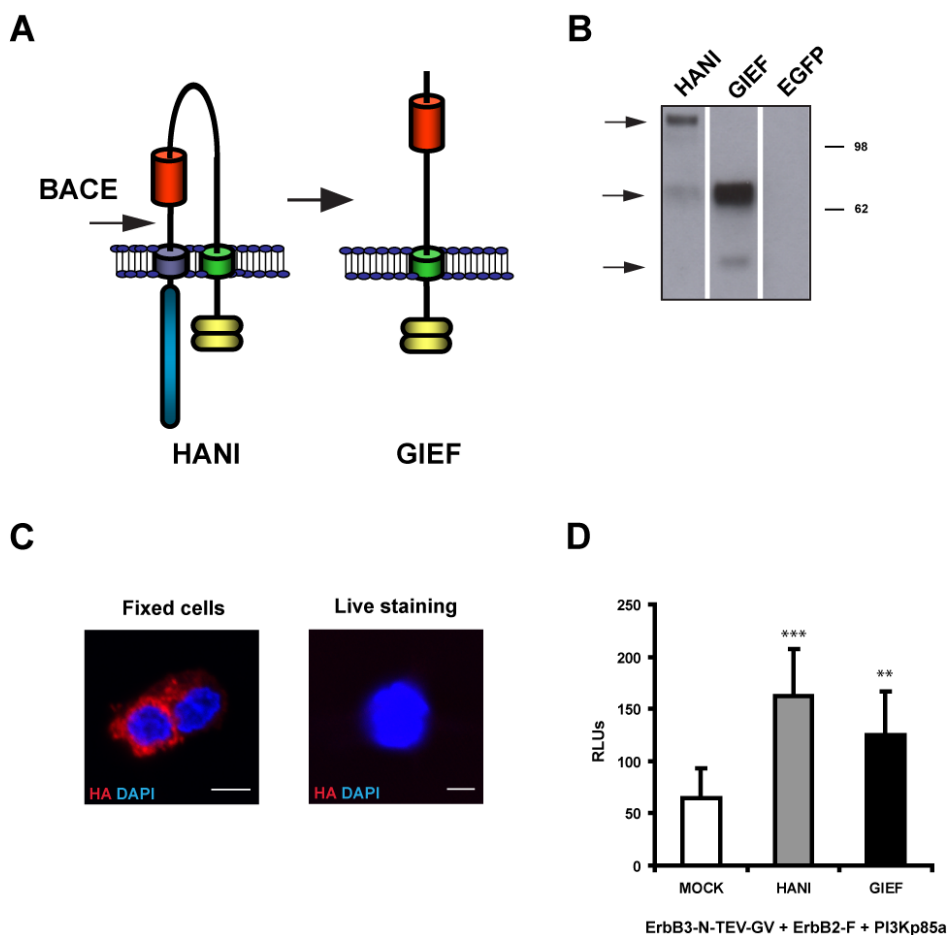
Fig. 3 *In vitro* expression and functional analysis of NRG1 variants

(A) Schematic representation of the HANI and GIEF protein structures. Note that the 'GIEF' protein represents the proteolytic cleavage product of HANI by BACE1 (indicated with an arrow). Specific domains are indicated by color coded boxes: EGF-like domain (red); cystein rich domain (green); transmembrane domain (dark blue); a-type cytoplasmic tail (light blue); HA tag (yellow).

(B) Anti HA tag WB on PC12 cell lysates. Cells were transfected with HANI, GIEF and EGFP expression plasmids. The upper 140kD band corresponds to the full length NRG1 variant HANI (arrow). The ~70kD band of full length GIEF protein corresponds in size to the BACE1-processed HANI protein (arrow). ~38kD band detected in GIEF lysates (arrow) represents potentially processed GIEF protein. Specific NRG1 protein bands detected by anti HA antibody are absent from the EGFP control lysates.

(C) Immunocytochemistry (ICC) on GIEF transfected PC12 cells. GIEF (red) is localized to the membrane detected by HA antibody after permeabilization. The intracellular HA tag is not detected by non (live) ICC without permeabilization. Scale bar 5 µm.

(D) Assesment of biological activity of HANI and GIEF by split-Tev assay. PI3K recruitment was used as a surrogate marker for ErbB receptor dimerization in a 2-cell split-TEV assay. Induction of luciferase reporter expression was significantly increased by HANI (p<0.001) and GIEF (p<0.01) overexpression in PC12 cells compared to MOCK transfected controls. Results are given as relative luminescence units (RLUs) ±STDEV, n=6.

4.2 *In vitro* expression analysis of full length and BACE1 processed NRG1 type III-β_1

As modifications in the primary structure can affect protein folding and mature conformation of the native proteins, expression and function of the modified proteins were tested *in vitro*. For *in vitro* expression analysis HANI and GIEF constructs cloned into the pCMV2 expression vector were used. Western blot (WB) was performed on HANI and GIEF transfected PC12 cells lysates using an antibody directed against HA tag. Tagged full length NRG1 showed expected 140kD full length protein band and ~70kD processed N-terminal protein fragment as previously reported (Wang et al., 2001) (Fig. 3B; arrows, first lane). Size of the GIEF protein corresponds to the ~70kD fragment after proteolytic cleavage of HANI (Fig. 3B; second lane). An additional band of ~38kD detected by HA antibody in GIEF transfected cell lysates, could result from an additional processing event by BACE1 or another protease which could lead to a release of the EGF signalling domain (Horiuchi et al., 2005). Protein bands detected by HA antibody were HANI and GIEF specific as no immunoreactivity was detected in EGFP transfected control cell lysate (Fig. 3B; third lane). Amino acid sequences that target the protein to specific cellular compartments are imprinted into the primary structure of the protein. Truncation of the NRG1 could lead to the loss of these signals in the GIEF protein sequence. Therefore we performed immunostaining on transfected PC12 cells. Immunodetection of the HA tag on GIEF transfected PC12 cells showed localization of GIEF protein in the membrane (Fig. 3C; left panel). Additionally we applied a live staining protocol that prevents antibodies from entering the intracellular space. With this approach we could show that once it reaches the membrane, GIEF protein is inserted with the N-terminus facing the intracellular space, as we could not detect the N-terminal tag extracellularly (Fig. 3C; right panel). NRG1 mediates numerous functions through the EGF-like signalling domain by activating ErbB receptor tyrosine kinases (Burden and Yarden, 1997; Falls, 2003; Yarden and Sliwkowski, 2001). To determine the functionality of the modified NRG1 proteins, with help of Dr. Michael Wehr we assessed their potential to induce ErbB2/ErbB3 receptor dimerization and the recruitment of downstream PI3K in the two-cell Split-TEV assay (Wehr et al., 2006; Wehr et al., 2008). Both HANI and GIEF proteins expressed on the surface of the PC12 cells were potent in inducing ErbB receptors heterodimerization on neighboring cells and downstream signalling detected by the activation of luciferase reporter. Measured luminescence intensity (RLUs) was significantly increased in assays containing HANI (161.74±45.16; [***]p<0.001) and GIEF (124.53±41.77; [**]p<0.01) transfected cells compared to MOCK transfected control assays (64.67±28.23) (Fig.

3D). This was another indirect proof of a correct membrane orientation of the tagged NRG1 variants with the EGF domain exposed to the extracellular environment.

4.3   *In vitr*o processing of NRG1 type III-β$_1$ by BACE1

BACE1 mediates processing of NRG1 *in vitro* (Hu et al., 2008; Willem et al., 2006). *In vivo*, BACE1 knock out mutants accumulate full length (140kD) NRG1 in the brain (Willem et al., 2006) suggesting that NRG1 processing is BACE1 mediated. Even though it is widely accepted that signalling of NRG1 type III is mediated in a paracrine manner it remains possible that the EGF like domain is released by an additional cleavage (Birchmeier and Nave, 2008; Wang et al., 2001; Willem et al., 2009). To confirm the processing of NRG1 by BACE1 in our system and to further analyze GIEF protein processing by BACE1 we have overexpressed *in vitro* HANI or GIEF in HEK 293T cells with or without overexpressing BACE1 and performed WB on cell lysates using HA antibody. Overexpression of BACE1 *in vitro* induces a potent cleavage of the 140 kD HANI band and a shift to the ~70 kD processed band which in size corresponds to the GIEF protein (Fig. 4A; lanes 3 and 5). The effect of BACE1 on HANI processing was specifically blocked by β secretase IV inhibitor treatment (2 µM) (Fig. 4A lane 4). Residual base line processing pattern of the HANI protein in HEK 293T cells remains even after the inhibition of BACE1 (Fig. 4A lanes 1 and 2) suggesting the existence of other proteases cleaving HANI in these cells. Since the ADAMs family of proteases is known to cleave NRG1 (Horiuchi et al., 2005) we also applied the general ADAMs inhibitor GM6001 to transfected cells. ADAMs inhibitor treatment (1µM and 5µM) did not abolish base line processing of the HANI protein in HEK 293T cells (Fig. 4B). The integrity of the ~70 kD and ~38 kD GIEF protein bands pattern were unaffected after overexpression of BACE1, excluding further cleavage of GIEF and the release of EGF like domain by BACE1 (Fig. 4A; lane 6). Similar to HANI baseline processing of the GIEF did not change after the cells were exposed to BACE1 and ADAMs proteases inhibitors (Fig. 4A; lane 5 and 6; Fig. 4B). This observation suggests the existence of other protease entity besides BACE1 and ADAMs family that participates in NRG1 processing.
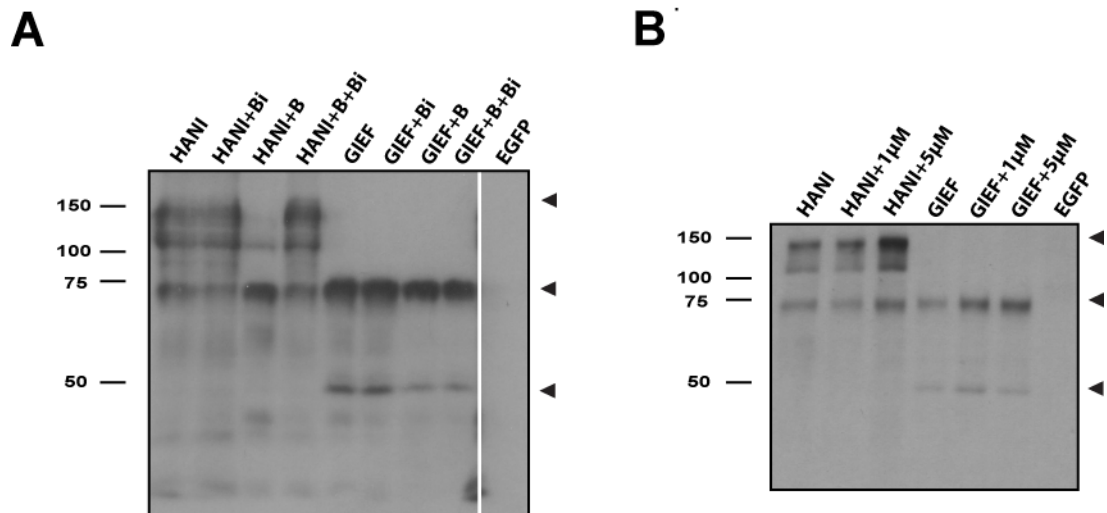
Fig. 4 *In vitro* processing of NRG1 variants HANI and GIEF

(A) WB of HEK293T cell lysates transfected with HANI, GIEF, BACE1 and EGFP expression plasmids using HA tag antibody. BACE1 activity in the selected assays was blocked by 2 μM β-secretase inhibitor (Bi). The 140kD band (arrowhead) of the full length NRG1 detected in all HANI lysates was lost after coexpression of BACE1 (HANI+B) and shifted to the ~70kD processed N-terminal band. The 140kD processed HANI band corresponds in size to a higher molecular weight band of GIEF protein (arrowhead). The BACE1 effect on HANI is blocked by the β-secretase inhibitor (HANI+B+Bi). GIEF ~70kD and ~38kD protein bands intensity is unaltered upon cotransfection of BACE1 (GIEF+B). Application of Bi does not affect base line processing of HANI and GIEF (HANI or GIEF+Bi).
(B) Anti HA antibody WB. ADAMs activity in the HEK293T cells was blocked by broad spectrum ADAMs inhibitor GM6001 (1μM and 5μM). It should be noted that the HANI 140kD and ~70kD and GIEF ~70kD and ~38kD protein bands intensity remains unchanged following inhibitor treatment.

4.4 Thy1 promoter driven neuronal overexpression of the GIEF *in vivo*

Neuronal overexpression of NRG1 type III-β_1 under control of the Thy1 promoter in mice promotes PNS myelination (Michailov et al., 2004). We have used the same approach to asses the function of BACE1 processed NRG1 in myelination *in vivo*. Accordingly, GIEF transgenic mice were generated using the Thy1.2 expression cassette (Caroni, 1997) which confines trasngene expression to neurons. The GIEF construct was cloned via XhoI site into the open reading frame of the Thy1 gene (Fig. 5A). Pronuclear microinjection of the linearized GIEF transgenic cassette resulted in two genetic founders as determined by genotyping PCR with transgene specific primers (Fig. 5B; asterisk). Only one of the two founders (#48) produced the transgenic offspring. To verify the quality of the genomic DNA samples primers amplifying a short sequence of the ErbB2 gene were included into the PCR reaction as a control. Presence of transgenic DNA in the mouse genome does not always ensure the functional expression of the transgene. Therefore, as a next step transgenic expression was analyzed. At two months of age, a transgenic GIEF mouse and a wt littermate from

the F1 generation were analyzed for the transgene expression on the RNA level. RT-PCR performed on spinal cord cDNA using intron spanning transgene specific primers (Fig. 5A; black arrows) revealed the presence of a transgenic transcript in the GIEF cDNA sample but not in WT and negative controls (Fig. 5C). Transgenic mice originating from founder #48 are fertile and without obvious phenotypes.
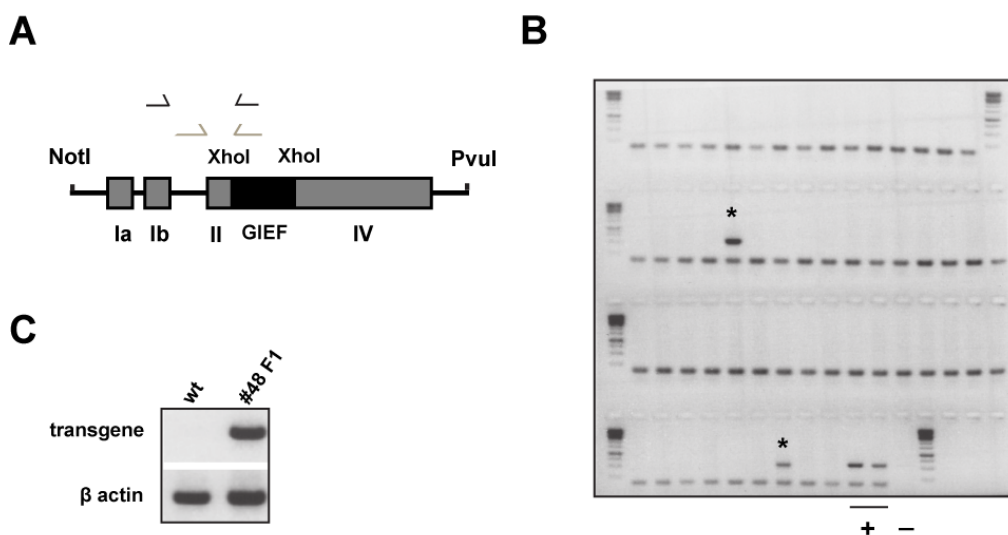
Fig. 5 Transgenic overexpression of GIEF NRG1-variant

(A) Schematic model of the Thy1-GIEF construct. The GIEF cDNA variant was PCR amplified from mouse NRG1 type III-β_1 cDNA with two additional HA tags at its 5' end. Gray arrows depict the position of genotyping primers. Black arrows represent RT-PCR primers.
(B) Screening of GIEF genomic founders by transgene specific genotyping PCR. Two animals positive for GIEF transgenic sequences are labeled with asterisk. Lower PCR band represents amplified ErbB2 fragment used to control for DNA quality.
(C) Transgene specific RT-PCR on spinal cord cDNA derived from founder (#48) F1 offspring at 2 months. Transgene derived transcript is detected in transgenic offspring. β-actin specific RT-PCR was performed as a cDNA quality control.

4.5 Analysis of the onset and the expression levels of the GIEF and HANI transgene.

Myelination program in developing Schwann cells is triggered perinatally (Jessen and Mirsky, 2005). As we wanted to study effects of the HANI and GIEF overexpression on myelination we have next determined the onset of transgene expression. We have prepared cDNA from spinal cord of newly born mice at postnatal day 1 (P1). Transgene specific PCR confirmed the presence of both transgene transcripts in spinal cord neurons at the onset of myelination (Fig. 6A). The expression level of the transgene can vary depending on the number of integrated transgene copies and the level of transcription at the transgene integration site. Different transgenic lines even with the same expression cassette can therefore exhibit very different transgene expression

levels. Comparison of transgene expression levels between two different transgenic lines allows more accurate comparison and interpretation of the observed phenotypes. We therefore evaluated relative expression levels of the GIEF and HANI transgenes in the spinal cord at two months of age by quantitative RT-PCR using primers specific for the type III isoforms. To obtain a highly accurate estimation of the expression, experiment was carried out in the setting of 5 experimental replicates per genotype and 4 technical replicates each. Expression was normalized to β actin. The mean relative expression of GIEF transgene was increased 9 fold (8.9±6.06; ***p<0.001) when compared to wt NRG1 type III (1±0.3), whereas HANI overexpressors had only 3 fold increase (2.9±1.8; *p< 0.05) (Fig. 6B; left panel).
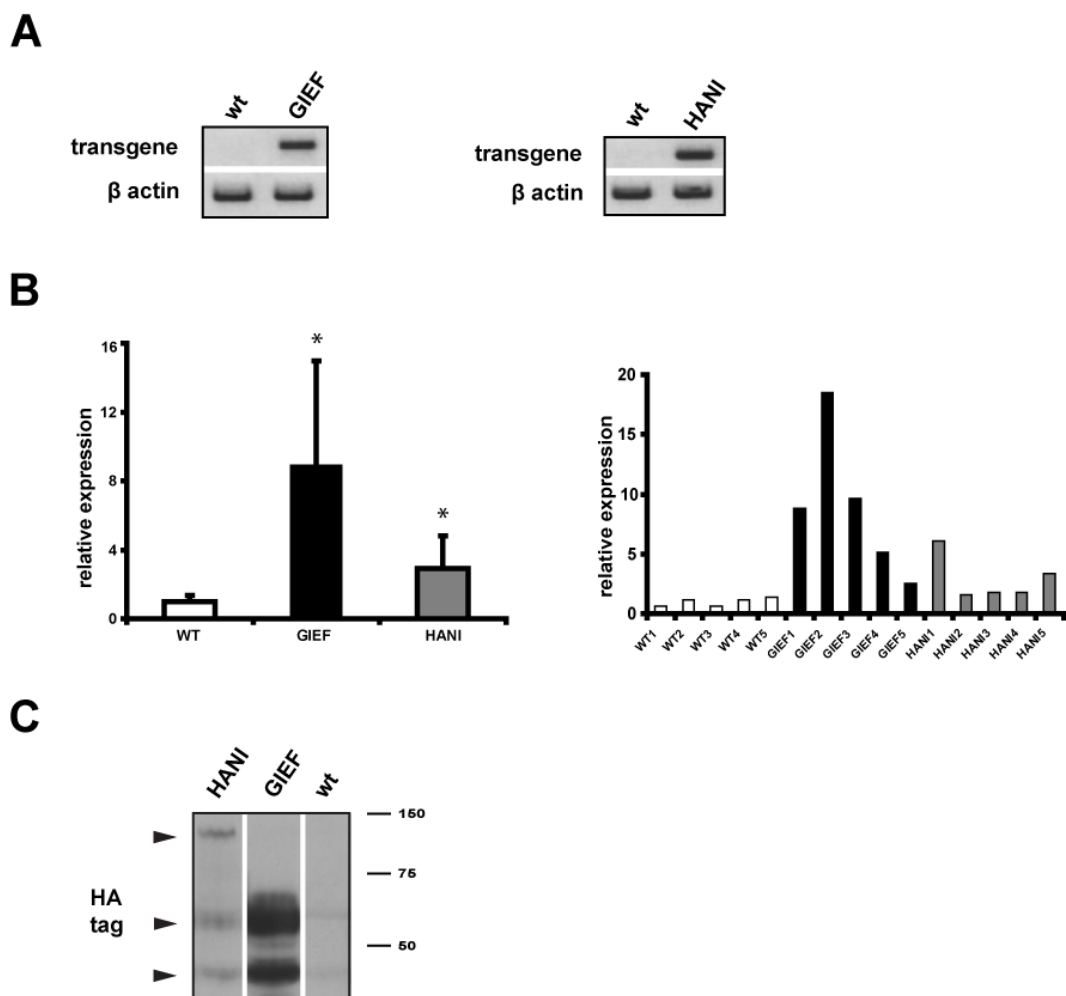
Fig. 6 Analysis of the expression profiles of HANI and GIEF transgenes

(A) Transgene specific RT-PCR on spinal cord cDNA from P1 GIEF and HANI transgenics and wt littermate controls. GIEF and HANI transgenes are expressed at the onset of myelination. β-actin-specific RT-PCR was used as cDNA quality control.
(B) CRD-NRG1 specific qRT-PCR performed on a spinal cord cDNA from wt, GIEF and HANI animals at 8 weeks of age (5 animals/genotype; 4 technical replicates each). Expression levels are normalized to β-actin. The average expression level values (± STDEV) are displayed (left panel). The HANI transgene

expression is 3 fold increased (*p< 0.05) and GIEF 9 fold (**p< 0.01) compared to wt. Individually plotted relative transgene expression levels depicting large variability in expression between the individual animals (right panel).

(C) Spinal cord protein lysates with 40 μg of protein from HANI, GIEF and wt mice immunobloted with HA antibody. Stronger overexpression of GIEF transgenics compared to HANI on mRNA level translates into increased protein amounts.

Three fold differences in the relative expression between GIEF and HANI lines were taken into consideration during the interpretation and comparisons of the phenotypes in GIEF and HANI transgenics Both transgenic lines display large expression level variability between individual animals (Fig. 6B; right panel). This important information was taken carefully into account during analysis as we expected to observe corresponding phenotype variability. We finally wanted to see if the difference in an expression level translates in to the amount of the synthesized protein. We have performed the WB on a spinal cord lysates from HANI, GIEF and wt mice. Membrane was probed with the HA antibody and expected protein band patterns were observed for both transgenic proteins. It is obvious from the WB that the difference in gene expression translates into a difference in the transgenic proteins amounts. 40 μg of protein lysate contains higher amount of GIEF than HANI transgenic protein (Fig. 6C).

4.6   Absence of pathology observed in mice upon early onset of the GIEF transgene overexpression

We have next analyzed if the GIEF protein overload in transgenic mice has a toxic effect on neurons. Since the Thy1 cassette is expressed in spinal cord ventral horn motor neurons that project into the sciatic nerve, we decided to examine the spinal cord and sciatic nerve for the presence of pathology. By HE staining of the spinal cord cross sections, we did not observe obvious changes in number and overall neuronal morphology at 4 months time point, in GIEF transgenic mice compared to controls (Fig. 7; arrowheads). Transgenic spinal cord tissue was also examined for the presence of astrogliosis or microglial activation which are the markers of inflammation, disturbed homeostasis and neuronal tissue pathology (Eng and Ghirnikar, 1994; Hanisch and Kettenmann, 2007). Immunostaining for astrocytic marker GFAP (glial fibrillary acidic protein) showed absence of astrocytes proliferation in GIEF mice when compared to the wt (Fig. 7; not quantified). Immunostaining for the MAC3 marker of the activated microglia revealed no inflammation induced by the GIEF overexpression (Fig. 7) Integrity of sciatic nerve axons was also unchanged in mutants when compared to WT littermates as shown by neurofilament and MBP myelin staining (Fig. 8A). Mutant mice also did not exhibit axon pathology and axonal loss in sciatic nerves as no difference in total number of axons between mutants and wt controls was observed when quantified

on Methyleneblue-Azur II stained semi thin sections of sciatic nerves (p=0.28) (Fig. 8B).
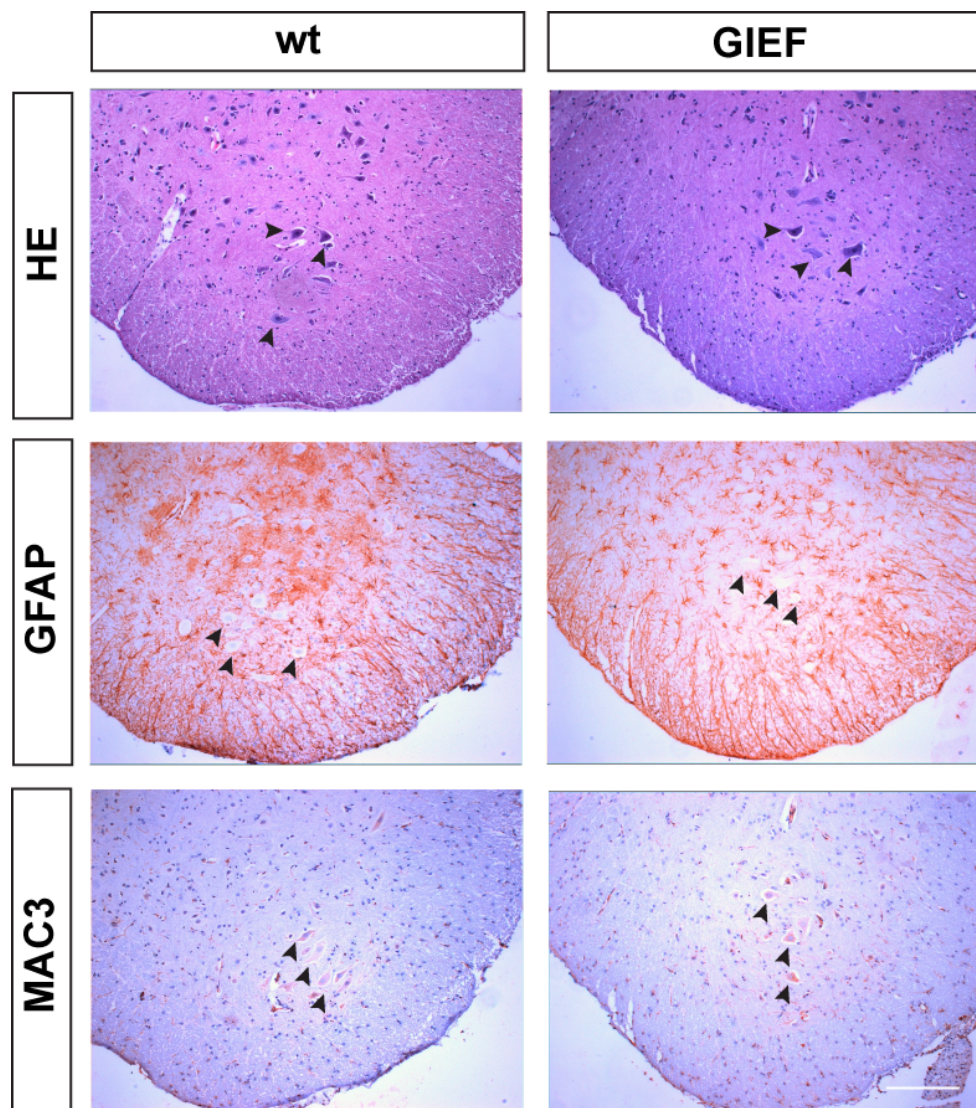
Fig. 7 Absence of pathological changes in the spinal cord of GIEF transgenic mice

Paraffin-embedded 0.5 µm spinal cord cross sections of wt and GIEF mice (4 months) were stained for pathology markers. Ventral horns of spinal cords containing GIEF expressing motor neurons are depicted (arrowheads). HE histological staining reveals normal gross morphology in the spinal cord. Chromogenic GFAP IHC shows no sign of astrogliosis. Chromogenic immunostaining for MAC3 a marker for activated microglia shows absence of inflammation. Scale bar 500 µm.
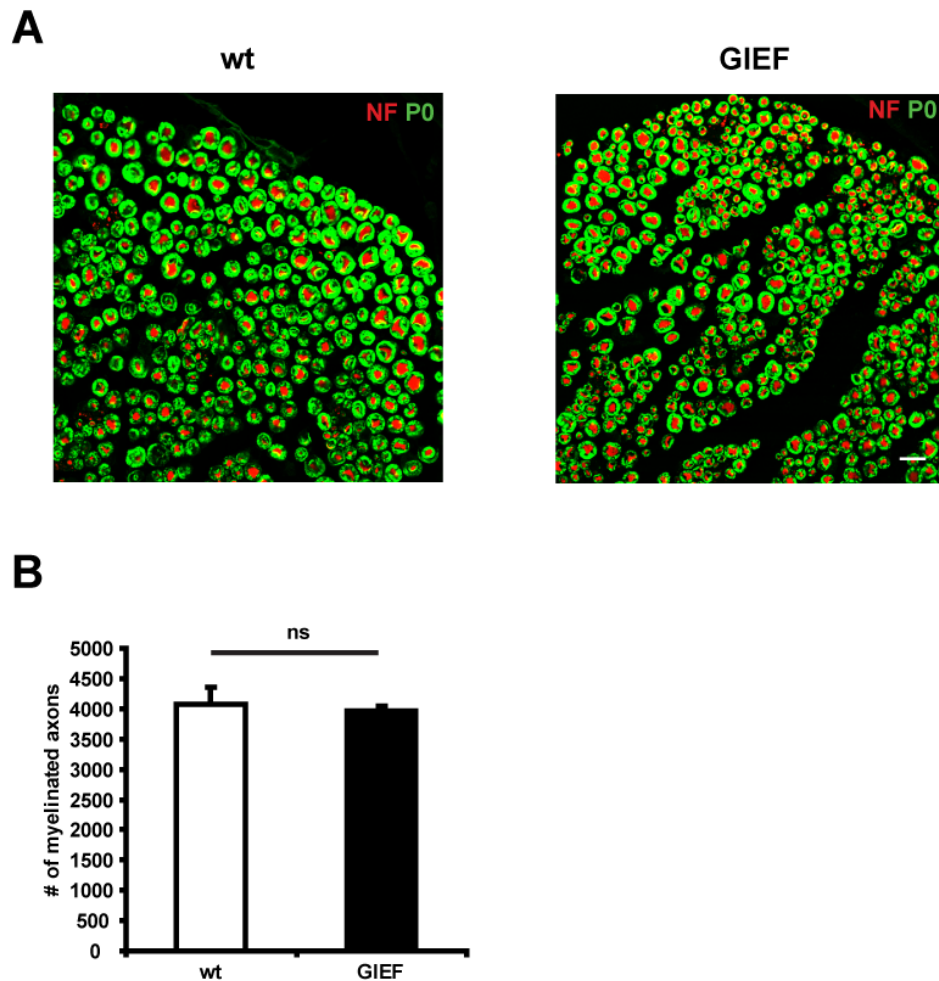
Fig. 8 Unaltered sciatic nerve morphology upon GIEF overexpression

(A) 5µm thick cross sections were cut from paraffin embedded sciatic nerves of wt and GIEF transgenic animals. No apparent change in morphology was observed based on immunofluorescent assessment of NF (red) and P0 (green) expression. Scale bar 10µm.

(B) Quantification and comparison of the number of myelinated fibers on sciatic nerve semithin sections (0.5µm) of wt and GIEF animals (n=3). The average total number of axons is displayed (average±STDEV) showing no significant difference (p=0.28). No axonal degeneration was detectable after overexpression of GIEF.

4.7 GIEF overexpression induces hypermyelination of PNS axons

Overexpression of full length NRG1 type III-β_1 *in vitro* and *in vivo* induces hypermyelination of peripheral axons (Michailov et al., 2004; Taveggia et al., 2005). To study the effect of GIEF overexpression on myelination we analyzed sciatic nerve semi-thin sections stained with Methylenblue-Azur II. GIEF mutant nerves exhibit hypermyelination compared to the myelin of the wt control nerves (Fig. 9A). Further morphological analysis of the same nerves by electron microscopy (EM) showed no changes in myelin ultrastructure in the GIEF transgenics (Fig. 9B). Myelin sheet of

increased thickness maintained a normal myelin membranes spacing periodicity (Fig. 9C).
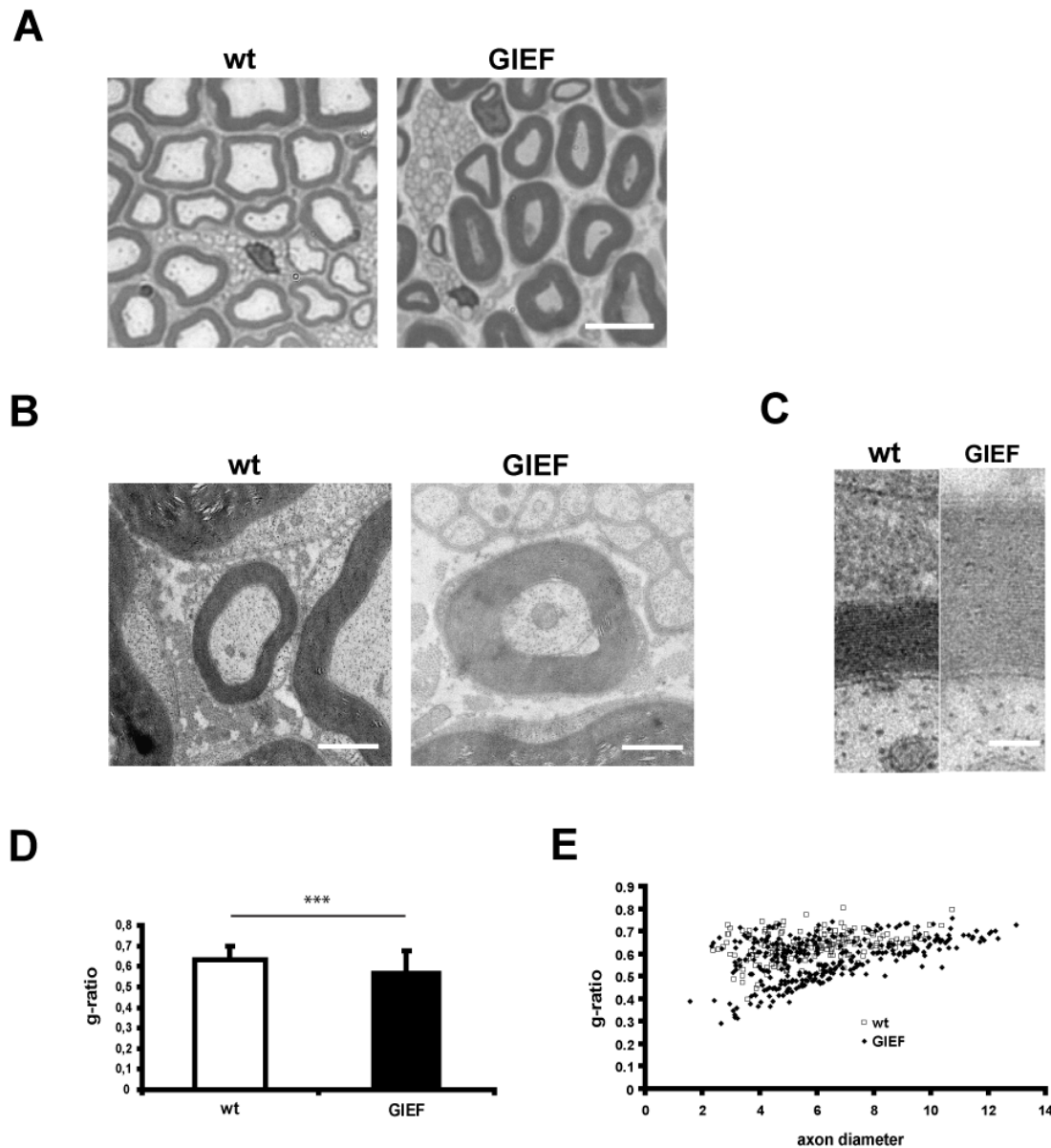
Fig. 9 Hypermyelination in the PNS of GIEF transgenic mice

(A) Semithin cross sections (0.5µm) of sciatic nerves comparing wt control and GIEF overexpressing mice at 2 months of age. GIEF transgenic mice are hypermyelinated with thicker myelin sheaths. Scale bar 10µm
(B) Electron micrograph of ultrathin cross sections (50nm) of the sciatic nerves comparing individual axons of the same diameter in wt and GIEF mutants. Considerably thicker myelin sheath of the GIEF axon is apparent compared to wt. Scale bar 1µm.
(C) Blow-up of aligned wt and GIEF myelin sheaths depicting unchanged myelin ultrastucture and radial periodicity upon increase in myelin thickness. Scale bar 200nm
(D) Quantification of the myelin sheath thickness by g-ratio measurement comparing wt and GIEF mice. Average of at least 100 myelinated axons per animal is depicted (average±STDEV) (wt n=2; GIEF n=4). Average g-ratio in GIEF mice is significantly decreased (***p< 0.001).
(E) Scatter plot depicting g-ratio as function of axon diameter. Smaller caliber axons are more strongly affected by hypermyelination.

Thus, increased thickness occurred as a consequence of the additional myelin membrane wrappings formed by the Sc, similar to previously observed with the full length NRG1 (Brinkmann et al., 2008; Michailov et al., 2004). To quantify myelin thickness we determined the ratio between axon and myelin diameter (g-ratio). Four GIEF mutants and two wt animals were analyzed and g-ratios of randomly selected myelinated axons (n=100/nerve) were measured. The average g-ratio value of axons determined for GIEF mice was significantly decreased when compared to wt controls (0.57 ± 0.09 vs 0.63 ± 0.06; [***]$p < 0.001$) (Fig. 9D). A scatter plot depicting g-ratio as a function of axon diameter shows more pronounced hypermyelination of smaller diameter axons (Fig. 9E). This is in line with the idea that larger axons require proportionally more "signal" to achieve the same level of hypermyelination. Not all axons were affected by hypermyelination, probably due to the mosaic expression of the Thy1 transgenic promoter (Caroni, 1997). This finding supports the hypothesis that the N-terminal fragment formed after BACE1 mediated cleavage is active and sufficient to perform the myelination promoting function of full length NRG1 type III-β_1 *in vivo.* Additionally, it demonstrates that the C-terminal fragment of NRG1 is dispensable for myelination promoting function.

4.8 GIEF mice are ectopically myelinated

Multiple layers of myelin are formed by myelinating Sc around PNS axons typically larger than 1 µm in diameter (Friede, 1972). Smaller axons are grouped and ensheated by non myelinating Sc in so called Remak bundles without a formation of multilamellar myelin sheath. NRG1 is the factor on the axon that translates the axon diameter into the myelination status of the axon and determines one of the alternative phenotypes of the Sc at least *in vitro* (Taveggia et al., 2005). Upon overexpression of NRG1 type III *in vivo* and *in vitro* myelin sheath is formed around normally unmyelinated small diameter axons (Taveggia et al., 2005) (Humml, Unpublished). We have investigated on ultrathin cross section of sciatic nerve by EM how GIEF overexpression affects the myelination status of Remak axons. Overexpression of GIEF on the surface of small diameter axons induces ectopic myelination of these axons (Fig. 10A; EM micrograph). Axons smaller than 1 µm in diameter normally found in Remak bundles are being sorted out and myelinated in mutant mice (Fig. 10A; labeled with asterisk). Quantification of this observation on semithin cross sections of sciatic nerve, 3 animals per genotype, showed significant increase of the ectopically myelinated fibers (<1µm) in mutants compared to the control animals (11.66 ± 2.66 vs 3.6 ± 0.8; [*]$p < 0.05$) (Fig. 10A; right panel).
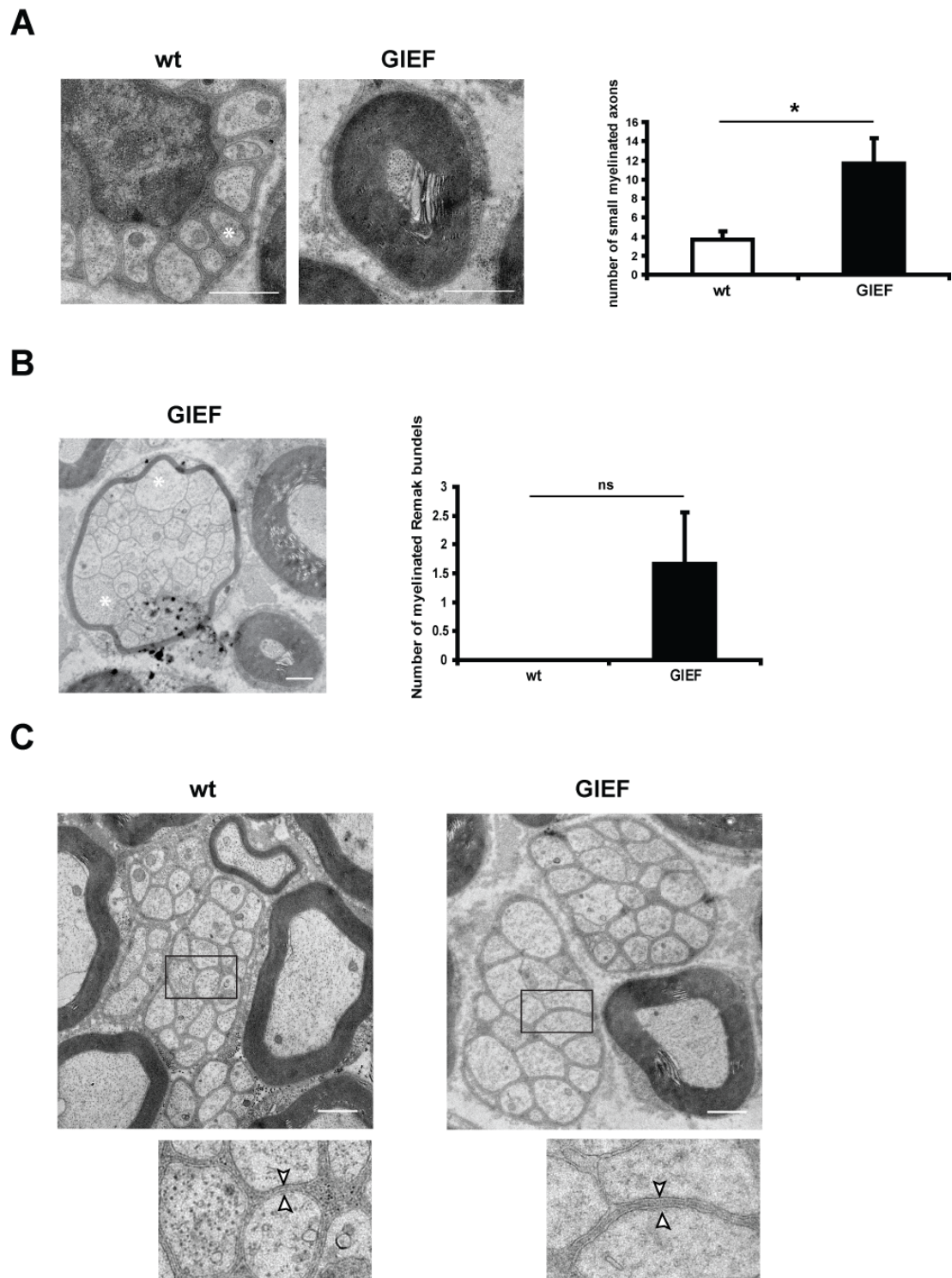
Fig. 10 GIEF overexpression induces ectopic myelination of small caliber axons

(A) Electron micrographs of sciatic nerves showing wt Remak bundle and an example of out sorted and ectopically myelinated small diameter axon in GIEF sciatic nerve. Asterisk labels the axon in the Remak bundle of the same diameter as an ectopically myelinated one. Number of ectopically myelinated axons quantified on sciatic nerve semithin cross sections (n=3) reveals a significant fourfold increase in mutant animals (average±SEM; *p< 0.05).

(B) Ultrathin (50 nm) cross section of a sciatic nerve with an example of myelinated Remak bundle structure, which is never found in wt animals. The myelinated Remak bundle contains unsegregated axons and larger diameter axons typically not found within Remak bundles (asterisk). Quantification (n=3;

average±SEM) revealed low incidence of this structure in mutants (1.5 in average) without significant increase compared to wt (p=0.06).
(C) The examples of Remak bundle structures in wt and GIEF sciatic nerves on ultra thin (50nm) cross sections. The majority of mutant Remak bundles show normal structure comparable to wt. Note in the blow up box that the spacing between axons (arrowheads) within Remak bundles of GIEF mutants is larger than in the wt (observation not quantified).

Additionally in mutant Sciatic nerves we found the Remak bundles surrounded by a multilamellar myelin sheath without segregation of individual axons within the Remak bundle, as if the whole bundle of small axons was perceived as one axon of the large diameter (Fig. 10B; left panel). "Myelinated" Remak bundles also contained axons larger than 1 µm in diameter (Fig. 10B; asterisk). In mutants, the incidence of this Remak morphology was low but it was newer observed in wt animals (1.66 ± 0.88 vs 0; p=0.06) (Fig. 10B; right panel). Besides previously mentioned examples of the aberrant Remak morphology, EM analysis showed no substantial morphological alteration in the majority of the Remak bundles in mutant animals. Remak bundles showed normal gross morphology comparable to the wt controls (Fig. 10C). Axons in the Remak bundles are properly compartmentalized by the nmSc cytoplasm (Fig. 10C; blow up lower panel). However while not quantified we have observed an increase in spacing between individual axons in mutant Remak bundles (Fig. 10C; arrowheads).

4.9 Overexpression of the GIEF does not induce Schwann cell proliferation

Besides its crucial role in myelination, NRG1 type III has also been trusted to control earlier stages of Sc development, including proliferation and survival of Sc precursors in peripheral nerves before the onset of myelination (Birchmeier and Nave, 2008; Dong et al., 1995; Garratt et al., 2000a) Therefore, we investigated if GIEF overexpression effects Sc proliferation. For that we determined the absolute number of Sc on the semithin sciatic nerve cross section (n=3) by counting nuclei of mSc and nmSc (Fig. 11A). We did not identify a significant change in the number of mSc in GIEF mutants compared to the WT animals (126±14.93 vs 152.66±36.52; p=0.15) (Fig. 11B; upper panel). Moreover, there was also no difference in nmSc number observed between mutants and WT controls (75.±19.6 vs 58±8.71;p=0.11) (Fig. 11B; lower panel). We also evaluated the cell proliferation in sciatic nerves by counting DAPI positive nuclei on paraffin nerve cross section (n=3) at 4 months of age. No increase was observed as the number of nuclei per mm^2 was unchanged in mutants compared to wt controls (158.87±38.66 vs 148.35±38.3; p=0.1) (Fig. 11C).
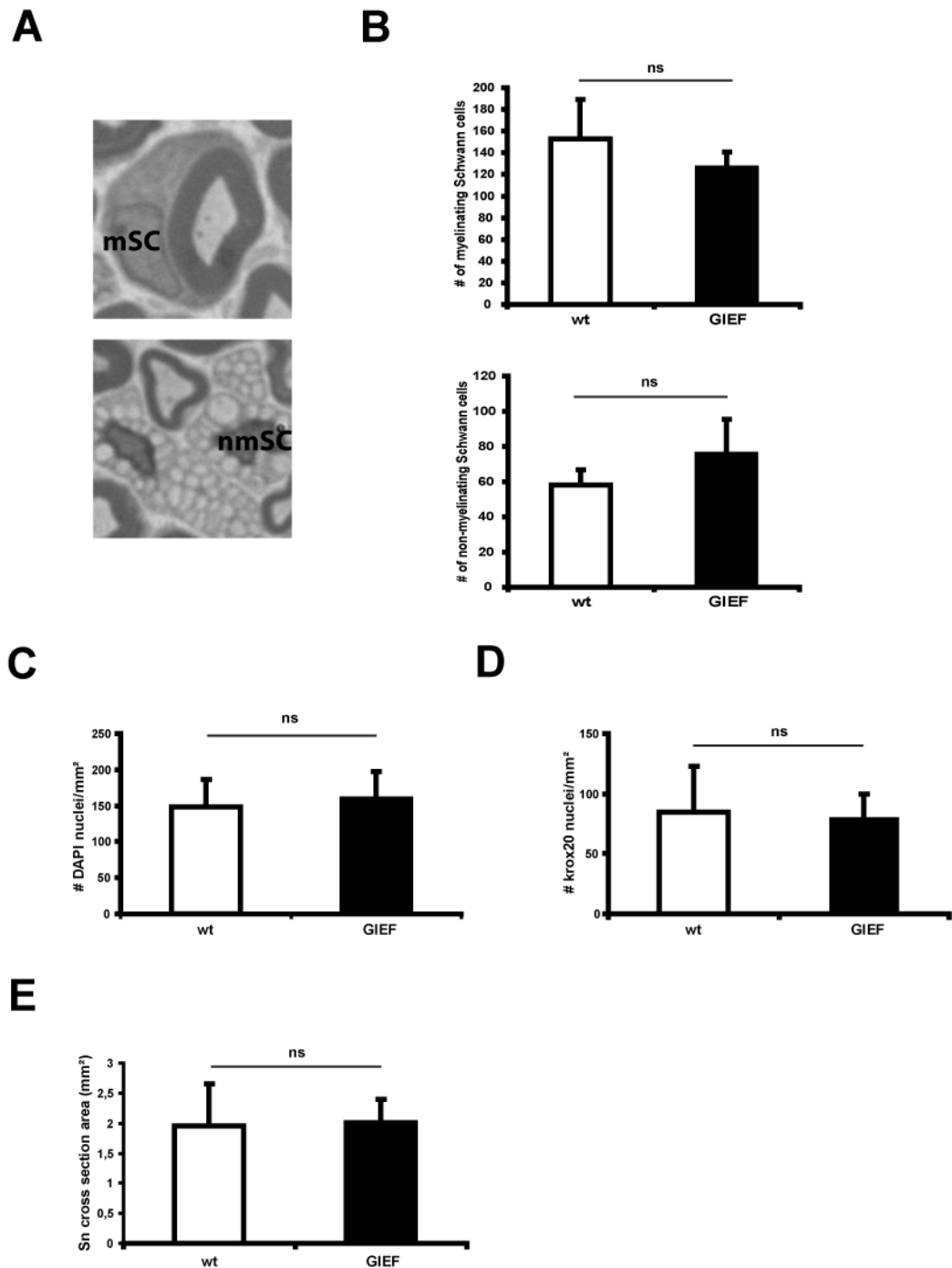
Fig. 11 Absence of Schwann cell proliferation upon overexpression of GIEF

(A) The examples of mSc and nmSc on semithin cross section of sciatic nerve counted for analysis of proliferation.

(B) The number of mSc per mm^2 is not significantly different in GIEF mutants compared to a wt (n=3; average±STDEV; p=0.15) Quantified average number of nmSc in GIEF mutants was slightly increased compared to the wt animals without significant difference (n=3; average±STDEV; p=0.11)

(C) Quantification of the DAPI positive nuclei per mm^2 of sciatic nerve cross section (n=3) shows no significant change in mutants compared to the control animals (average±STDEV; p=0.1).

(D) The Krox20 positive nuclei number per mm^2 (n=3) was not significantly changed between mutants and wt (average ±STDEV; p=0.4).

(E) Measurement of the sciatic nerve cross section area in mm^2 (n=3). No difference between the genotypes was observed (average±SEM; p=0.4).

To examine if GIEF overexpression recruits more Schwann cell precursors to myelinate axons we have also stained the sciatic nerve cross section for Krox20. Krox20 is a major transcriptional regulator the myelination program in Schwann cells (Topilko et al., 1994). Quantification of the number of Krox 20 positive nuclei per mm^2 of GIEF and wt sciatic nerve cross section showed unchanged numbers of Schwann cells engaged in myelination (79.98±19.78 vs 84.35±38.63;p=0.4) (Fig. 11D). From these results, we could conclude that GIEF overexpression does not induce proliferation of Sc or change in Sc profiles in the sciatic nerve. Correspondingly, there was no increase in overall section area size of sciatic nerve in the mutants compared to the wt (2±0.38 vs1.95±0.69; p=0.4) (Fig. 11E).

4.10 ErbB receptor stimulation by overexpression of GIEF induces mild tomacula formation.

NRG1 signalling promotes myelination through activation of ErbB receptor and PI3-kinase-Akt pathway, at least *in vitro* (Maurel and Salzer, 2000). Strong constitutive activation of the PI3K (pAkt-mTor) pathway by conditional PTEN (phosphatase and tensin homolog) inactivation induces hypermyelination and aberrant myelin swellings termed tomaculas (Göbbels et. al submitted). Tomacula structures can be grouped into different categories based on characteristic morphology formed by the aberrantly growing myelin membranes. We have asked if similar aberrant myelin growth is induced as a consequence of ErbB receptor stimulation and activation of PI3K pathway by strongly overexpressed GIEF variant. We have identified two different types of tomaculas in the transgenic nerves at two months of age. One type is defined by axon compression induced by the growing myelin membranes (Fig. 12A; left panel). The second one forms out folding of the myelin sheath and is termed as "myelin budding" (Fig. 12A; right panel). Tomacula formation was quantified on semi thin cross sections of sciatic nerves in a setting of three animals per genotype. Compressed axon tomacula never occurred in wt animals, whereas mutants showed a modest incidence of this type of tomacula formation with average of 6 tomaculas per sciatic nerve (6±2.08 vs 0; *p< 0.05) (Fig. 12B; upper panel). Myelin budding occurred with a higher incidence (27±17 vs 1±0.58) and with high variability between transgenic animals, due to which the 27 fold increase in transgenics was not statistically significant compared to wt controls (p=0.1) (Fig. 12B; lower panel). Therefore, we will include more mice in future analysis. According to the mild tomacula phenotype, it is most likely that even substantial GIEF overexpression does not induce a strong upregulation of PI3K signalling in Sc as after PTEN inactivation.
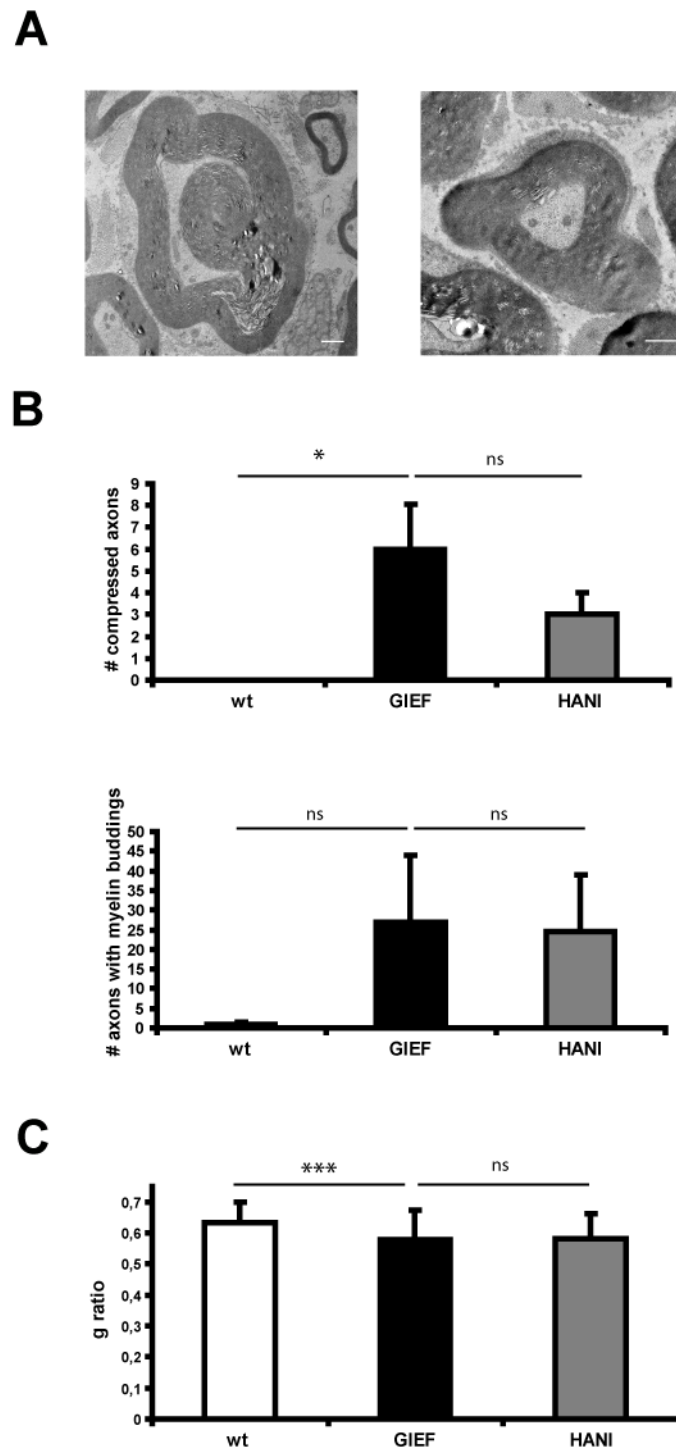
Fig. 12 GIEF overexpression induces mild tomacula formation

(A) Electron micrograph (50nm) of sciatic nerves showing examples of tomacula morphology. Compressed axon tomacula (left panel). Myelin budding (right panel). Scale bar 1 µm.

(B) Quantification of tomacula on sciatic nerve cross semithin (0.5µm) sections form wt (n=3), GIEF (n=3), and HANI (n=2) animals. Values are expressed as average±SEM. Number of compressed axons is significantly higher than in wt (*p< 0.05) where tomacula formation is not found. Difference between GIEF and HANI is not significant (p=0.18). Considerable increase in the number of myelin buddings (average±SEM) in GIEF mutants is not significant compared to wt (p=0.1). No significant difference can be observed between GIEF and HANI (p=0.46).

(C) Comparison of g-ratios between GIEF (n=3) and HANI (n=2). At least 100 axons per animal were measured on semithin sciatic nerve cross sections. HANI and GIEF transgenics display similar g-ratio values (average±STDEV p=0.39)

4.11 GIEF and HANI lines show comparable potential in promoting myelination

Overexpression of GIEF in neurons provides excess amounts of the mature NRG1 type III-β1 fragment with the EGF like signalling domain available to activate ErbB receptors in Schwann cells. According to the currently accepted concept (Falls, 2003), the full length NRG1 is processed in the stalk region by proteases, predominantly BACE1 (Willem et al., 2006) or ADAMs (Horiuchi et al., 2005) before it binds to ErbB receptors. Therefore we have hypothesized that GIEF must be more potent in inducing phenotypes characteristic for NRG1 type III-β1 overexpression. To asses this we first compared the myelination promoting potential of HANI and GIEF overexpressing mice. Comparison of g-ratios (HANI n=2; GIEF n=4) showed no difference between these transgenic lines (0.58±0.08 vs 0.57±0.09; p=0.39) (Fig. 12C). We next examined if HANI mice show signs of tomacula formation similar to those in GIEF mice. Again, HANI compared to GIEF transgene has been equally potent in inducing tomacula formation. There was no significant difference in number of compressed axons between GIEF and HANI mice (6±2.08 vs 3±1; p=1.18) (Fig. 12B; upper panel). Finally the incidence of myelin budding was also without significant difference between GIEF and HANI mice (27±17 vs 24.5±14.5; p=0.46) (Fig. 12B; lower panel). Overexpression of BACE1 processed NRG1 type III-β1 phenocopied all the hallmarks of myelin morphology alterations seen after overexpression of the full length NRG1 type III-β1, showing that GIEF is not per se more potent than the full length NRG1. The similarity of the phenotype seen after overexpression of the full length and BACE1 activated NRG1 variant also shows that C-terminus is not required for myelination promoting function of NRG1.

4.12 Functional interaction between NRG1 myelination promoting function and BACE1 *in vivo*

Neuronal overexpression of BACE1 in transgenic mice increases amyloidogenic processing of APP in the brain (Willem et al., 2004). We wanted to investigate if NRG1 type III-β1 and activity is also increased upon BACE1 overexpression resulting in further stimulated myelination. After breeding BACE1 transgenic mice to HANI overexpressors, BACE1/HANI double transgenics, HANI transgenics and wt littermate controls were analyzed at three months of age. Sciatic nerves semithin cross sections were analyzed by light microscopy. Obtained sections were used for the quantification

of myelin thickness. Quantification of myelin thickness by g-ratio measurement of (n=100 axons/nerve) showed that NRG1 induced hypermyelination was not further promoted by BACE1 overexpression (0.535±0.005 vs 0.532±0.005; p=0.36) (Fig. 13D). Thus, BACE1 is not rate limiting for the myelination promoting function of the NRG1 *in vivo*. Endogenous amounts of BACE1 have the capacity to activate increased levels of NRG1 in HANI transgenic mice. Inactivation of BACE1 throughout development leads to the formation of extremely thin myelin sheath around PNS axons (Willem et al., 2006) (Fig. 13A; BACE-/-). This phenotype is supposedly caused by abolished or decreased processing of NRG1 (Willem et al., 2006) as it phenocopies hypomyelination seen in NRG1 heterozygous mutants (Michailov et al., 2004). We therefore wanted to investigate if the absence of BACE1 would affect the myelination promoting function in HANI overexpressing mice. To achieve HANI overexpression in a BACE1 null background, HANI transgenics, which were heterozygous for mutant BACE1 allele, were bred to heterozygous BACE1 mutants. Sciatic nerves were processed for semithin sections and analyzed. Light microscopy pictures showed increased myelin thickness in a sciatic nerve of the HANI, and BACE1-/-/HANI when compared to the wt animal (Fig. 13A; axons of the same diameter labeled with asterisk). We also observed significantly thinner myelin of BACE1-/- compared to wt (Fig. 13A) as previously described (Willem et al., 2006). To quantify these observations we measured g-ratios. Overexpression of NRG1 in the complete absence of BACE1 still induced peripheral hypermyelination, but not to the same extent as observed in the presence of active BACE1 (0.580±0.005 in HANI vs 0.616±0.007 in BACE1-/-/HANI; [***]p< 0.001) (Fig. 13B; upper panel). Scatter plot depicting g-ratio as a function of axon diameter for HANI and BACE1-/-/HANI displays an equal shift in g-ratio values regardless of the axon diameter (Fig. 13C; upper panel). Thus, we could show a functional interaction of BACE1 and NRG1 during myelination *in vivo*. However, this result also suggests the existence of compensatory protease that (partially) activates NRG1 or the ability of NRG1 to mediate signalling without being previously proteolytically processed. Another interesting perspective is the finding that hypomyelination in BACE1-/- mutants is rescued by providing more NRG1 protein as seen in BACE1-/-/HANI (0.776±0.003 vs 0.616±0.007; [***]p< 0.001) (Fig. 13B; lower panel). The corresponding scatter plot shows that smaller diameter axons of BACE1-/- are more potently rescued (Fig. 13C; lower panel). This is consistent with a proportionally lower NRG1 level required on small-diameter axons compared to large-diameter axons to reach a certain g-ratio.
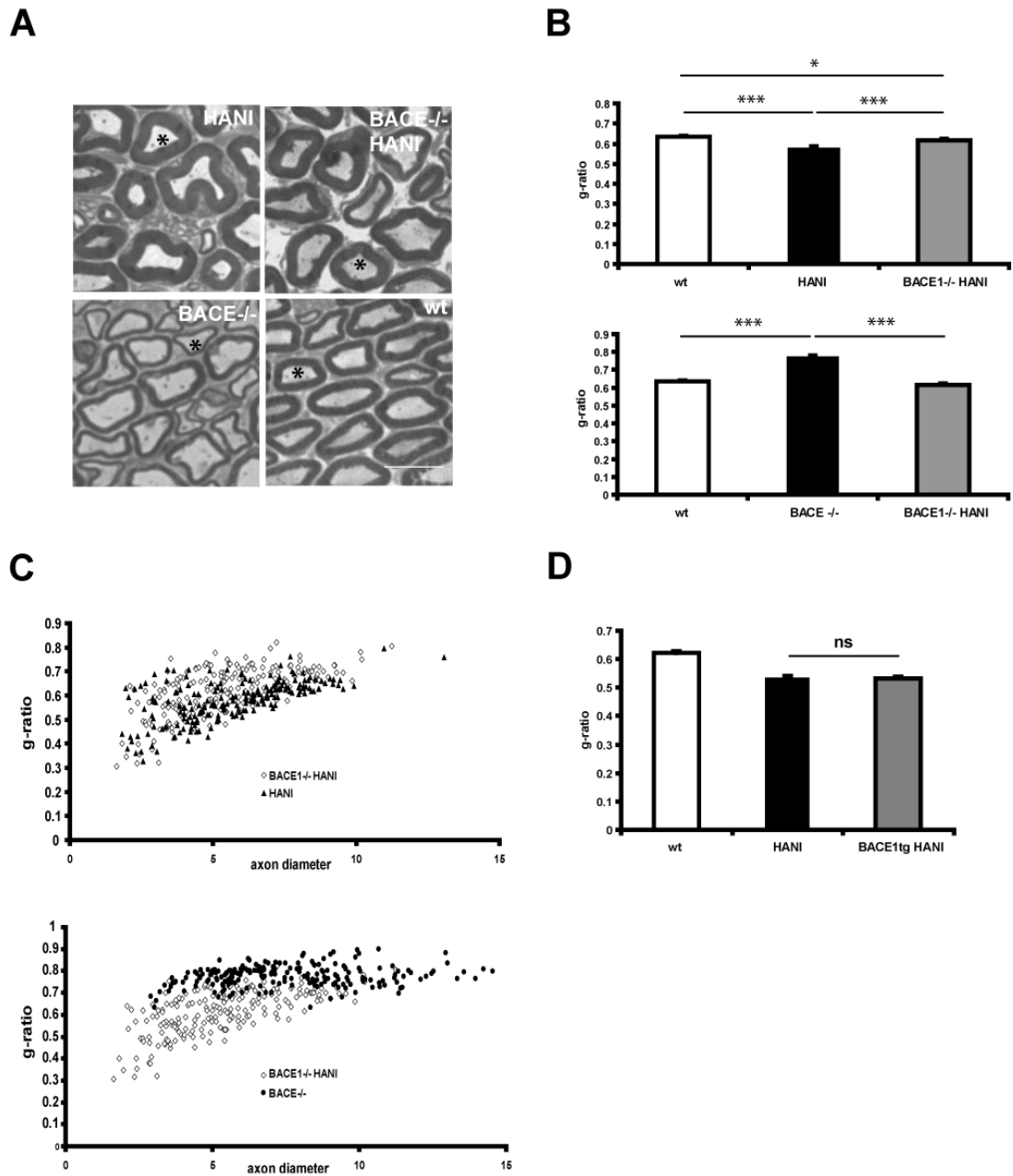
Fig. 13 NRG1 type III overexpression rescues hypomyelination in the PNS of BACE1 null mutants

(A) Semithin sciatic nerve cross sections (0.5µm). Metyleneblue stained myelin in HANI, HANI/BACE1-/- , BACE1-/- and wt animals at 2 months of age. Asterisk labels axons of equal diameter. It is apparent that the myelin sheaths in sciatic nerves of HANI/BACE1-/- animals have a comparable thickness to HANI mutants, while they are hypermyelinated when compared to wt animals. BACE1-/- mutants show hypomyelination of SN axons. Scale bar 10 µm.

(B) Analysis of myelin sheath thickness by g-ratio measurement performed on 2 animals per genotype and 100 axons per sciatic nerve. NRG1 myelin promoting function partially depends on the presence of BACE1. g-ratio values (average±SEM) in HANI/BACE1-/- are significantly decreased compared to wt animals ($p< 0.05$). g-ratio values of HANI/BACE1-/- are significantly increased compared to HANI mutants (***$p< 0.001$). BACE1-/- hypomyelination is rescued after overexpression of NRG1. BACE1-/- g-ratio values are increased compared to wt controls (***$p< 0.001$). Note the extreme decrease in g-ratio values of HANI/BACE1-/- mutants compared to BACE1-/- (***$p< 0.001$).

(C) Individual g-ratio values plotted against axon diameter. Shift in HANI/BACE1-/- g-ratio values compared to HANI is equal through out the axon diameter distribution range. Difference in g-ratio values between BACE1-/- and HANI/BACE1-/- mutants is higher for smaller diameter axons.

(D) BACE1 is not rate limiting for myelination promoting function of NRG1. G-ratio values (average±SEM) comparing HANI, HANI/BACE transgenic animals and wt animals at 3 months of age (n=2). G-ratio values are not significantly changed between HANI and HANI/BACEtg (p=0.36)

4.13 HANI and GIEF protein are detected on the surface of the spinal cord motor neurons *in vivo*

Neuregulin1 type III-β1 is produced as a proprotein harboring two TM-domains. It is believed that it is converted in to a mature signalling molecule by proteolytic processing in the stalk region after which "U" shaped NRG1 opens to expose the EGF like domain (Nave and Salzer, 2006; Wang et al., 2001). However, trafficking routes of newly synthesized NRG1, and sites as well as the order of processing are not well understood. The lack of functional NRG1 antibodies has made it difficult to specifically visualize the protein and address these questions. Only one antibody directed against C-terminus (sc-348 against 'a' type cytoplasmic tail of NRG1) yields satisfactory results as it detects elevated NRG1 protein in the tissue of transgenic overexpressors. By introducing the HA tag at the N-terminus of NRG1 in our transgenic animals (HANI and GIEF), we have enabled the detection of the N-terminal fragment of NRG1 type III *in vivo*. To investigate the cellular localization of NRG1 we performed immunostaining of the lumbar spinal cord that contains the somata of motor neurons that project axons into the sciatic nerve. Spinal cords of HANI, GIEF and wt animals (n=3 per genotype) at 12 days and 4 moths of age were processed for paraffin sections. NRG1 was detected by fluorescent immunostaining on spinal cord cross sections using HA and C-terminus specific antibodies recognizing antibodies. Using the C-terminal antibody in wt control animals NRG1 was detected at both time points on the cell surface of the motor neurons where it displayed a patchy pattern of localization (red) (Fig. 14; wt arrowheads). As expected HA immunoreactivity (green) was absent in wt controls. We speculate that the patchy membrane domains could correspond to postsynaptic compartments on the motor neuron soma as we have data colocalizing HANI protein in CNS with PSD-95 (Gummert unpublished observation). This finding has to be addressed in more detail using antibodies directed against pre- and post-synaptic markers such as PSD-95, synapsin, VGLUT, and GAD65. Another possibility is that the patches represent lipid raft membrane microdomains. It has been previously reported that NRG1 is localized to lipid rafts *in vivo* (Frenzel and Falls, 2001). In HANI overexpressing mice at both time points, neuronal cell surface domains containing the N-termini of NRG1 were widened and immunoreactivity of the N- and C-terminal antibody completely overlapped (yellow) (Fig. 14; HANI arrowheads). It is not clear if full length NRG1 is first delivered to the membrane surface before being cut in the stalk region or the cut already occurs in the Golgi network. The GIEF variant was localized to

neuronal surface, but also detected in the intracellular compartments presumably ER and Golgi networks (Fig. 14; GIEF). The HA signal intensity in the GIEF overexpressor was stronger than in HANI mice presumably due to the stronger overexpression of the GIEF transgene. Interestingly, in GIEF mice membrane domains containing transgene detected by HA tag antibody (green) did not overlap with the domains containing endogenous NRG1 detected by C-terminal antibody (red) (Fig. 14; arrowheads; far low right panel). Thus, GIEF was transported into a domain different to endogenous NRG1. This finding is in line with a previous *in vitro* study (Frenzel and Falls, 2001) where authors showed that N-terminal fragment of NRG1 localized to a non lipid raft membrane compartment in contrast to full length NRG1 and the C-terminal fragment, which were found in a detergent insoluble lipid raft membrane fraction.
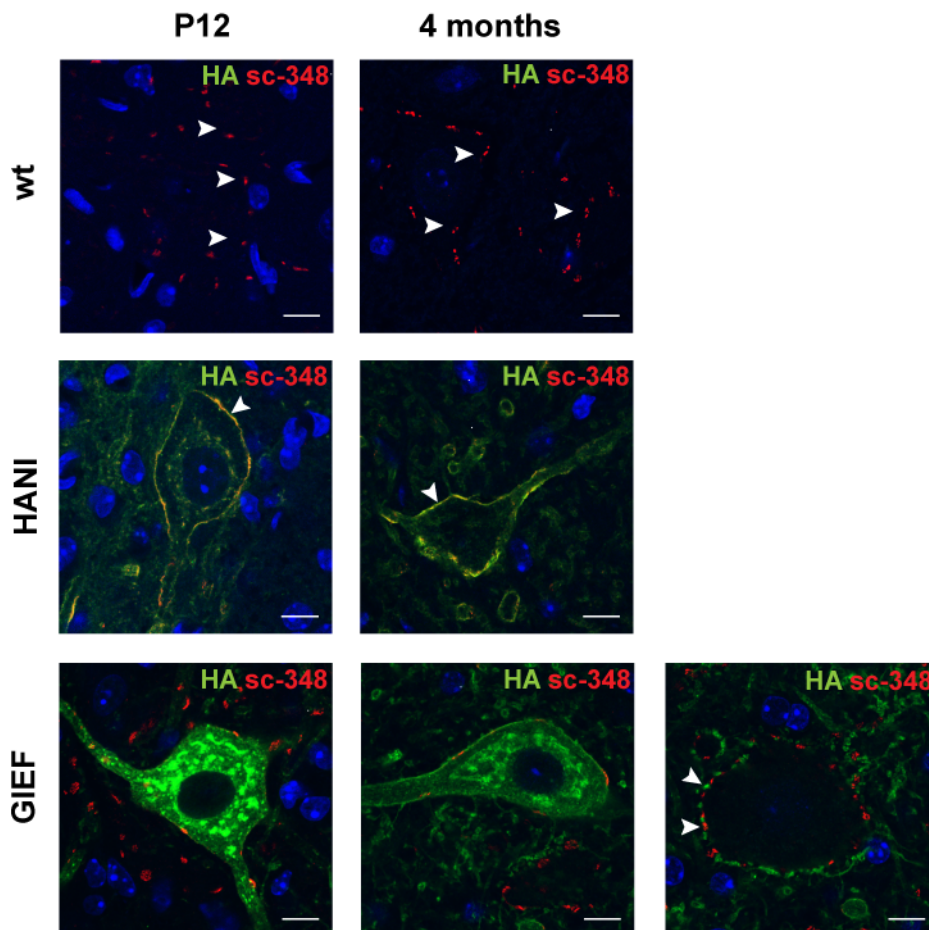
Fig. 14 NRG1 type III is localized on the surface of spinal cord motor neurons of wt and NRG1 transgenic mice

Paraffin spinal cord cross sections (5μm) of wt, HANI and GIEF mice at P12 and 4 months. Immunostaining was performed using anti HA (green) and sc-348 (red) antibodies. Nuclei are stained with DAPI (blue). Confocal images showing NRG1 signal on spinal cord motor neurons. Wt and transgenic NRG1 variants localize to neuronal surface (arrowheads). In GIEF mutants transgenic protein is additionally enriched in the intracellular compartment.

Far down right panel depicting an example of a motor neuron in GIEF mutants. wt -NRG1 (red) and GIEF transgenic proteins (green) are found in distinct membrane compartments (arrowheads). Scale bar 10 µm.

4.14 Transport of the NRG1 fragments from neuronal soma in to the axonal compartment is limited

According to the functional role of NRG1 in myelination (Michailov et al., 2004; Taveggia et al., 2005) NRG1 has to be transported from the neuronal cell body into the axonal compartment to stimulate signalling in Sc. After cleavage of the NRG1 type III-$\beta1$ proprotein in the stalk region, C- and N- terminal fragments are separated (Falls, 2003). The EGF-like signalling domain, responsible for ErbB receptor activation is located at the membrane anchored N-terminal fragment. To further address the mechanism of NRG1 action we have assessed the transport of NRG1 fragments in to the sciatic nerve. To detect NRG1 *in vivo* in axonal compartment we have performed immunostaining on paraffin sciatic nerve cross sections of wt, HANI and GIEF animals at P12 and 4 months of age in a setting of 3 animals per genotype. Nerves were immunolabeled for neurofilament (NF) to define the axonal compartment (red) and with HA antibody to detect NRG1 (green) (Fig. 15). As expected NRG1 staining of wt nerves with the HA antibody did only result in background signal and served as a negative control (Fig. 15A, B). In HANI transgenic NRG1 was localized to the axonal membrane forming a ring structure around the NF labeled axon at the P12 time point (Fig. 15A arrowhead and inset). However, the number of labeled axons was low (observation not quantified). NRG1 immunoreactivity at the axonal surface could not be detected in HANI sciatic nerves at 4 months of age probably due to the low amount of available NRG1 protein below the sensitivity threshold of the staining method (Fig. 15B). The fact that NRG1 was detected on neuronal cell somata, but not on the axons suggests limited transport of the protein into the axonal compartment. HA antibody staining detected the GIEF fragment on the axonal surface at both time points (Fig. 15A, B; arrowheads). The GIEF fragment was clearly localized to the axonal surface forming ring like structure around the axon (Fig. 15A, B inset). At the 4 months time point we, could also see vesicle like structures in the axonal lumen, potentially representing vesicles transporting GIEF protein from the soma via fast axonal transport (Fig. 15B; inset) .

A

P12

WT

HANI

GIEF

B

4 monhs

WT
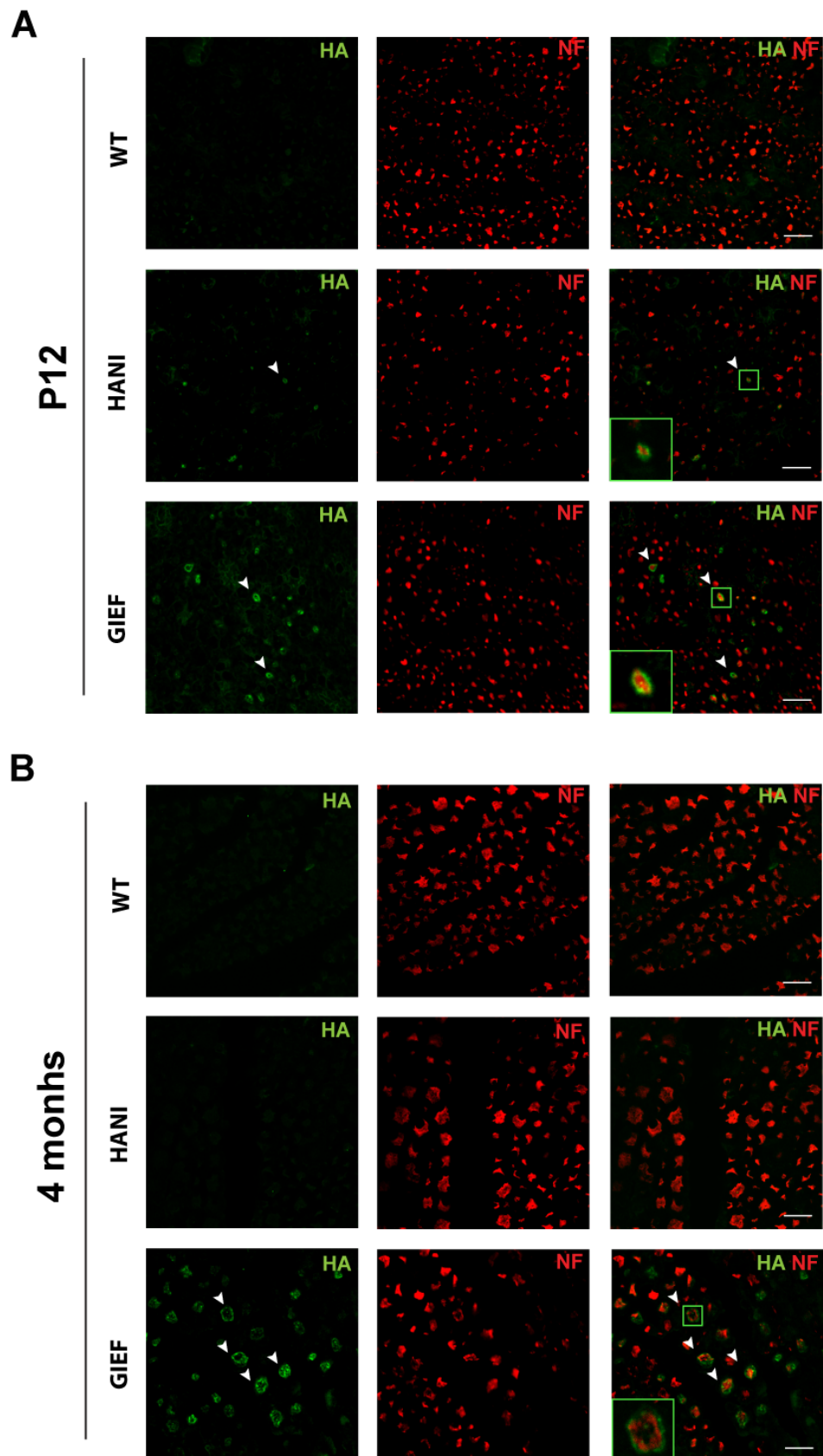
HANI

GIEF

Fig. 15 Immunohistological detection of the N-terminal fragment of NRG1 type III in sciatic nerve

71

Paraffin embedded sciatic nerve cross sections (5µm) of wt, HANI and GIEF animals (P12) immunostained with antibodies against the N-terminal HA tag in HANI and GIEF transgenics are shown in green, neurofilament is shown in red.

(A) At P12 in HANI and GIEF transgenics NRG1 protein can be detected on axons (arrowheads). It is apparent with higher magnification that the tg-derived protein localizes to the axonal membrane surface. Transport of NRG1 into the axonal compartment is limited. Scale bar 10µm.

(B) At 4 months of age transgene derived protein is not detected in HANI sciatic nerve. GIEF transgenic protein is detected on the axonal surface (arrowheads; inset). The vesicular structures containing NRG1 are apparent in the axonal lumen (inset).

To asses the transport of the C-terminal fragment at P12 and 4 months, HANI sciatic nerves were stained with an antibody against tubulin (Tuj1, green) and an antibody directed against NRG1 C-terminus (red) (Fig. 16) At both time points, the C-terminal fragment of NRG1 could not be detected in the axonal compartment.
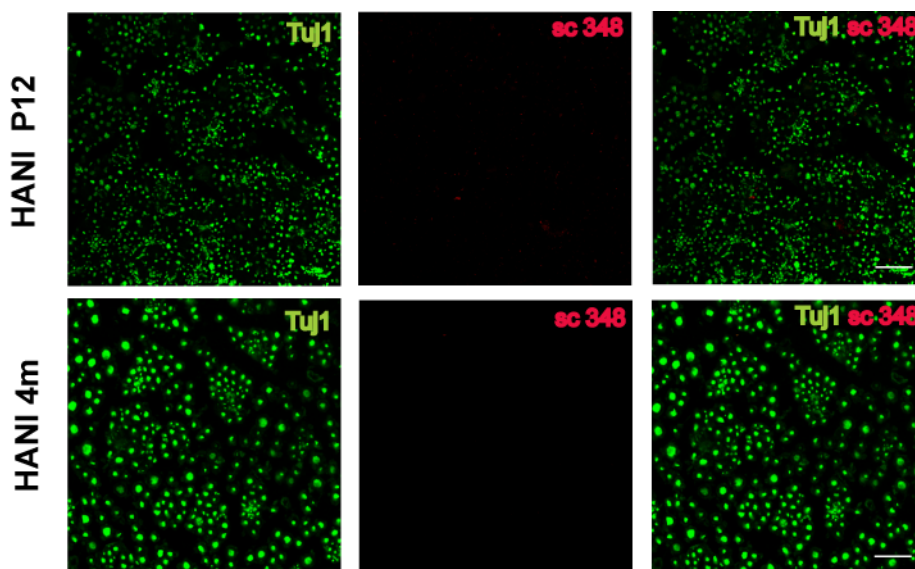
Fig. 16 Immunohistological detection of the C-terminal fragment of NRG1 type III in sciatic nerve

Paraffin embedded sciatic nerve cross sections (5µm) of HANI animals (P12 and 4 moths) immunostained with sc-348 antibody against NRG1 C-terminus (red) and tubulin (green). The sciatic nerves examined were devoid of NRG1 C-terminal fragment evidenced by the lack of fluorescent signal.

To study the transport of NRG1 fragments into the sciatic nerve, we have performed the WB analysis of spinal cord and sciatic nerve protein lysates. HANI and GIEF mutants were sacrificed at 2 months of age and three animals per genotype were analyzed. Protein lysates containing 40 µg of protein were analyzed and tubulin was used as a loading control. Immunoblotting of the HANI spinal cord and sciatic nerve supported the limited transport theory. Western blotting of the spinal cord lysates using the HA antibody, revealed typical processing pattern consisting of 140kD full length protein and processed ~70kD and ~38kD N-terminal fragments (Fig. 17A; first three

lanes). Corresponding bands were absent from sciatic nerve lysates containing the same protein amount and only unspecific bands could be detected (Fig. 17A; second three lanes). Protein lysates from wt spinal cord and sciatic nerve were used as controls (Fig. 17A; last two lanes). Immunodetection of the C-terminal fragment in the HANI and wt spinal cord and sciatic nerve protein lysates produced similar results. A 140kD full length protein and a processed ~60kD C-terminal protein fragment were detected in the HANI spinal cord while corresponding bands in the wt were very weak (Fig. 17B). Corresponding bands could not be detected in sciatic nerve lysates of both wt and overexpressing mutants (Fig. 17B).
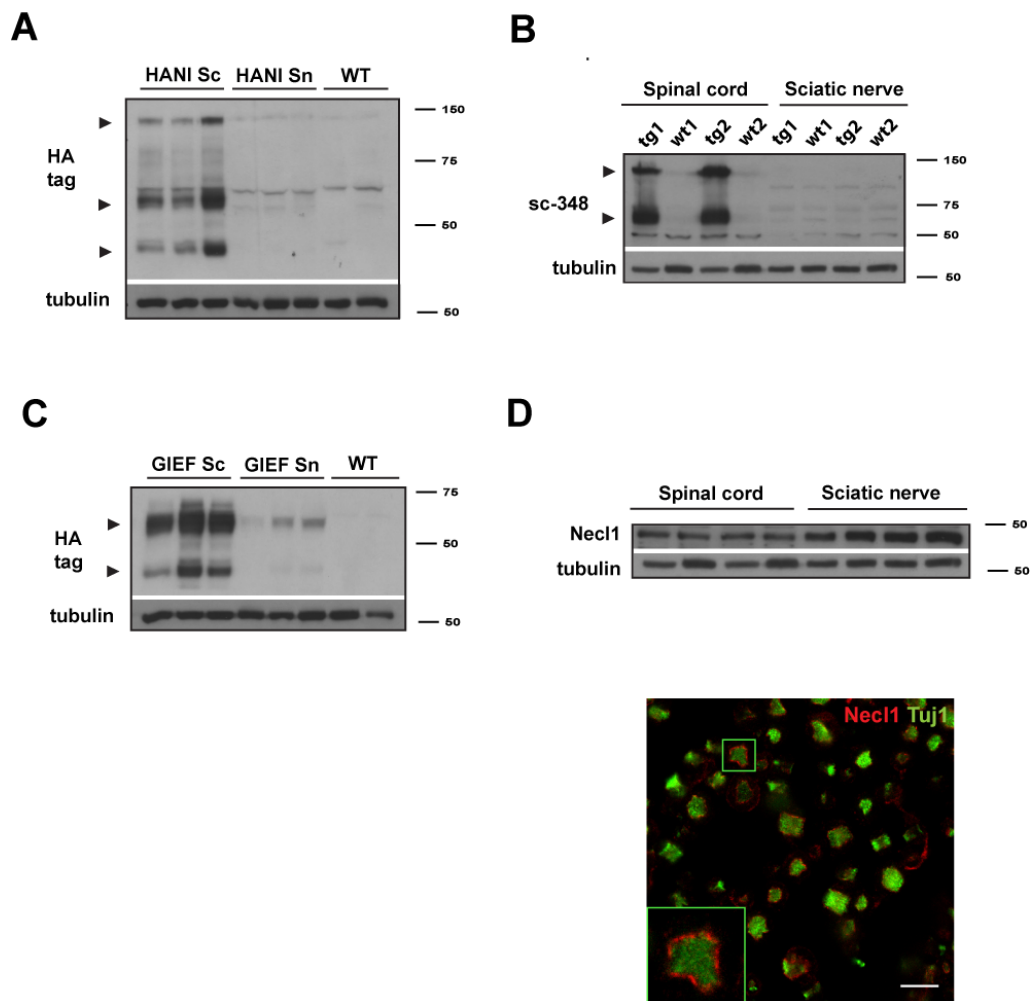
Fig. 17 WB analysis supports limited transport of NRG1 from neuronal somata into axonal compartments

(A) WB of the spinal cord and sciatic nerve lysates (40 µg) of HANI (n=3) and wt mice containing 40 µg of protein, performed with the anti HA antibody. The 140kD band corresponding to the full length HANI and a processed N-terminal ~70kD and ~38kD bands (arrows) are detected in spinal cord lysates. Corresponding bands are not visible in sciatic nerve lysates. Transgenic protein bands are absent in the wt lysates. β-tubulin was used as a loading control in all blots.
(B) WB of the HANI and wt spinal cord and sciatic nerve lysates (n=2) containing 40 µg of protein performed with a sc-348 antibody to NRG1 C-terminus. The 140kD full length and 60kD processed C-

terminal NRG1 band are detected (arrows) in the spinal cord, with obvious increase in the protein amounts in transgenic animals. Corresponding bands are not detected in sciatic nerve lysates.
(C) WB showing GIEF transgenic protein bands detected in the spinal cord and sciatic nerve using anti HA antibody. The full length GIEF protein band ~70kD and a processed band of ~38kD are detected in spinal cord and sciatic nerve lysates (arrows). Reduced amount of the protein in sciatic nerve is evident.
(D) WB showing enrichment in Necl1 protein in sciatic nerve compared to spinal cord (n=4).Paraffin embedded sciatic nerve cross sections (5µm) of a HANI mouse stained for Necl1 (red) and tubulin (green). Necl1 appears to be localized to the axonal membrane. Scale bar 10 µm.

Western blotting performed with GIEF protein lysates revealed the presence of the typical transgene protein bands of ~70kD and ~38kD in a sciatic nerve, which were strongly reduced, compared to spinal cord (Fig. 17C). Taken together western blot analysis agrees with theory of *in vivo* limited transport of NRG1 from the neuronal soma where protein is synthesized in to the axonal compartment, supporting data from immunostainings. To exclude technical reasons for the difficulties to detect NRG1 in sciatic nerves of HANI mutants we performed western blotting and immunostaining for Necl1 protein which is known to be localized at the axonal surface (Spiegel et al., 2007). On WB, we could detect Necl1 protein in both spinal cord and sciatic nerve protein lysates with enrichment in the sciatic nerve (Fig. 17D). Immunostaining of sciatic nerve cross sections also revealed localization of Necl1 on the axonal surface forming ring-like structures (red) surrounding the tubulin labeled axon (green) (Fig. 17D; lower panel).

4.15 Inhibition of ADAMs proteases promotes *in vitro* myelination in DRG-Sc co-culture

In our experiments with transgenic mice NRG1 stimulated myelination even in the absence of BACE1 protease. NRG1 activation was probably compensated for by other proteases, most likely belonging to the ADAMs family such as TACE (Horiuchi et al., 2005). To asses the effect of ADAMs activity on myelination we took advantage of Dorsal root ganglion-Schwann cell (DRG-Sc) co-cultures in which myelination can be stimulated by addition of ascorbic acid. This *in vitro* myelination system proved to be compatible with our *in vivo* findings. HANI and GIEF constructs were cloned into lentiviral expression plasmid pLenti6/V5-DEST (Invitrogen) using gateway cloning. Expression was confirmed *in vitro* by immunostaining against HA tag after transfection of HEK 293T cells (Fig. 18A). In experiments made in collaboration with Dr. Carla Taveggia, similar to our transgenic mice, lentivirally overexpressed HANI and GIEF proteins in DRG neurons strongly promoted myelination by Sc after 7 days in myelinating conditions. HANI and GIEF infected cultures have a considerable increase in number of MBP positive myelin segments (red) compared to a non infected control cultures (not quantified) (Fig. 18B).
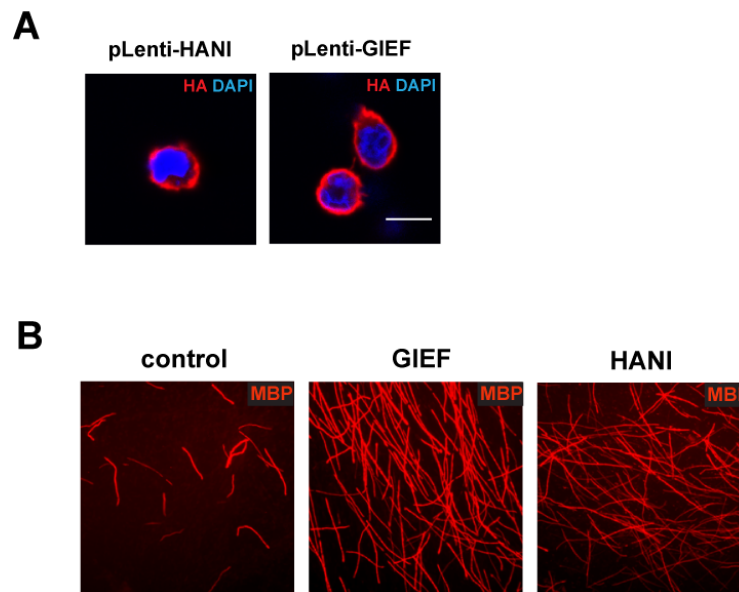
Fig. 18 Lentiviral overexpression of GIEF promotes myelination in DRG-Sc co-cultures.

(A) Functional assessment of viral expression plasmids pLenti6/V5-DEST containing HANI and GIEF expression constructs. Anti HA tag immunocytochemistry (red) was done to detect HANI and GIEF expression in HEK 293T cells 24h post transfection.
(B) Extent of myelination in DRG-Sc co-culture detected by immunostaining for MBP myelin protein (shown in red). Sc were cultured for a week with in the presence of neurons that virally overexpressing HANI or GIEF. Controls represent non infected cultures. Myelination is strongly promoted in co-cultures overexpressing HANI and GIEF compared to controls, as evidenced by the increase in number of MBP positive myelin segments (not quantified).

We therefore used this system for pharmacological treatment with protease inhibitors. Treatment with the BACE1 inhibitor (2µM β secretase inhibitor IV in DMSO) almost completely blocked myelination. Only few MBP positive myelin segments (green) were found after two weeks in myelinating condition (Fig. 19A, upper panel) representing 3.12% of the average number of myelin segments counted in control DMSO treated cultures (Fig. 19A; lower panel). Inhibition of myelination *in vitro* by pharmacological BACE1 inactivation was thus in agreement with the hypomyelination phenotype of BACE1 null mouse mutants. To block ADAMs activity we used a broad spectrum ADAMs inhibitor GM6001 (1µM). After two weeks in myelinating conditions, cultures were stained for MBP and unexpectedly we observed a considerable increase in the number of MBP positive myelin segments (green) when compared to DMSO treated control cultures (Fig. 19A; upper panel) Quantification of MBP positive myelin segments was done on there independent cultures with 2 coverslips per culture. ADAMs inhibitor treatment significantly promoted myelination, such that the average number of myelin segments was increased by 1.9 fold compared to DMSO cultures (100% vs 190.13%±32.5; [**]$p < 0.01$) (Fig. 19A; lower panel). From these experiments we conclude that BACE1 and ADAMs have opposing effects on myelination, possibly

by differential processing of NRG1. Changed number of myelin segments after inhibitor treatment could result from changes in the number of Sc associated with axons. Thus we quantified the number of Sc aligning with axon bundles (Fig. 19B; upper panel). Two independent cultures treated with BACE1 and ADAMs inhibitors were analyzed after one week in myelinating conditions. DAPI-positive Sc nuclei aligning with axon bundles were counted on confocal images (3 coverslips/culture; 3 bundels/coverslip) and percentage average number of nuclei/µm/axon in treated culture relative to control was displayed as a result. BACE1-inhibitor treatment did not significantly change the number of Schwann cells in contact with the axon (Fig. 19B; lower panel). BACE1 treated cultures had almost unchanged number compared to DMSO treated cultures (94%±5.1 vs 100%; p=0.17). In ADAMs inhibitor treated cultures, compared to controls, more Sc aligned with the axons (144%±23.24 vs 100%). However the increase in number was not statistically significant (p=0.09). This result strongly suggests that inhibition of BACE1 and ADAMs induces changes in myelination relevant signalling between axons and Sc rather than a change in the number of myelination competent Sc. We therefore preformed a WB to evaluate changes in the activation of PI3K and MAPK pathways upon inhibitor treatment. Protein lysates from DRG co-culture were immunobloted with the antibodies directed against phosphorylated PI3K and MAPK proteins. Unexpectedly the phosphorylated levels of PI3K and MAPK after inhibitor treatment were unchanged compared to control cultures (Fig. 19C). In a pilot experiment we asked if ADAMs inhibition has similar effects on myelination by oligodendrocytes. Co-cultures of cortical neurons and oligodendrocyte precursors cells (OPC) were treated with the ADAMs inhibitor (1µM) for four days and oligodendrocytes were analyzed. As previously described (Stevens et al., 2002) we could clearly identify in culture 5 stages of oligodendrocyte differentiation towards the mature myelinating stage (Fig. 20A). When we quantified the number of oligodendrocytes with morphology of the developmental stage V (Fig. 20A myelin stage), a 2.14 fold increase in the number of myelinating oligodendrocytes was observed in ADAMs inhibitor treated CNS co-cultures compared to the DMSO treated control cultures (1 vs 2.14±0.32 ; [**]p<0.01) (Fig. 20B). Further studies are required to address if the ADAMs inhibition promotes differentiation or proliferation of oligodendrocytes. Nevertheless, with these experiments we showed that ADAMs activity opposes BACE1 at least *in vitro* to affect the extent of myelination by Sc and oligodendrocytes.

A

B

C
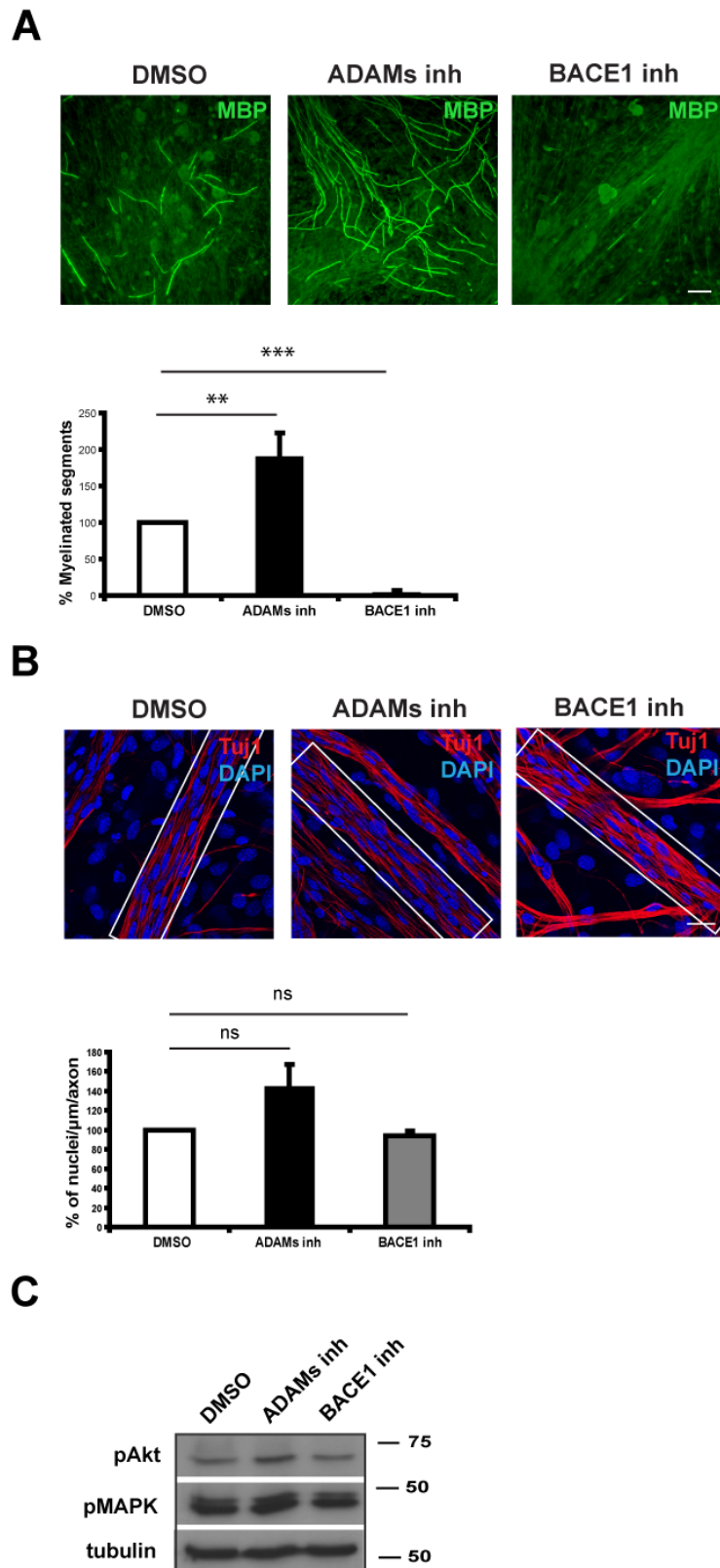
Fig. 19 Inhibition of ADAMs activity promotes myelination in DRG-Sc co-cultures

(A) Effects of ADAMs inhibitor (1 µM GM6001) and BACE1 inhibitor (2 µM β-secretase inhibitor IV) on myelination in DRG-Schwann cell co-culture. Extent of myelination is detected by immunostaining for MBP myelin protein (green) after 2 weeks in myelinating conditions. Treatment with ADAMs inhibitor treatment promoted myelination apparent by the increase in MBP positive myelin segments compared to control DMSO treated cultures. Almost no myelin can be detected in BACE1 inhibitor treated cultures. Scale bar

segments (3 cultures; 2 coverslips/culture) is expressed in percentage relative to the wt ±SEM. Average increase in number of myelin segments is almost two fold after ADAMs inhibition compared to control culture (**p< 0.01). Decrease in number after BACE1 inhibition is significant (***p< 0.001) compared to the control.

(B) Confocal images of the DRG-Schwann cell co-cultures (1 week in myelinating conditions) immunostained for tubulin (red) with DAPI stained nuclei (blue). Example of an axon bundle (boxed) is used for quantification of the Sc association with the axon. Scale bar 20 µm. Two independent cultures were quantified (3 coverslips; 3 bundles/coverslip). Numbers of nuclei/axon /µm are expressed in percentage±SEM relative to the DMSO treated controls. 40% increase after ADAMs inhibition compared to control was not significant (p=0.07). BACE1 inhibition induced 2% decrease compared to control (p=0.17)

(C) WB was performed on DMSO and inhibitors treated DRG Schwann cell co-culture (7 days in myelinating conditions). 40µg of protein was used for WB. The WB was probed with antibodies against pAkt and pMAPK. No change in the amount of pAkt and pMAPK is detected upon inhibitor treatment. β-tubulin was used as a loading control.
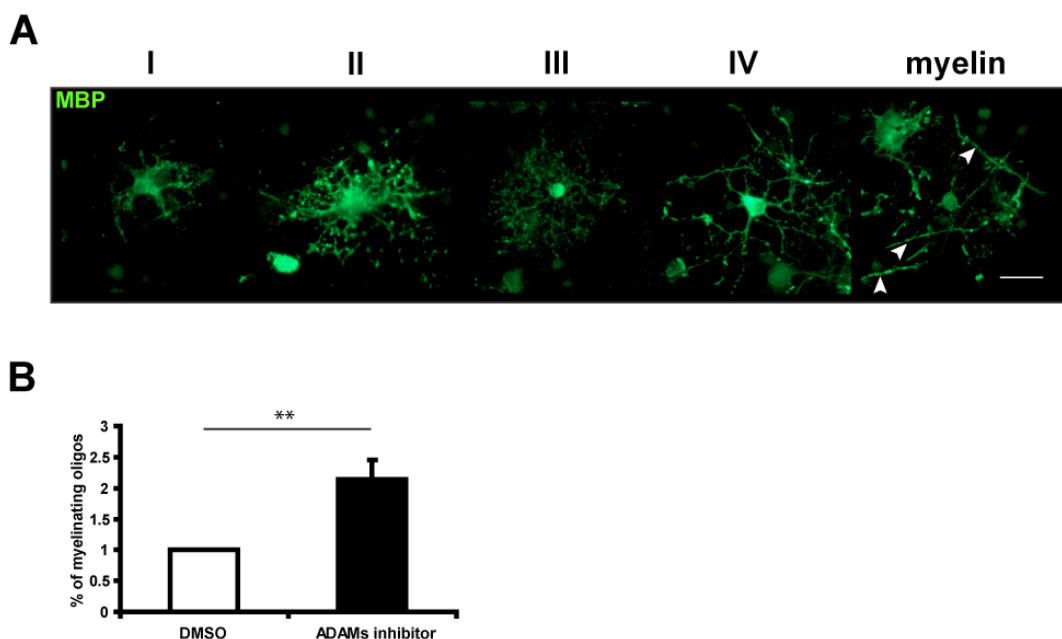
Fig. 20 Inhibition of ADAMs activity promotes myelination in cortical neuron oligodendrocyte co-cultures

(A) Different developmental oligodendrocyte stages with distinct morphology visualized by MBP staining (green) after 4 days co-culture with neurons. The myelinating stage is defined by formation of myelin segments (arrowheads). Scale bar 100µm.

(B) Quantification of the number of myelinating oligodendrocytes in 3 independent cultures (2 coverslips/culture) treated with ADAMs inhibitor (1µM GM6001) and DMSO treated controls. Numbers are expressed as an average percentage±SEM relative to DMSO treated cultures. Inhibition of ADAMs increases the number of myelinating oligodendrocytes by twofold compared to controls (**p< 0.01).

78

5 DISCUSSION

5.1 Transgenic overexpression of tagged NRG1 variants in transgenic mice - advantages and disadvantages of the approach.

The goal of this study was to further explore the role of BACE1 in the NRG1 type III-β_1 mediated control of peripheral myelination, and to decipher the structure of the "active" form of NRG1 type III-β_1 *in vivo*. Furthermore, we wanted to address the subcellular localization of NRG1 in spinal cord motor neurons. For the purpose of this study, we have generated a transgenic mouse line that harbors a Thy1-promoter (Caroni, 1997) driven cDNA encoding a BACE1 processed N-terminally tagged NRG1 type III-β_1 (GIEF).The "GIEF" construct represents an N-terminal fragment of full length NRG1 type III-β_1 tagged at the N-terminus (HANI), resulting after BACE1 cleavage in the stalk region (Fig. 3). We have decided to introduce an HA-tag at the N-terminus due to the lack of the appropriate NRG1 antibodies. This allowed us to detect and follow N-terminal NRG1 fragment supposed to carry the EGF like signaling domain (Wang et al., 2001). Previous studies which successfully analyzed processing of NRG1 proteins *in vitro* also relied on the indirect detection of NRG1 by introducing peptide tags (HA, myc, fluorescent) at different positions of the NRG1 protein (Hu et al., 2008; Shirakabe et al., 2001; Wang et al., 2001; Yokozeki et al., 2007). Alternatively, shedding of the NRG1 was indirectly measured by the level of enzymatic activity detected after release of alkaline phosphatase linked to the NRG1 ectodomain (Horiuchi et al., 2005; Willem et al., 2004). However, this has the disadvantage, that the cell culture system cannot provide the full complexity of the *in vivo* system, thus only allows basic protein characterization. The NRG1 processing pattern observed in cell culture does not necessarily correlate to the *in vivo* situation. In our approach, we went one step beyond the *in vitro* analysis of transfected cells, as we studied NRG1 processing *in vivo*. Transgenic overexpression of the tagged NRG1 variants, "HANI" (Gummert unpublished) and GIEF under the neuron specific Thy1-promoter (Caroni, 1997) allowed us to visualize products of NRG1 type III-β_1 processing. This approach made stage for a more detailed analysis of the processing pattern of NRG1 type III-β_1 *in vivo* especially with regard to the evaluation of the possible further processing of N-terminal protein fragments and the putative release of the EGF signalling domain (Fig. 1). These studies have not been possible previously, since the only reliable NRG1 antibody recognizes the C-terminus of NRG1. Additionally, overexpression of tagged NRG1 variants in neurons creates the venue for answering question of neuronal localization of NRG1 fragments *in vivo*. The levels of the overexpressed proteins are likely to be

above the sensitivity threshold of applied staining methods and the HA-tag enabled us to detect the N-terminus which previously has not been visualized *in vivo*. As the Introduced HA-tag could have an impact on maturation and protein function and we wanted to asses the activity of the GIEF variant in myelination *in vivo,* it was important verify normal intracellular trafficking and targeting as well as preserved function in signalling. Therefore, the integrity and function of GIEF and HANI-variants were confirmed in a battery of *in vitro* experiments, which showed transmembrane localization of GIEF-variant as well as unchanged activity in inducing ErbB receptor dimerization (Fig. 3). Importantly transgenic approaches carry several disadvantages that need to be taken under consideration before interpretation of phenotypes. One disadvantage is the virtual absence of control over the integrated transgene copy number and the transgene integration site. This random integration effect can induce different levels of transgene expression and it is hampering the comparison between two independent transgenic lines. Moreover, the onset of the transgene expression can vary depending on the transgene integration site. Our study addressing the role of NRG1 variants in myelination required that the transgene is expressed early postnatally at the onset of myelination. We have therefore analyzed the onset of transgene expression and expression levels in HANI and GIEF lines before making conclusive statements regarding the myelination phenotypes. Both Thy1 driven transgenes were expressed at P1 at the beginning of myelination similar to previously described Thy1 driven mouse line overexpressing full length wt NRG1 type III-β_1 (Michailov et al., 2004) (Fig. 6). Transgenic overexpression in the GIEF-line was three fold higher when compared to HANI (Fig. 6) which was taken under consideration when phenotypes were compared. Taken together, transgenic NRG1 mouse lines used and generated in our study have satisfied experimental criteria necessary to reveal if BACE1 processing activates NRG1 *in vivo.* Additionally, overexpression of tagged NRG1 variants in neurons created the opportunity to address the transport and localization of NRG1 *in vivo.*

5.2 BACE1 activates NRG1 type III-β_1 to promote myelination

Myelin formation is controlled to provide optimal conduction properties of myelinated fibers, which are necessary for functional integration of the nervous system (Waxman, 1997). Structural parameters, such as myelin sheath thickness and internodal length, are not randomly chosen but strictly defined relative to axon diameter to provide millisecond precision in neuronal signal transmission. The identity of one of the axonal signals that regulate myelin sheath thickness was revealed 50 years later after the question was asked (Rushton, 1951) with the identification of axonal membrane

derived growth factor NRG1 type III-β_1 (Michailov et al., 2004). The amount of NRG1 type III presented to the Sc was found to be a measure of axon diameter that signalls to the Sc how many myelin wraps to produce. To generate a mature signalling fragment, NRG1 type III-β_1 is believed to be proteolytically cleaved. Recent work discovered a physiological role of BACE1 in myelination (Hu et al., 2006; Willem et al., 2006). Lack of BACE1 in mouse mutants causes hypomyelination similar to the previously described phenotype of NRG1 type III heterozygous mice (Michailov et al., 2004). The similarity of these phenotypes led to the conclusion that the phenotype observed in BACE1-/- mice is linked to impaired NRG1 processing. Even though the inactivation of BACE1 induces accumulation of full length NRG1 type III-β_1 in the brain, it is not known if impaired processing of NRG1 also occurs in the PNS and thus whether a direct functional link exists between BACE1 and NRG1. Transgenic overexpression of the epitope-tagged GIEF construct, mimicking BACE1 processing of the tagged NRG1 type III-β_1 (HANI), induces hypermyelination in the PNS (Fig. 9). Very similar to full length NRG1 type III-β_1 (HANI). This is compatible with the hypothesis that BACE1 cleaves NRG1 type III-β_1 in the stalk region to generate a protein fragment which is competent in promoting myelination *in vivo*. This is the first *in vivo* observation of a functional interaction between BACE1 and NRG1 type III-β_1 in myelination. As the GIEF fragment alone is sufficient to induce hypermyelination *in vivo*, we conclude that back signalling to the nucleus by the cytoplasmic tail of NRG1 (Bao et al., 2004; Bao et al., 2003) does not play a role in myelination promotion by NRG1 type III-β_1. The effect of the GIEF fragment on myelination seems to be specific for its primary structure rather than the paracrine signalling mode. Another type III isoform highly expressed in PNS neurons known as SMDF (Ho et al., 1995; Schroering and Carey, 1998) only differs from the GIEF-variant by the EGF-β_3 domain. Neuronal overexpression of NRG1 type III-β_3 under control of the neuron specific enolase (NSE) promoter has no effect on myelination despite the incredible structural similarity to the GIEF-variant (Gomez-Sanchez et al., 2009). Indeed, biochemical analysis of NRG1 type III-β_3 suggest a topological model in which its C-terminus interacts with the membrane and bends the extracellular part of the protein possibly creating different signalling by the EGF-β_3 domain (Cabedo et al., 2002). Thus, it is possible that processing by BACE1 is important to create a specific EGF domain environment, which is competent for myelination. Inactivation of all type III isoforms induces a 50% reduction in the number of spinal motor and sensory neurons (Wolpowitz et al., 2000). It has been speculated that the mechanism of NRG1 type III, which mediates neuronal survival involves back signalling by its C-terminus. Considering the fact that NRG1 type III-β_3 does not contain a cytoplasmic tail, the type III-β_1 isoform represents a mayor candidate for NRG1 type

III mediated neuron survival. Taken together, we propose that NRG1 type III-β_1 evolved to serve two distinct independent functions in neuronal cells that are mediated by its N-terminal and C-terminal domains. After proteolytic cleavage by BACE1 or/and other proteases, the N-terminal fragment harboring EGF serves a myelination function by forward signalling, whereas the C-terminus ensures neuronal survival by back signalling.

5.3 Ectopic myelination in mice overexpressing BACE1 cleaved NRG1 type III-β_1

NRG1 type III is an instructive signal for the binary choice between axon ensheathment and myelination (Taveggia et al., 2005). Small caliber axons (<1µm) expressing low dosage of NRG1 type III are not myelinated but ensheathed by a nmSc, which results in formation of Remak bundles. Proper formation of Remak bundles has been shown to be sensitive to the dosage of NRG1 type III (Taveggia et al., 2005). Mice haploinsuficient for the type III-isoform have aberrantly organized Remak bundles with axons unsegregated by the nmSc cytoplasm. Overexpression of the GIEF variant on small caliber axons induces ectopic myelination (Fig. 10). Thus, axons normally found in Remak bundles are sorted out and acquire a compacted myelin sheath. We also observed the formation of myelinated Remak bundles containing unsegregated axon fibers (Fig. 10). Otherwise, Remak bundles did not show major structural aberrations, as they display normal gross morphology with properly segregated axons (Fig. 10). Taken together, nmSc appear to be less sensitive to the increased doses of the GIEF variant than mSc. It is very interesting that in contrast to GIEF overexpression, NRG1 type III-β_3 overexpression in neurons induces major disturbances of Remak bundles (Gomez-Sanchez et al., 2009). Most of the Remak bundles have unsegregated axons and ~ 20% of the Remak bundles are myelinated. Even though we are comparing two different transgenic lines, it is tempting to speculate that after initial ensheathment versus myelination choice, which is defined by NRG1 type III-β_1 correct structural organization of the Remak bundle depends more on type III-β_3 isoform. In light of all these findings it is also possible that the Remak bundle phenotype observed in NRG1 type III +/- mice (Taveggia et al., 2005) is caused manly by the loss of the β_3 isoform but not by the β_1 isoform.

5.4 GIEF and HANI are equally potent in promoting myelination

Activation of the PI3K-pAkt pathway was shown to be required for the initial events of myelination *in vitro* (Maurel and Salzer, 2000). Accordingly increasing PI3 kinase activity induces downstream pAkt and promotes myelination in DRG-Sc co-culture

(Ogata et al., 2004). PI3K-pAkt activation was shown to be mediated by axonal surface presented NRG1 type III-β_1 *in vitro* (Taveggia et al., 2005). Although overexpression of NRG1 type III-β_1 and hypermyelination are not clearly coupled to an upregulation of the PI3K-pAkt pathway in transgenic mice (Humml unpublished observation), constitutive activation of the PI3 kinase pathway by conditional inactivation of PTEN in Sc induces hypermyelination and tomacula formation (Göbbels et al., submitted). GIEF overexpression induced formation of tomacula, which are similar in structure to the tomacula observed in PTEN mutants (Fig. 12). Originally, we hypothesized that the GIEF variant represents a "ready to signal" NRG1 type III-β_1 variant which might be more potent in activating Akt. However, quantification of tomacula revealed that the phenotype is very mild in comparison to PTEN mutants. Myelin in GIEF transgenic mice, aside from mild tomacula formation, has a normal ultrastructure and increased myelin thickness is a result of an additional myelin membrane wraps (Fig. 9). Moreover, analysis of HANI transgenic mice revealed the same potency to induce tomacula (Fig. 12). This was unexpected considering the three-fold higher expression of the GIEF-variant compared to HANI. Similarly, HANI and GIEF transgenic mice also displayed a comparable level of hypermyelination as g-ratios values are not significantly different (Fig. 12). This could be explained by a saturating effect of ErbB2/ErbB3 receptor heterodimers by increased levels of NRG1. The available amount of receptors for NRG1 ligand binding might be below the capacity to fully translate the increased NRG1 signal into a corresponding increase in activity of the p-Akt signaling pathway. By PTEN inactivation p-Akt is activated downstream of the receptor level and the saturation effect is omitted resulting in a severe tomacula phenotype. It is also likely that the activation of alternative pathways downstream of p-Akt strongly depend on specific ligand-receptor complexes. Tomacula formation of the PTEN mutants is mediated through the m-Tor pathway (Göbbels et al., submitted) known for it implication in cell mass growth and tumorigenesis (Liu et al., 2009; Wullschleger et al., 2006). As the exact mechanisms of myelin membrane growth are still not known, it is possible that HANI and GIEF overexpression activate alternative pathways that enhance myelin growth, which is distinct from the cell mass growth induced by the m-TOR pathway.

5.5 Absence of the Sc proliferation upon GIEF overexpression

NRG1 induces proliferation of Sc *in vitro* (Dong et al., 1995; Lemke and Brockes, 1984; Levi et al., 1995). However, in most cases a recombinant EGF domain of NRG1 was used in these experiments. A role of NRG1 type III in Sc survival was also shown. Inactivation of NRG1 type III isoforms reduces the numbers of Sc precursors

(Wolpowitz et al., 2000). However, neuronal overexpression of the NRG1 type III-β_1 *in vivo* does not effect the proliferation of Sc (Michailov et al., 2004). In a recent study, *in vivo* overexpression of NRG1 type III-β_3 induced the proliferation of nmSc but not mSc (Gomez-Sanchez et al., 2009). Overexpression of GIEF, which is very similar in structure to type III-β_3, did not effect the proliferation of both mSc and nmSc (Fig. 11). It has been shown previously that two major pathways activated in Sc upon NRG1 signaling (MAP kinase and PI3 kinase) serve opposing function in the process of Sc differentiation (Ogata et al., 2004). Thus, it is possible that a difference in the primary structure of a NRG1 ligand can engage ErbB2/ErbB3 receptors differentially resulting in a different biological response of Sc. Moreover, NRG1 affects also differentiation of Sc. Stimulation by NRG1 in cell culture promotes differentiation of SCP (Dong et al., 1995). Viral overexpression of the HANI variant of NRG1 type III-β_1 in DRG neurons promotes myelination in co-culture (Fig. 18). In addition, overexpression of GIEF in DRG-Sc co-culture recruited more Sc to myelinate resulting in increased number of myelin segments in DRG-Sc co-culture. Overexpression of GIEF *in vivo* did not recruit more SCP to further differentiate towards myelinating phenotype showed by the unchanged number of Krox 20 positive Sc (Fig. 11). *In vivo* overexpression of GIEF affected apparently only myelinating Sc in the close contact with the axon, in the final phase of the myelination process. Mechanisms adjusting the number of Sc to the number of myelin segments during development (Grinspan et al., 1996; Syroid et al., 1996) are not affected by the GIEF overexpression similar to the overexpression of NRG1 type III-β_1 (Michailov et al., 2004)

5.6 NRG1 promotes myelination in the absence of BACE1: Implications for the existence of compensatory mechanism.

BACE1 mutants and transgenic mice were generated to support the efforts in establishing therapeutic approaches in Alzheimer disease (AD) (Willem et al., 2009). Their analysis revealed that overexpression of BACE1 promotes production of amyloid β peptide, whereas inactivation of BACE1 completely abolished APP processing (Dominguez et al., 2005; Willem et al., 2004). However, inhibition of BACE1 as a therapy of Alzheimer disease was shaded after the discovery that inactivation of the BACE1 causes hypomyelination (Hu et al., 2006; Willem et al., 2006). NRG1 as a substrate of BACE1 was implied to be responsible for this effect. We here show for the first time *in vivo,* that BACE1 contributes to the activation of NRG1 during myelination. However, this contribution is surprisingly mild as NRG1 type III-β_1 is still capable to induce hypermyelination in the absence of BACE1, albeit with reduced potency (Fig. 13). Complete absence of NRG1 type III *in vivo* results in reduced numbers of Sc in

sciatic nerve (Wolpowitz et al., 2000). Cultured DRG neurons from type III -/- mice are not myelinated by Sc *in vitro* (Taveggia et al., 2005). It is therefore intriguing that even though thickness is greatly reduced, compact myelin still forms in the absence of BACE1 *in vivo*, similar to the NRG1 type III +/- mice. This suggests that some NRG1 type III activity persists in the absence of BACE1 and/or that other molecules can signal a "baseline" myelination program *in vivo*. Surprisingly, overexpression of the HANI-variant with absence of BACE1, albeit at reduced levels induces hypermyelination (Fig. 13). This finding can be explained by compensatory processing by other proteases, such as ADAM17, ADAM19 or (partial) myelin-promoting competence of uncut NRG1 type III. Biochemical analysis of protein extracts from spinal cord and sciatic nerve of HANI-transgenic mice with absence of BACE1 will allow to address this question. It will be interesting to see if in the absence of BACE1, GIEF is more potent than HANI in promoting myelination. In that case, we could suggest the relevance of BACE1 over compensatory proteases in NRG1 activation for myelination. Taken together myelination by NRG1 type III-β_1 only partially depends on BACE1.

5.7 Does BACE1 cut twice to activate NRG1?

The function of NRG1 in myelination is restricted to the type III NRG1 isoform as overexpression of the type I isoform does not induce hypermyelination (Michailov et al., 2004). According to the current concept of NRG1 signalling, type I and II isoforms signal in a paracrine manner through a shedded EGF like domain and type III isoforms mediate paracrine signalling (Falls, 2003). Moreover, it has been shown that virally overexpressed NRG1 type III-β_1 in DRG neuron presents its EGF domain bound to the membrane (Taveggia et al., 2005). Accordingly, it is thought that axonally presented NRG1 type III-β_1 juxtacrine signal is essential for NRG1 function in myelination. Nevertheless recently, based on *in vitro* biochemical analysis recently, has been speculated that the EGF domain of type III is released once the first myelin wraps are formed to complete myelin maturation in a paracrine signaling manner (Birchmeier and Nave, 2008). The subsequent cleavage and release of NRG1 type III after ErbB receptor binding makes sense in terms of signaling promotion. It has been shown the NRG1 signalling in neurons by ErbB4 requires receptor internalization to activate PI3K and MAPK pathways. This occurs only with the soluble ligands (Liu et al., 2007). After initial receptor binding, the release of the membrane tethered ligand also could enhance receptor dimerization and downstream signaling by increasing diffusion of the receptor-ligand complex (Blobel, 2005). Both BACE1 and ADAMs proteases are candidates for the second cleavage releasing the EGF domain (Willem et al., 2009).

Analysis of the processing pattern of full length NRG1 type III-β_1 and BACE1 processed GIEF, strongly suggests that the GIEF-variant results from BACE1-mediated processing of HANI. The ~70kD protein product resulting from BACE1 cleavage of HANI *in vitro* exactly corresponds in size to the GIEF-isoform on a WB (Fig. 4). In addition, WB analysis of spinal cord lysates from HANI and GIEF overexpressors revealed that the GIEF-variant corresponds in size to the N-terminal product of HANI cleavage (Fig. 4). Moreover, the existence of two bands (~70kD and ~38kD) in cells transfected with GIEF construct and spinal cord lysates suggest further processing in the extracellular domain. At least *in vitro,* no evidence was obtained that this processing is BACE1 mediated (Fig. 4), as the processing pattern in the GIEF transfected cell lysates remained unchanged after cotransfection with BACE1 and application of the BACE1 inhibitor. Application of the broad spectrum ADAMs inhibitor also did not influence processing pattern of both HANI and GIEF proteins *in vitro* (Fig. 4). Thus we can not exclude the presence of additional proteases different from BACE1 and ADAMs in HEK239T cells such as nardilysin (Ohno et al., 2009) that cleaves NRG1 under baseline conditions and that the activity of this protease was not affected by our manipulations. After breeding our transgenic lines to BACE1 mutants, we will also test *in vivo* if a second cleavage by BACE1 occurs. Finding that overexpression of GIEF promotes myelination *in vivo* strongly indicates that NRG1 type III-β_1 is cleaved by BACE1 in the stalk region to be activated for myelination function. Furthermore, analysis of the hypermyelination status of GIEF transgenics in a BACE1 null background will allow us to address whether BACE1 mediates a second processing step that is required for the myelination promoting function of GIEF. This will provide a more detailed picture of the structure of an NRG1 signaling complex responsible for myelination.

5.8 Localization of NRG1 in neurons *in vivo*

Studies of the trafficking and subcellular localization of NRG1 have been hampered by the lack of appropriate antibodies and sensitivity levels of the staining methods. Our transgenic mouse lines that overexpress HA-tagged NRG1-variants offer an opportunity to investigate the subcellular localization of NRG1 in neurons *in vivo.* By immunostaining with antibodies directed against the N- and C- terminus of NRG1, we were able to show that N- and C- terminal protein products colocalize at the cell surface of spinal cord motor neurons (Fig. 14). WB analysis of spinal cord protein lysates identified a ~70kD N-terminal fragment resulting after processing of the 140kD full length NRG1 (Fig. 17). We suggest that NRG1 is transported to the cell surface to be processed by BACE1. However, processing might already occur in the Golgi

compartment. Thus, even though N- and C-terminal fragments colocalize on the cell surface of transgenic mice that overexpress full length NRG1 type III-β_1, it is possible that they are delivered to the membrane already separated by the cleavage in the stalk region. Available BACE1 antibodies did not produce conclusive information about the subcellular localization of BACE1. Therefore, to further elucidate the site of NRG1 cleavage by BACE1 it will be necessary to perform WB analysis after subcellular fractionation, which will allow us to identify if NRG1 is already processed in the intracellular compartment. The GIEF variant is strongly enriched within the intracellular vesicular compartment, but also detected at the cell surface of spinal cord motor neurons (Fig. 14). Endogenous NRG1, detected by the C-terminal antibody is localized in patchy pattern on the neuronal surface which could correspond to lipid rafts micro domains. Interestingly, the endogenous C-terminal fragment occupies distinct membrane microdomains when compared to the GIEF variant. Thus, N- and C-terminal fragments are transported to a distinct membrane compartments. Accordingly, the GIEF variant would than localize to non lipid raft domains. These findings are in line with previously described biochemical assays which revealed that full length NRG1 and the C-terminal fragment harboring the transmembrane domain localize to the lipid raft membrane fraction in transfected cells (Frenzel and Falls, 2001). In contrast, the HA tagged N-terminal fragment was detected in a non lipid raft membrane fraction. In this study lipid raft localization was suggested to be significant for NRG1 signalling. This is in agreement with the proposed function of lipid rafts in the compartmentalization of signaling complexes and formation of platforms for proteolytic processing (Brown and London, 2000; Simons and Ikonen, 1997; Simons and Toomre, 2000). Indeed, *in vitro* studies showed that the processing of NRG1 by ADAM19 takes place within lipid raft microdomains (Wakatsuki et al., 2004). BACE1 is also compartmentalized to lipid rafts (Riddell et al., 2001) and it is possible that NRG1 type III-β_1 processing by BACE1 requires lipid raft colocalization. After processing of the full length NRG1 N-terminal fragment is probably released to the non lipid raft microdomain. We also found that the transport of NRG1 into the axonal compartment is limited. While wt and transgenic variants of NRG1 were prominently expressed in spinal cord motor neurons, sciatic nerve expression was very low or even undetectable (Fig. 14, Fig. 15, Fig. 16, Fig. 17). Strong overexpression in the GIEF transgenic line increased protein transport into the sciatic nerve above a level that allowed immunodetection. Immunostaining of sciatic nerve cross sections identified an HA-tagged N-terminal fragment on the axonal membrane. Moreover, vesicles containing the N-terminal fragment were present in the axonal lumen presumably transporting the N-terminal fragment from the neuronal cell body. It is still an open question to which extent the C-terminus is transported in to the

axon at all since it was not detected in sciatic nerve of NRG1 overexpressing mice (Fig. 15, Fig. 16, Fig. 17,). In contrast to our findings authors of the study analyzing NRG1 levels in sciatic nerve of wt and Erbin mutant mice detected by WB full length NRG1 protein of 140kD and ~60kD processed C-terminal fragment (Tao et al., 2009). We assume that by increasing in protein levels in the homozygous HANI mice will allow us to resolve this question. Taken together, our findings suggest that the regulated transport of NRG1 into the axon serves as a mechanism to provide appropriate level of NRG1 on the axonal membrane for myelination control compatible with the finding that the amount of NRG1 rather than ErbB receptors appears to be rate limiting for myelin formation (Michailov et al., 2004). Therefore, the amount of NRG1 in the nerve must be tightly regulated to produce the appropriate amounts of myelin. Indeed, our data show that only a fraction of the synthesized NRG1 is transported into the axonal compartment as we detect only small amounts of NRG1 in the sciatic nerve by WB and immunostaining. The identity of the mechanisms involved in regulation of axonal trafficking of NRG1 is currently unknown. We speculate that proteolytic cleavage could be one of the checkpoints. It is also possible that transport into the axon is regulated by the level of endosomal vesicle release. Taken together, we propose that NRG1 accumulates in lipid rafts and it is transported to the neuronal surface to be proteolyticaly cleaved by BACE1. Subsequently, the N-terminal fragment diffuses into non-lipid raft compartments from where it is internalized and transported into the endosome. Vesicles containing NRG1 are subsequently transported from the recycling endosome into the axon and integrated into the axonal membrane. The C-terminal fragment most likely stays behind in the neuronal soma to mediate neuronal survival by back signalling to the nucleus.(Fig. 21).
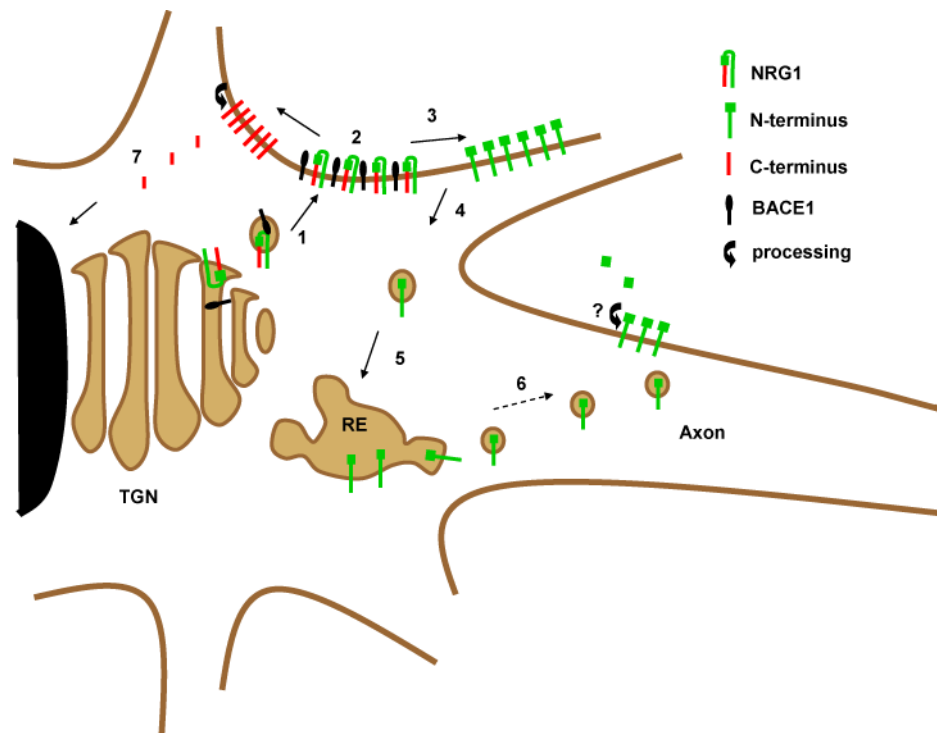
Fig. 21 Model of NRG1 trafficking in neurons

(1) Synthesized NRG1 and BACE1 transported in vesicles from trans-Golgi network (TGN) to the neuronal cell surface. After proteolytic processing (2) NRG1-N-terminal fragment (green) is localized to distinct membrane compartment (3) to NRG1-C-terminal fragment (red). N-terminal fragment is than internalized (4) and transported to recycling endosome (RE) (5). From RE vesicles containing NRG1-N terminus are transported to the axon (6) and integrated into the membrane. N-terminus on axonal membrane is potentially further cleaved (labeled with question mark) to release the EGF-like domain. C-terminus most likely remains in the neuron soma to mediate back signalling to the nucleus (7).

5.9   Inhibition of ADAMs proteases stimulates myelination *in vitro* u

We have shown that BACE1 is required to fully activate the myelination promoting function of NRG1. However, the potential of overexpressed NRG1 to promote myelination remains, albeit at lover levels, even in the absence of BACE1. Therefore, we wanted to investigate possible processing of NRG1 by other proteases in the absence of BACE1. Members of the ADAMs family, ADAM17 and ADAM19, which have been shown to mediate NRG1 cleavage *in vitro* (Horiuchi et al., 2005; Shirakabe et al., 2001) and are attractive candidates. Unexpectedly, inhibition of ADAMs activity in DRG-Sc co-cultures by a broad spectrum inhibitor (GM6001) promoted myelination and increased the number of myelin segments by twofold in comparison to control culture (Fig. 19). We speculate that this effect might also be observed *in vivo* as DRG co-cultures replicate other *in vivo* effects. For instance, BACE1 inhibition almost completely abolished myelination, and viral overexpression of GIEF and HANI-variants in DRG neurons promoted myelination, very similar to finding in transgenic mice (Fig. 18,Fig. 19). The molecular targets and mechanisms responsible for this effect are

currently not clear. However, we found that the association of Sc with the DRG axons is largely unchanged upon treatment with ADAMs and BACE1 inhibitors. This would suggest that proteolytic processing is not required for the initial stage of Sc-axon association but controls axo-glial signalling after an initial contact has been established (Fig. 19). Nevertheless, PI3K and MAPK activities were not significantly changed upon inhibitor treatment (Fig. 19). However, it is possible that other downstream signalling cascades involved in Sc differentiation are affected by the treatment such as calcineurin/NFAT, shown to be activated in Sc after addition of NRG1 *in vitro* (Kao et al., 2009). Even though the ADAMs inhibitor is not specific for ADAM17, it blocks ADAM17 activity in low-nanomolar concentrations (Moss and Rasmussen, 2007) Based on the importance of NRG1 signalling in PNS myelination (Michailov et al., 2004), one obvious explanation is therefore that inhibition of ADAM17 activates NRG1 to promote myelination. This hypothesis implicates that proteolytic processing can also negatively regulate NRG1 signalling, which is beyond the simple model of proteolysis mediated activation. APP can be cleaved by BACE1 and ADAM17 to produce two functionally different protein fragments (Turner et al., 2003). Therefore, it is possible that a similar scenario exists for NRG1 processing. While currently, no data directly connect ADAMs inhibition with NRG1 processing it will be interesting to study if the GM6001 inhibitor can promote myelination or remyelination after nerve crush *in vivo*. This would open and avenue for the therapy of peripheral neuropathies. Interestingly, we observed a similar effect of ADAMs inhibition in co-cultures of CNS neurons and oligodendrocytes. Here the number of myelinating oligodendrocytes was increased by twofold compared to control cultures (Fig. 20). It will be an important task for future experiments to determine if the effect is a consequence of induced oligodendrocytes proliferation at if ADAMs inhibition mainly affects post mitotic oligodendrocytes. It is tempting to speculate that treatment with ADAMs inhibitor could be used in future as a potential treatment to stimulate OPC differentiation in MS lesions and repair of damaged myelin sheaths.

6   SUMMARY AND CONCLUSIONS

NRG1 type III-β_1 is a master regulator of peripheral myelination (Michailov et al., 2004; Taveggia et al., 2005). It has been suggested that NRG1 isoforms undergo proteolytic cleavage to generate mature signalling ligands (Mei and Xiong, 2008). Although NRG1 processing by the ADAMs family of metalloproteases has been widely studied, (Horiuchi et al., 2005) the identity of the protease activating NRG1 type III and the exact structure of signaling fragment that regulates myelination remained elusive. Recently studies of BACE1-/- mutants revealed hypomyelination of the PNS axons and described a physiological role of BACE1 in the PNS myelination (Willem et al., 2006). Even though processing of the type III NRG1 isoform by BACE1 has been shown *in vitro* (Hu et al., 2008) the importance of BACE1 processing for NRG1 type III-β_1 mediated myelination *in vivo* has not been directly demonstrated.

Neuronal overexpression of a NRG1 variant mimicking BACE1 processed NRG1 type III-β_1 in transgenic mice promotes myelination in the PNS similar to the full length NRG1 protein. This result strongly suggests that BACE1 processing occurs *in vivo* to activate NRG1 type III-β_1 in myelination. Thereby we also showed that back signalling by cytoplasmic tail of NRG1 type III-β_1 is not required for the myelination promoting function against previous speculations. Our finding also implies different signalling function of type III-β_1 and type III-β_3 NRG1 isoforms.

We could show that BACE1 cleavage in the stalk region functionally activate NRG1. Analysis of the processing pattern of NRG1 type III-β_1 *in vivo* and *in vitro* support this first opening cut. *In vitro* analysis shows no evidence that BACE1 further cuts NRG1 to release EGF domain, but our results strongly suggest cleavage by another protease. Analysis of the myelination as well as biochemical analysis of mice with GIEF overexpression in the absence of BACE1 will resolve whether second cleavage step by BACE1 occurs *in vivo* and whether it is necessary for the function in myelination.

BACE1 overexpression does not further promotes myelination in NRG1 type III-β_1 overexpressing mice. In the absence of BACE1, overexpressed NRG1 type III-β_1 retains the potential to promote myelination, albeit to the less extent showing for the first time functional interaction between BACE1 and NRG1 *in vivo*. It remains to be elucidated if BACE1 activity is compensated by another protease or NRG1 function in myelination can be independent of processing mediated activation.

NRG1 protein fragments localize to the cell surface of spinal cord motor neurons and the transport into axonal compartment is limited. Proteolytic processing represents possible rate limiting step for the axonal transport.

Inhibition of the ADAMs proteases promotes myelination *in vitro*. This finding presents potential approach to stimulate myelination in demyelinating diseases. Whether NRG1 participates in the effect observed with ADAMs inhibitor is not clear, but could be possible mechanism of proteolytic inactivation of NRG1.

7   APPENDIX

Despite the fact that the following project was discontinued, I will briefly introduce and discus it in the following chapter. I have attempted to generate a NRG1-antibody fusion protein, as an experimental therapy in a mouse model of Multiple sclerosis (MS). This project, done in collaboration with Dr. Moses Rodriguez at Mayo clinic USA, led to the identification of an antibody that following intraperitoneal injection (i.p.) binds to axons in the spinal cord of Theiler's murine encephalomyelitis virus (TMEV) mediated mouse model of MS.

7.1   NRG1 as a potential therapy of MS

Multiple sclerosis is a chronic progressive inflammatory demyelinating disease of the CNS. MS is the most common cause of neurological disability in the world population affecting more than 2.5 million individuals (Hauser and Oksenberg, 2006). Pathological hallmarks of the disease are focal plaques of demyelination characterized by inflammation, axonal loss and gliosis (Bruck, 2005). T-cell and antibody mediated inflammatory mechanisms and oligodendrogliopathies lead to the myelin damage in the lesions (Lassmann et al., 2001) impeding axonal saltatory conduction. Clinical manifestations in the early phase of the disease are believed to result form the inflammatory reactions due to the recurrent autoimmune attacks (Bruck, 2005). Later on, axonal injury in MS plaques (Ferguson et al., 1997; Trapp et al., 1998) further contributes to the loss of neuronal functional integrity and it is thought to be the main cause of neurological symptoms in the progressive phase of the disease (Trapp and Nave, 2008). Remyelination in MS plaques is a beneficial regenerative process that can restore the conduction velocity and appears to confer axonal protection (Irvine and Blakemore, 2008; Kornek et al., 2000). Unfortunately, the extent of remyelination in the course of MS is inefficient and inadequate, leaving the majority of lesions largely demyelinated (Franklin, 2002). During remyelination myelin sheaths are formed by newly differentiated oligodendrocytes from OPCs pool residing in the CNS (Blakemore and Keirstead, 1999; Gensert and Goldman, 1997). It is not clear why remyelination fails in MS. Critical points in the process of remyelination are recruitment of the OPCs into demyelinated regions, proliferation and subsequent differentiation resulting in formation of new myelin sheaths (Franklin and Ffrench-Constant, 2008). Therefore, stimulation of these processes could potentially increase the efficiency of remyelination. This in turn would lead to restored functional integrity of CNS axons and improvement clinical picture in MS patients.

NRG1, given its role in the oligodendrocyte development is one of the candidates for stimulation of OPCs differentiation in MS. Immature oligodentrocytes fail to develop in cultured spinal cord explants derived from NRG1 null mutants (Vartanian et al., 1999). Proliferation and survival of OPCs and oligodendrocytes *in vitro* is stimulated after addition of NRG1 (Canoll et al., 1996). Similarly increasing NRG1 levels in optic nerve *in vivo* also promotes survival of oligodendrocytes (Fernandez et al., 2000). Astrocytic NRG1 has been found to be decreased in MS lesions suggesting that altered levels of NRG1 contribute to the disturbed homeostasis in MS lesions (Viehover et al., 2001). Therapeutic attempts employing recombinant NRG1 to stimulate remyelination have previously been carried out. Systemic application of the recombinant NRG1 in mice with experimental autoimmune encephalomyelitis (EAE) improved the extent of remyelination in this model (Cannella et al., 1998; Marchionni et al., 1999). In a follow up study in which recombinant NRG1 was directly injected in to the gliotoxin-induced demyelinated CNS lesion, no improvement in remyelination was observed (Penderis et al., 2003). In light of the fact that the underlying pathology in EAE models is to a great extend caused by inflammatory immune system responses, the beneficial effect of NRG1 on remyelination in this model was probably due to modulation of immune responses as no improvement in myelination was found in gliotoxin model. The NRG1 isoform used in previous experiments is the type II isoform differ from the type III shown to promote myelination in PNS (Michailov et al., 2004). It is believed that NRG1 type III signals in a juxtacrine manner while the type II isoform signals in a paracrine fashion. It has been speculated that the failure of NRG1 to promote myelination in the gliotoxin model is due to the inadequately presented NRG1 signal. Previous studies underscore this hypothesis: Addition of recombinant NRG1 to oligodendrocytes in culture was shown to block differentiation and induce dedifferentiation of matured oligodendrocytes (Canoll et al., 1999; Canoll et al., 1996). A similar de-differentiation effect was observed in DRG neuron-Sc co-cultures (Zanazzi et al., 2001). Based on these findings by it was hypothesized that a possible way to promote myelination in the CNS could be achieved by elevating the levels of axonally presented NRG1 type III. Indeed, overexpression of NRG1 type III in neurons under transcriptional control of the Thy1 promoter induces early onset of myelination in optic nerve and hypermyelination in the corpus callossum of transgenic mice (Brinkmann et al., 2008).

We therefore hypothesized that for NRG1 to be effective in remyelination NRG1 has to be delivered to the surface of demyelinated axons following systemic administration. To direct recombinant NRG1 to the surface of demyelinated axons, we thought to create a fusion protein composed of the NRG1 EGF-like domain coupled to the variable region of a single chain antibody recognizing axonal surface epitope. Theoretically, this would

allow NRG1-antibody fusion product to cross the disrupted blood brain barrier (BBB) in MS and to bind to the demyelinated axons increasing the levels of NRG1 on their surface. This in turn could potentially induce remyelination given that mere elevation of NRG1 protein levels on axonal surface is sufficient for oligodendrocytes to initiate the complete remyelination program.

7.2 Characterization of the axon binding antibody from IgM auto antibody repertoire

The first step towards generation of single chain antibody-NRG1 fusion protein is to identify an axon-specific antibody that will bind to CNS axons after i.p. injection in a mouse model of MS. We have tested a repertoire of human and mouse natural IgM and IgG autoantibodies for axon binding properties. These antibodies were obtained from the Mayo Clinic archive (Rochester, MN). Human derived antibodies originate from sera of patients suffering from Waldenström syndrome, multiple myeloma, monoclonal gammopathy (Rodriguez et al., 2009) and from human fetal cord blood B-cell clone derived hybridoma (Warrington et al., 2004). Natural autoantibodies are polyreactive to self antigens and serve as effectors of rapid immune response to pathogens (Coutinho et al., 1995). These antibodies were of great interest for our re-myelination approach, because of previous findings showing that sHIgM22 antibody from this repertoire enters the CNS after i.p. injection and binds to oligodendrocytes to stimulate remyelination in a TMEV mouse model of MS (Warrington et al., 2000). For preliminary characterization we have tested the binding properties of these antibodies on acute unfixed 225 μm thick spinal cord cross sections. The unfixed tissue was used to preserve native structure of the epitopes. A subset of antibodies which were found to bind in a preliminary analysis, were tested on acute unfixed longitudinal spinal cord sections of the TMEV infected mice (4 moths post infection). Floating sections were incubated with IgM antibodies and fluorescently labeled for microscopy. Imaging of the lateral column of spinal cord revealed that antibodies sHIgM42 showed axonal distribution pattern (Fig. 22; arrowheads). The sHIgM42 antibody has been previously shown to bind to cerebellar granule cells and promote neuronal outgrowth in culture (Warrington et al., 2004). The oligodendrocyte-binding rIgM22 antibody was localized to axonal tracts in the spinal cord. Two additional antibodies, mIgM79.08 and CB2bG8, were found to label spinal cord resident cells possibly astrocytes.
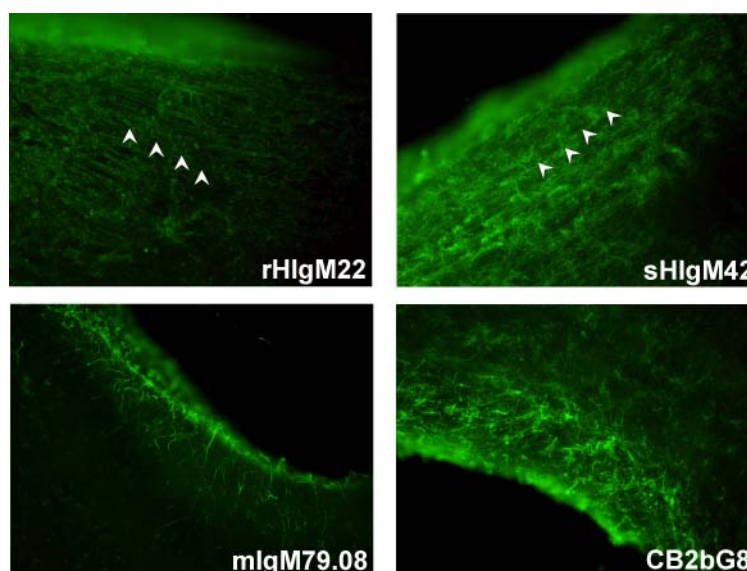
Fig. 22 Characterization of IgM auto-antibodies for axon binding in the mouse spinal cord

Characterization of IgM auto-antibodies for axon binding in the mouse spinal cord
Acute floating longitudinal sections (225µm) of spinal cord labeled with HIgM antibodies rHIgM22, sHIgM42, mIgM79.08, CB2bG8. Fluorescent images of lateral column of spinal cord showing staining pattern of antibodies. Oligodendrocyte binding rHIgM22 antibody and neuron binding rHIgM42 show axonal staining pattern (arrowheads). The antibody mHIgM79 labels cells possibly astrocytes and CB2bG8 displays staining of undefined structures in spinal cord different from axons.

7.3 Antibody-mediated targeting of CNS axons following *in vivo* injection

As a next step we injected sHIgM42 antibody into TMEV infected mice (4 months post infection) to assess *in vivo* binding to CNS axons. A small cohort of three mice was injected i.p. with 650µl PBS containing 500µg of sHIgM42 antibody. Control mice were injected with the same amount of sHIgM39 antibody, which previously showed no binding to cells within the CNS (Warrington et al., 2004). 24 hours post injection mice were perfused with 4% PFA and spinal cords were processed for cryosectioning. Longitudinal spinal cord cryosections (10-12 µm) were fluorescently labeled with anti human IgM secondary antibodies. Microscopic analysis revealed that sHIgM42 signal could be detected on the axons in discrete regions in the lateral columns of the spinal cord (Fig. 23A, arrow heads). The nuclear staining with DAPI showed massive immune cell infiltrates characteristic of lesions (asterisk). Similar signals were never found in spinal cords of mice injected with sHIgM39 (Fig. 23C). Spinal cords contained lesions where sHIgM42 antibody did not bind (Fig. 23B), probably due to the difference in the pathology of different demyelinated lesions concerning BBB opening, level of demyelination and axon preservation. This is corroborated by Gallyas staining on spinal cords of TMEV infected mouse showing lesions infiltrated by immune cells (asterisk) (Fig. 23D) with largely preserved myelin in contrast to heavily demyelinated

regions (Fig. 23D; boxed). To show that the sHIgM42 binds to demyelinated regions consecutive paraffin section of spinal cords was fluorescently co-labeled to detect sIgM42 and anti neurofilament antibodies. Demyelinated region in the spinal cord (Fig. 23D; boxed) corresponded to the region in which axonal localization of IgM42 was detected (Fig. 23E)
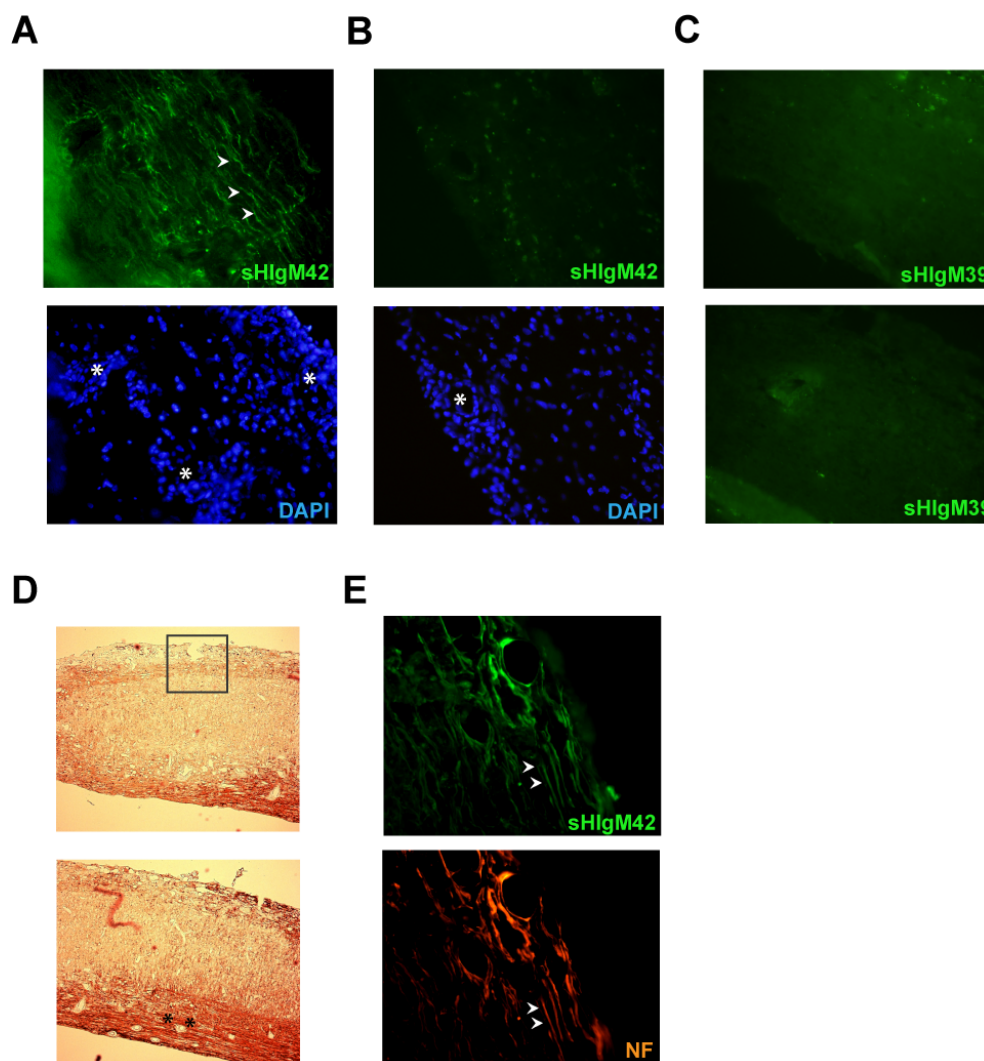
Fig. 23 Human IgM42 binds to spinal cord axons after *in vivo* injection into a Theiler's mouse model of MS.

TMEV infected mice 4 months post infection were injected intreperitoneally with 500µg of sHIgM42 or sHIgM39 antibodies. Spinal cord tissue collected after 24 hours was processed for cryosectioning. Longitudinal spinal cord sections (10µm) were immunolabeled with FITC-anti human IgM antibody (green). (A) Image of a region in the lateral column of spinal cord region showing axons labeled with rHIgM42 antibody (arrowheads). DAPI staining shows massive immune cell infiltrates (asterisk). (B) Region of the same spinal cord without labeled axons. Region is clearly overlaps with a lesion with infiltrated immune cells showed by DAPI staining. (C) Two different spinal cord regions of a mouse injected with a control sHIgM39 antibody. Staining similar to rHIgM42 could not be observed.
(D) Gallyas myelin stain on a longitudinal spinal cord paraffin section (5µm) from a TMEV infected mouse injected with rHIgM42. Boxed demyelinated area corresponds to the region in depicted in (C). Not all lesioned regions infiltrated by immune cell are demyelinated (asterisk).

(E) Consecutive longitudinal spinal cord section, labeled with neurofilament antibody. Images of a lateral spinal cord showing overlap between rHIgM42 (green) signal and NF (red) (arrowheads).

During the course of this project, data concerning the CNS myelination revealed that the contribution of NRG1 to CNS myelin formation and stimulation of remyelination is less essential (Brinkmann et al., 2008). In contrast to the PNS, NRG1 is dispensable for myelination in the CNS. Conditional mouse mutants lacking NRG1-β isoforms in the CNS show no disruption in myelin formation. Additionally, myelination appears to be unaffected in the absence of NRG1 receptors ErbB3 and ErbB4 expressed by oligodendrocytes. Importantly, CNS remyelination in mice overexpressing NRG1 type III in CNS neurons did not promote remyelination in the spinal cords of following lysolecithin-induced focal demyelination (Brinkmann et al., 2008). In the light of these results NRG1-based strategies for myelin regeneration in MS no longer appear to present a promising therapeutic approach.

8 REFERENCES

Arroyo, E.J., and S.S. Scherer. 2000. On the molecular architecture of myelinated fibers. *Histochem Cell Biol.* 113:1-18.

Balice-Gordon, R.J., L.J. Bone, and S.S. Scherer. 1998. Functional gap junctions in the schwann cell myelin sheath. *J Cell Biol.* 142:1095-104.

Bao, J., H. Lin, Y. Ouyang, D. Lei, A. Osman, T.W. Kim, L. Mei, P. Dai, K.K. Ohlemiller, and R.T. Ambron. 2004. Activity-dependent transcription regulation of PSD-95 by neuregulin-1 and Eos. *Nat Neurosci.* 7:1250-8.

Bao, J., D. Wolpowitz, L.W. Role, and D.A. Talmage. 2003. Back signaling by the Nrg-1 intracellular domain. *J Cell Biol.* 161:1133-41.

Bermingham-McDonogh, O., Y.T. Xu, M.A. Marchionni, and S.S. Scherer. 1997. Neuregulin expression in PNS neurons: isoforms and regulation by target interactions. *Mol Cell Neurosci.* 10:184-95.

Birchmeier, C., and K.A. Nave. 2008. Neuregulin-1, a key axonal signal that drives Schwann cell growth and differentiation. *Glia.* 56:1491-7.

Birnboim, H.C., and J. Doly. 1979. A rapid alkaline extraction procedure for screening recombinant plasmid DNA. *Nucleic Acids Res.* 7:1513-23.

Black, R.A., C.T. Rauch, C.J. Kozlosky, J.J. Peschon, J.L. Slack, M.F. Wolfson, B.J. Castner, K.L. Stocking, P. Reddy, S. Srinivasan, N. Nelson, N. Boiani, K.A. Schooley, M. Gerhart, R. Davis, J.N. Fitzner, R.S. Johnson, R.J. Paxton, C.J. March, and D.P. Cerretti. 1997. A metalloproteinase disintegrin that releases tumour-necrosis factor-alpha from cells. *Nature.* 385:729-33.

Blakemore, W.F., and H.S. Keirstead. 1999. The origin of remyelinating cells in the central nervous system. *J Neuroimmunol.* 98:69-76.

Blobel, C.P. 2005. ADAMs: key components in EGFR signalling and development. *Nat Rev Mol Cell Biol.* 6:32-43.

Brinkmann, B.G., A. Agarwal, M.W. Sereda, A.N. Garratt, T. Muller, H. Wende, R.M. Stassart, S. Nawaz, C. Humml, V. Velanac, K. Radyushkin, S. Goebbels, T.M. Fischer, R.J. Franklin, C. Lai, H. Ehrenreich, C. Birchmeier, M.H. Schwab, and K.A. Nave. 2008. Neuregulin-1/ErbB signaling serves distinct functions in myelination of the peripheral and central nervous system. *Neuron.* 59:581-95.

Brown, D.A., and E. London. 2000. Structure and function of sphingolipid- and cholesterol-rich membrane rafts. *J Biol Chem.* 275:17221-4.

Bruck, W. 2005. The pathology of multiple sclerosis is the result of focal inflammatory demyelination with axonal damage. *J Neurol.* 252 Suppl 5:v3-9.

Burden, S., and Y. Yarden. 1997. Neuregulins and their receptors: a versatile signaling module in organogenesis and oncogenesis. *Neuron.* 18:847-55.

Cabedo, H., C. Luna, A.M. Fernandez, J. Gallar, and A. Ferrer-Montiel. 2002. Molecular determinants of the sensory and motor neuron-derived factor insertion into plasma membrane. *J Biol Chem.* 277:19905-12.

Cai, H., Y. Wang, D. McCarthy, H. Wen, D.R. Borchelt, D.L. Price, and P.C. Wong. 2001. BACE1 is the major beta-secretase for generation of Abeta peptides by neurons. *Nat Neurosci.* 4:233-4.

Cannella, B., C.J. Hoban, Y.L. Gao, R. Garcia-Arenas, D. Lawson, M. Marchionni, D. Gwynne, and C.S. Raine. 1998. The neuregulin, glial growth factor 2, diminishes autoimmune demyelination and enhances remyelination in a chronic relapsing model for multiple sclerosis. *Proc Natl Acad Sci U S A.* 95:10100-5.

Canoll, P.D., R. Kraemer, K.K. Teng, M.A. Marchionni, and J.L. Salzer. 1999. GGF/neuregulin induces a phenotypic reversion of oligodendrocytes. *Mol Cell Neurosci.* 13:79-94.

Canoll, P.D., J.M. Musacchio, R. Hardy, R. Reynolds, M.A. Marchionni, and J.L. Salzer. 1996. GGF/neuregulin is a neuronal signal that promotes the proliferation and survival and inhibits the differentiation of oligodendrocyte progenitors. *Neuron.* 17:229-43.

Caroni, P. 1997. Overexpression of growth-associated proteins in the neurons of adult transgenic mice. *J Neurosci Methods*. 71:3-9.

Charles, P., S. Tait, C. Faivre-Sarrailh, G. Barbin, F. Gunn-Moore, N. Denisenko-Nehrbass, A.M. Guennoc, J.A. Girault, P.J. Brophy, and C. Lubetzki. 2002. Neurofascin is a glial receptor for the paranodin/Caspr-contactin axonal complex at the axoglial junction. *Curr Biol*. 12:217-20.

Chen, Z.L., W.M. Yu, and S. Strickland. 2007. Peripheral regeneration. *Annu Rev Neurosci*. 30:209-33.

Citri, A., and Y. Yarden. 2006. EGF-ERBB signalling: towards the systems level. *Nat Rev Mol Cell Biol*. 7:505-16.

Coutinho, A., M.D. Kazatchkine, and S. Avrameas. 1995. Natural autoantibodies. *Curr Opin Immunol*. 7:812-8.

Deadwyler, G.D., S. Pouly, J.P. Antel, and G.H. Devries. 2000. Neuregulins and erbB receptor expression in adult human oligodendrocytes. *Glia*. 32:304-12.

Dominguez, D., J. Tournoy, D. Hartmann, T. Huth, K. Cryns, S. Deforce, L. Serneels, I.E. Camacho, E. Marjaux, K. Craessaerts, A.J. Roebroek, M. Schwake, R. D'Hooge, P. Bach, U. Kalinke, D. Moechars, C. Alzheimer, K. Reiss, P. Saftig, and B. De Strooper. 2005. Phenotypic and biochemical analyses of BACE1- and BACE2-deficient mice. *J Biol Chem*. 280:30797-806.

Dong, Z., A. Brennan, N. Liu, Y. Yarden, G. Lefkowitz, R. Mirsky, and K.R. Jessen. 1995. Neu differentiation factor is a neuron-glia signal and regulates survival, proliferation, and maturation of rat Schwann cell precursors. *Neuron*. 15:585-96.

Dowsing, B.J., W.A. Morrison, N.A. Nicola, G.P. Starkey, T. Bucci, and T.J. Kilpatrick. 1999. Leukemia inhibitory factor is an autocrine survival factor for Schwann cells. *J Neurochem*. 73:96-104.

Eng, L.F., and R.S. Ghirnikar. 1994. GFAP and astrogliosis. *Brain Pathol*. 4:229-37.

Falls, D.L. 2003. Neuregulins: functions, forms, and signaling strategies. *Exp Cell Res*. 284:14-30.

Falls, D.L., K.M. Rosen, G. Corfas, W.S. Lane, and G.D. Fischbach. 1993. ARIA, a protein that stimulates acetylcholine receptor synthesis, is a member of the neu ligand family. *Cell*. 72:801-15.

Ferguson, B., M.K. Matyszak, M.M. Esiri, and V.H. Perry. 1997. Axonal damage in acute multiple sclerosis lesions. *Brain*. 120 (Pt 3):393-9.

Fernandez, P.A., D.G. Tang, L. Cheng, A. Prochiantz, A.W. Mudge, and M.C. Raff. 2000. Evidence that axon-derived neuregulin promotes oligodendrocyte survival in the developing rat optic nerve. *Neuron*. 28:81-90.

Franklin, R.J. 2002. Why does remyelination fail in multiple sclerosis? *Nat Rev Neurosci*. 3:705-14.

Franklin, R.J., and C. Ffrench-Constant. 2008. Remyelination in the CNS: from biology to therapy. *Nat Rev Neurosci*. 9:839-55.

Freese, C., A.N. Garratt, F. Fahrenholz, and K. Endres. 2009. The effects of alpha-secretase ADAM10 on the proteolysis of neuregulin-1. *FEBS J*. 276:1568-80.

Frenzel, K.E., and D.L. Falls. 2001. Neuregulin-1 proteins in rat brain and transfected cells are localized to lipid rafts. *J Neurochem*. 77:1-12.

Friede, R.L. 1972. Control of myelin formation by axon caliber (with a model of the control mechanism). *J Comp Neurol*. 144:233-52.

Garbay, B., A.M. Heape, F. Sargueil, and C. Cassagne. 2000. Myelin synthesis in the peripheral nervous system. *Prog Neurobiol*. 61:267-304.

Garratt, A.N., S. Britsch, and C. Birchmeier. 2000a. Neuregulin, a factor with many functions in the life of a schwann cell. *Bioessays*. 22:987-96.

Garratt, A.N., O. Voiculescu, P. Topilko, P. Charnay, and C. Birchmeier. 2000b. A dual role of erbB2 in myelination and in expansion of the schwann cell precursor pool. *J Cell Biol*. 148:1035-46.

Garrett, T.P., N.M. McKern, M. Lou, T.C. Elleman, T.E. Adams, G.O. Lovrecz, M. Kofler, R.N. Jorissen, E.C. Nice, A.W. Burgess, and C.W. Ward. 2003. The crystal structure of a truncated ErbB2 ectodomain reveals an active

conformation, poised to interact with other ErbB receptors. *Mol Cell.* 11:495-505.

Gensert, J.M., and J.E. Goldman. 1997. Endogenous progenitors remyelinate demyelinated axons in the adult CNS. *Neuron.* 19:197-203.

Giese, K.P., R. Martini, G. Lemke, P. Soriano, and M. Schachner. 1992. Mouse P0 gene disruption leads to hypomyelination, abnormal expression of recognition molecules, and degeneration of myelin and axons. *Cell.* 71:565-76.

Gomez-Sanchez, J.A., M. Lopez de Armentia, R. Lujan, N. Kessaris, W.D. Richardson, and H. Cabedo. 2009. Sustained axon-glial signaling induces Schwann cell hyperproliferation, Remak bundle myelination, and tumorigenesis. *J Neurosci.* 29:11304-15.

Graham, F.L., J. Smiley, W.C. Russell, and R. Nairn. 1977. Characteristics of a human cell line transformed by DNA from human adenovirus type 5. *J Gen Virol.* 36:59-74.

Greene, L.A., and A.S. Tischler. 1976. Establishment of a noradrenergic clonal line of rat adrenal pheochromocytoma cells which respond to nerve growth factor. *Proc Natl Acad Sci U S A.* 73:2424-8.

Grinspan, J.B., M.A. Marchionni, M. Reeves, M. Coulaloglou, and S.S. Scherer. 1996. Axonal interactions regulate Schwann cell apoptosis in developing peripheral nerve: neuregulin receptors and the role of neuregulins. *J Neurosci.* 16:6107-18.

Guy, P.M., J.V. Platko, L.C. Cantley, R.A. Cerione, and K.L. Carraway, 3rd. 1994. Insect cell-expressed p180erbB3 possesses an impaired tyrosine kinase activity. *Proc Natl Acad Sci U S A.* 91:8132-6.

Hanisch, U.K., and H. Kettenmann. 2007. Microglia: active sensor and versatile effector cells in the normal and pathologic brain. *Nat Neurosci.* 10:1387-94.

Harrisingh, M.C., E. Perez-Nadales, D.B. Parkinson, D.S. Malcolm, A.W. Mudge, and A.C. Lloyd. 2004. The Ras/Raf/ERK signalling pathway drives Schwann cell dedifferentiation. *EMBO J.* 23:3061-71.

Hartline, D.K., and D.R. Colman. 2007. Rapid conduction and the evolution of giant axons and myelinated fibers. *Curr Biol.* 17:R29-35.

Hauser, S.L., and J.R. Oksenberg. 2006. The neurobiology of multiple sclerosis: genes, inflammation, and neurodegeneration. *Neuron.* 52:61-76.

Ho, W.H., M.P. Armanini, A. Nuijens, H.S. Phillips, and P.L. Osheroff. 1995. Sensory and motor neuron-derived factor. A novel heregulin variant highly expressed in sensory and motor neurons. *J Biol Chem.* 270:26722.

Holmes, W.E., M.X. Sliwkowski, R.W. Akita, W.J. Henzel, J. Lee, J.W. Park, D. Yansura, N. Abadi, H. Raab, G.D. Lewis, and et al. 1992. Identification of heregulin, a specific activator of p185erbB2. *Science.* 256:1205-10.

Hooper, N.M., E.H. Karran, and A.J. Turner. 1997. Membrane protein secretases. *Biochem J.* 321 (Pt 2):265-79.

Horiuchi, K., H.M. Zhou, K. Kelly, K. Manova, and C.P. Blobel. 2005. Evaluation of the contributions of ADAMs 9, 12, 15, 17, and 19 to heart development and ectodomain shedding of neuregulins beta1 and beta2. *Dev Biol.* 283:459-71.

Hu, X., W. He, C. Diaconu, X. Tang, G.J. Kidd, W.B. Macklin, B.D. Trapp, and R. Yan. 2008. Genetic deletion of BACE1 in mice affects remyelination of sciatic nerves. *FASEB J.* 22:2970-80.

Hu, X., C.W. Hicks, W. He, P. Wong, W.B. Macklin, B.D. Trapp, and R. Yan. 2006. Bace1 modulates myelination in the central and peripheral nervous system. *Nat Neurosci.* 9:1520-5.

Irvine, K.A., and W.F. Blakemore. 2008. Remyelination protects axons from demyelination-associated axon degeneration. *Brain.* 131:1464-77.

Jackson, L.F., T.H. Qiu, S.W. Sunnarborg, A. Chang, C. Zhang, C. Patterson, and D.C. Lee. 2003. Defective valvulogenesis in HB-EGF and TACE-null mice is associated with aberrant BMP signaling. *EMBO J.* 22:2704-16.

Jensen, F.C., A.J. Girardi, R.V. Gilden, and H. Koprowski. 1964. Infection of Human and Simian Tissue Cultures with Rous Sarcoma Virus. *Proc Natl Acad Sci U S A*. 52:53-9.

Jessen, K.R., and R. Mirsky. 1998. Origin and early development of Schwann cells. *Microsc Res Tech*. 41:393-402.

Jessen, K.R., and R. Mirsky. 2005. The origin and development of glial cells in peripheral nerves. *Nat Rev Neurosci*. 6:671-82.

Jones, J.T., R.W. Akita, and M.X. Sliwkowski. 1999. Binding specificities and affinities of egf domains for ErbB receptors. *FEBS Lett*. 447:227-31.

Kao, S.C., H. Wu, J. Xie, C.P. Chang, J.A. Ranish, I.A. Graef, and G.R. Crabtree. 2009. Calcineurin/NFAT signaling is required for neuregulin-regulated Schwann cell differentiation. *Science*. 323:651-4.

Kitazume, S., Y. Tachida, R. Oka, K. Shirotani, T.C. Saido, and Y. Hashimoto. 2001. Alzheimer's beta-secretase, beta-site amyloid precursor protein-cleaving enzyme, is responsible for cleavage secretion of a Golgi-resident sialyltransferase. *Proc Natl Acad Sci U S A*. 98:13554-9.

Klapper, L.N., S. Glathe, N. Vaisman, N.E. Hynes, G.C. Andrews, M. Sela, and Y. Yarden. 1999. The ErbB-2/HER2 oncoprotein of human carcinomas may function solely as a shared coreceptor for multiple stroma-derived growth factors. *Proc Natl Acad Sci U S A*. 96:4995-5000.

Kojro, E., G. Gimpl, S. Lammich, W. Marz, and F. Fahrenholz. 2001. Low cholesterol stimulates the nonamyloidogenic pathway by its effect on the alpha -secretase ADAM 10. *Proc Natl Acad Sci U S A*. 98:5815-20.

Kornek, B., M.K. Storch, R. Weissert, E. Wallstroem, A. Stefferl, T. Olsson, C. Linington, M. Schmidbauer, and H. Lassmann. 2000. Multiple sclerosis and chronic autoimmune encephalomyelitis: a comparative quantitative study of axonal injury in active, inactive, and remyelinated lesions. *Am J Pathol*. 157:267-76.

Laird, F.M., H. Cai, A.V. Savonenko, M.H. Farah, K. He, T. Melnikova, H. Wen, H.C. Chiang, G. Xu, V.E. Koliatsos, D.R. Borchelt, D.L. Price, H.K. Lee, and P.C. Wong. 2005. BACE1, a major determinant of selective vulnerability of the brain to amyloid-beta amyloidogenesis, is essential for cognitive, emotional, and synaptic functions. *J Neurosci*. 25:11693-709.

Lammich, S., E. Kojro, R. Postina, S. Gilbert, R. Pfeiffer, M. Jasionowski, C. Haass, and F. Fahrenholz. 1999. Constitutive and regulated alpha-secretase cleavage of Alzheimer's amyloid precursor protein by a disintegrin metalloprotease. *Proc Natl Acad Sci U S A*. 96:3922-7.

Lappe-Siefke, C., S. Goebbels, M. Gravel, E. Nicksch, J. Lee, P.E. Braun, I.R. Griffiths, and K.A. Nave. 2003. Disruption of Cnp1 uncouples oligodendroglial functions in axonal support and myelination. *Nat Genet*. 33:366-74.

Lassmann, H., W. Bruck, and C. Lucchinetti. 2001. Heterogeneity of multiple sclerosis pathogenesis: implications for diagnosis and therapy. *Trends Mol Med*. 7:115-21.

Le Douarin, N.M. 1986. Cell line segregation during peripheral nervous system ontogeny. *Science*. 231:1515-22.

Lemke, G.E., and J.P. Brockes. 1984. Identification and purification of glial growth factor. *J Neurosci*. 4:75-83.

Levi, A.D., R.P. Bunge, J.A. Lofgren, L. Meima, F. Hefti, K. Nikolics, and M.X. Sliwkowski. 1995. The influence of heregulins on human Schwann cell proliferation. *J Neurosci*. 15:1329-40.

Li, Q., and J.A. Loeb. 2001. Neuregulin-heparan-sulfate proteoglycan interactions produce sustained erbB receptor activation required for the induction of acetylcholine receptors in muscle. *J Biol Chem*. 276:38068-75.

Li, Q., and T.C. Sudhof. 2004. Cleavage of amyloid-beta precursor protein and amyloid-beta precursor-like protein by BACE 1. *J Biol Chem*. 279:10542-50.

Li, Y., G.I. Tennekoon, M. Birnbaum, M.A. Marchionni, and J.L. Rutkowski. 2001. Neuregulin signaling through a PI3K/Akt/Bad pathway in Schwann cell survival. *Mol Cell Neurosci*. 17:761-7.

Lichtenthaler, S.F., D.I. Dominguez, G.G. Westmeyer, K. Reiss, C. Haass, P. Saftig, B. De Strooper, and B. Seed. 2003. The cell adhesion protein P-selectin glycoprotein ligand-1 is a substrate for the aspartyl protease BACE1. *J Biol Chem*. 278:48713-9.

Liu, P., H. Cheng, T.M. Roberts, and J.J. Zhao. 2009. Targeting the phosphoinositide 3-kinase pathway in cancer. *Nat Rev Drug Discov*. 8:627-44.

Liu, Y., Y.M. Tao, R.S. Woo, W.C. Xiong, and L. Mei. 2007. Stimulated ErbB4 internalization is necessary for neuregulin signaling in neurons. *Biochem Biophys Res Commun*. 354:505-10.

Loeb, J.A., and G.D. Fischbach. 1995. ARIA can be released from extracellular matrix through cleavage of a heparin-binding domain. *J Cell Biol*. 130:127-35.

Lowry, O.H., N.J. Rosebrough, A.L. Farr, and R.J. Randall. 1951. Protein measurement with the Folin phenol reagent. *J Biol Chem*. 193:265-75.

Marchionni, M.A., B. Cannella, C. Hoban, Y.L. Gao, R. Garcia-Arenas, D. Lawson, E. Happel, F. Noel, P. Tofilon, D. Gwynne, and C.S. Raine. 1999. Neuregulin in neuron/glial interactions in the central nervous system. GGF2 diminishes autoimmune demyelination, promotes oligodendrocyte progenitor expansion, and enhances remyelination. *Adv Exp Med Biol*. 468:283-95.

Marchionni, M.A., A.D. Goodearl, M.S. Chen, O. Bermingham-McDonogh, C. Kirk, M. Hendricks, F. Danehy, D. Misumi, J. Sudhalter, K. Kobayashi, and et al. 1993. Glial growth factors are alternatively spliced erbB2 ligands expressed in the nervous system. *Nature*. 362:312-8.

Maurel, P., S. Einheber, J. Galinska, P. Thaker, I. Lam, M.B. Rubin, S.S. Scherer, Y. Murakami, D.H. Gutmann, and J.L. Salzer. 2007. Nectin-like proteins mediate axon Schwann cell interactions along the internode and are essential for myelination. *J Cell Biol*. 178:861-74.

Maurel, P., and J.L. Salzer. 2000. Axonal regulation of Schwann cell proliferation and survival and the initial events of myelination requires PI 3-kinase activity. *J Neurosci*. 20:4635-45.

McGavern, D.B., P.D. Murray, C. Rivera-Quinones, J.D. Schmelzer, P.A. Low, and M. Rodriguez. 2000. Axonal loss results in spinal cord atrophy, electrophysiological abnormalities and neurological deficits following demyelination in a chronic inflammatory model of multiple sclerosis. *Brain*. 123 Pt 3:519-31.

Mei, L., and W.C. Xiong. 2008. Neuregulin 1 in neural development, synaptic plasticity and schizophrenia. *Nat Rev Neurosci*. 9:437-52.

Meier, C., E. Parmantier, A. Brennan, R. Mirsky, and K.R. Jessen. 1999. Developing Schwann cells acquire the ability to survive without axons by establishing an autocrine circuit involving insulin-like growth factor, neurotrophin-3, and platelet-derived growth factor-BB. *J Neurosci*. 19:3847-59.

Meyer, D., T. Yamaai, A. Garratt, E. Riethmacher-Sonnenberg, D. Kane, L.E. Theill, and C. Birchmeier. 1997. Isoform-specific expression and function of neuregulin. *Development*. 124:3575-86.

Meyer zu Horste, G., T. Prukop, D. Liebetanz, W. Mobius, K.A. Nave, and M.W. Sereda. 2007. Antiprogesterone therapy uncouples axonal loss from demyelination in a transgenic rat model of CMT1A neuropathy. *Ann Neurol*. 61:61-72.

Michailov, G.V., M.W. Sereda, B.G. Brinkmann, T.M. Fischer, B. Haug, C. Birchmeier, L. Role, C. Lai, M.H. Schwab, and K.A. Nave. 2004. Axonal neuregulin-1 regulates myelin sheath thickness. *Science*. 304:700-3.

Montero, J.C., L. Yuste, E. Diaz-Rodriguez, A. Esparis-Ogando, and A. Pandiella. 2000. Differential shedding of transmembrane neuregulin isoforms by the tumor necrosis factor-alpha-converting enzyme. *Mol Cell Neurosci*. 16:631-48.

Morris, J.K., W. Lin, C. Hauser, Y. Marchuk, D. Getman, and K.F. Lee. 1999. Rescue of the cardiac defect in ErbB2 mutant mice reveals essential roles of ErbB2 in peripheral nervous system development. *Neuron*. 23:273-83.

Morrissey, T.K., A.D. Levi, A. Nuijens, M.X. Sliwkowski, and R.P. Bunge. 1995. Axon-induced mitogenesis of human Schwann cells involves heregulin and p185erbB2. *Proc Natl Acad Sci U S A*. 92:1431-5.

Moss, M.L., S.L. Jin, M.E. Milla, D.M. Bickett, W. Burkhart, H.L. Carter, W.J. Chen, W.C. Clay, J.R. Didsbury, D. Hassler, C.R. Hoffman, T.A. Kost, M.H. Lambert, M.A. Leesnitzer, P. McCauley, G. McGeehan, J. Mitchell, M. Moyer, G. Pahel, W. Rocque, L.K. Overton, F. Schoenen, T. Seaton, J.L. Su, J.D. Becherer, and et al. 1997. Cloning of a disintegrin metalloproteinase that processes precursor tumour-necrosis factor-alpha. *Nature*. 385:733-6.

Moss, M.L., and F.H. Rasmussen. 2007. Fluorescent substrates for the proteinases ADAM17, ADAM10, ADAM8, and ADAM12 useful for high-throughput inhibitor screening. *Anal Biochem*. 366:144-8.

Mullis, K., F. Faloona, S. Scharf, R. Saiki, G. Horn, and H. Erlich. 1986. Specific enzymatic amplification of DNA in vitro: the polymerase chain reaction. *Cold Spring Harb Symp Quant Biol*. 51 Pt 1:263-73.

Nave, K.A., and J.L. Salzer. 2006. Axonal regulation of myelination by neuregulin 1. *Curr Opin Neurobiol*. 16:492-500.

Nave, K.A., M.W. Sereda, and H. Ehrenreich. 2007. Mechanisms of disease: inherited demyelinating neuropathies--from basic to clinical research. *Nat Clin Pract Neurol*. 3:453-64.

Nave, K.A., and B.D. Trapp. 2008. Axon-glial signaling and the glial support of axon function. *Annu Rev Neurosci*. 31:535-61.

Ni, C.Y., M.P. Murphy, T.E. Golde, and G. Carpenter. 2001. gamma -Secretase cleavage and nuclear localization of ErbB-4 receptor tyrosine kinase. *Science*. 294:2179-81.

Ogata, T., S. Iijima, S. Hoshikawa, T. Miura, S. Yamamoto, H. Oda, K. Nakamura, and S. Tanaka. 2004. Opposing extracellular signal-regulated kinase and Akt pathways control Schwann cell myelination. *J Neurosci*. 24:6724-32.

Ohno, M., Y. Hiraoka, T. Matsuoka, H. Tomimoto, K. Takao, T. Miyakawa, N. Oshima, H. Kiyonari, T. Kimura, T. Kita, and E. Nishi. 2009. Nardilysin regulates axonal maturation and myelination in the central and peripheral nervous system. *Nat Neurosci*.

Penderis, J., R.H. Woodruff, A. Lakatos, W.W. Li, M.D. Dunning, C. Zhao, M. Marchionni, and R.J. Franklin. 2003. Increasing local levels of neuregulin (glial growth factor-2) by direct infusion into areas of demyelination does not alter remyelination in the rat CNS. *Eur J Neurosci*. 18:2253-64.

Peschon, J.J., J.L. Slack, P. Reddy, K.L. Stocking, S.W. Sunnarborg, D.C. Lee, W.E. Russell, B.J. Castner, R.S. Johnson, J.N. Fitzner, R.W. Boyce, N. Nelson, C.J. Kozlosky, M.F. Wolfson, C.T. Rauch, D.P. Cerretti, R.J. Paxton, C.J. March, and R.A. Black. 1998. An essential role for ectodomain shedding in mammalian development. *Science*. 282:1281-4.

Poliak, S., and E. Peles. 2003. The local differentiation of myelinated axons at nodes of Ranvier. *Nat Rev Neurosci*. 4:968-80.

Riddell, D.R., G. Christie, I. Hussain, and C. Dingwall. 2001. Compartmentalization of beta-secretase (Asp2) into low-buoyant density, noncaveolar lipid rafts. *Curr Biol*. 11:1288-93.

Riethmacher, D., E. Sonnenberg-Riethmacher, V. Brinkmann, T. Yamaai, G.R. Lewin, and C. Birchmeier. 1997. Severe neuropathies in mice with targeted mutations in the ErbB3 receptor. *Nature*. 389:725-30.

Rodriguez, M., E. Oleszak, and J. Leibowitz. 1987. Theiler's murine encephalomyelitis: a model of demyelination and persistence of virus. *Crit Rev Immunol*. 7:325-65.

Rodriguez, M., A.E. Warrington, and L.R. Pease. 2009. Invited Article: Human natural autoantibodies in the treatment of neurologic disease. *Neurology*. 72:1269-76.

Rushton, W.A. 1951. A theory of the effects of fibre size in medullated nerve. *J Physiol*. 115:101-22.

Sahin, U., G. Weskamp, K. Kelly, H.M. Zhou, S. Higashiyama, J. Peschon, D. Hartmann, P. Saftig, and C.P. Blobel. 2004. Distinct roles for ADAM10 and ADAM17 in ectodomain shedding of six EGFR ligands. *J Cell Biol*. 164:769-79.

Salzer, J.L., P.J. Brophy, and E. Peles. 2008. Molecular domains of myelinated axons in the peripheral nervous system. *Glia*. 56:1532-40.

Salzer, J.L., A.K. Williams, L. Glaser, and R.P. Bunge. 1980. Studies of Schwann cell proliferation. II. Characterization of the stimulation and specificity of the response to a neurite membrane fraction. *J Cell Biol*. 84:753-66.

Sardi, S.P., J. Murtie, S. Koirala, B.A. Patten, and G. Corfas. 2006. Presenilin-dependent ErbB4 nuclear signaling regulates the timing of astrogenesis in the developing brain. *Cell*. 127:185-97.

Schlondorff, J., and C.P. Blobel. 1999. Metalloprotease-disintegrins: modular proteins capable of promoting cell-cell interactions and triggering signals by protein-ectodomain shedding. *J Cell Sci*. 112 (Pt 21):3603-17.

Schroering, A., and D.J. Carey. 1998. Sensory and motor neuron-derived factor is a transmembrane heregulin that is expressed on the plasma membrane with the active domain exposed to the extracellular environment. *J Biol Chem*. 273:30643-50.

Shah, N.M., M.A. Marchionni, I. Isaacs, P. Stroobant, and D.J. Anderson. 1994. Glial growth factor restricts mammalian neural crest stem cells to a glial fate. *Cell*. 77:349-60.

Shapiro, L., J.P. Doyle, P. Hensley, D.R. Colman, and W.A. Hendrickson. 1996. Crystal structure of the extracellular domain from P0, the major structural protein of peripheral nerve myelin. *Neuron*. 17:435-49.

Sherman, D.L., and P.J. Brophy. 2005. Mechanisms of axon ensheathment and myelin growth. *Nat Rev Neurosci*. 6:683-90.

Shirakabe, K., S. Wakatsuki, T. Kurisaki, and A. Fujisawa-Sehara. 2001. Roles of Meltrin beta /ADAM19 in the processing of neuregulin. *J Biol Chem*. 276:9352-8.

Simons, K., and E. Ikonen. 1997. Functional rafts in cell membranes. *Nature*. 387:569-72.

Simons, K., and D. Toomre. 2000. Lipid rafts and signal transduction. *Nat Rev Mol Cell Biol*. 1:31-9.

Simons, M., E.M. Kramer, C. Thiele, W. Stoffel, and J. Trotter. 2000. Assembly of myelin by association of proteolipid protein with cholesterol- and galactosylceramide-rich membrane domains. *J Cell Biol*. 151:143-54.

Smith, K.J., W.F. Blakemore, J.A. Murray, and R.C. Patterson. 1982. Internodal myelin volume and axon surface area. A relationship determining myelin thickness? *J Neurol Sci*. 55:231-46.

Spiegel, I., K. Adamsky, Y. Eshed, R. Milo, H. Sabanay, O. Sarig-Nadir, I. Horresh, S.S. Scherer, M.N. Rasband, and E. Peles. 2007. A central role for Necl4 (SynCAM4) in Schwann cell-axon interaction and myelination. *Nat Neurosci*. 10:861-9.

Steinthorsdottir, V., H. Stefansson, S. Ghosh, B. Birgisdottir, S. Bjornsdottir, A.C. Fasquel, O. Olafsson, K. Stefansson, and J.R. Gulcher. 2004. Multiple novel transcription initiation sites for NRG1. *Gene*. 342:97-105.

Stevens, B., S. Porta, L.L. Haak, V. Gallo, and R.D. Fields. 2002. Adenosine: a neuron-glial transmitter promoting myelination in the CNS in response to action potentials. *Neuron*. 36:855-68.

Stoffel, W., and A. Bosio. 1997. Myelin glycolipids and their functions. *Curr Opin Neurobiol*. 7:654-61.

Syroid, D.E., P.R. Maycox, P.G. Burrola, N. Liu, D. Wen, K.F. Lee, G. Lemke, and T.J. Kilpatrick. 1996. Cell death in the Schwann cell lineage and its regulation by neuregulin. *Proc Natl Acad Sci U S A*. 93:9229-34.

Tao, Y., P. Dai, Y. Liu, S. Marchetto, W.C. Xiong, J.P. Borg, and L. Mei. 2009. Erbin regulates NRG1 signaling and myelination. *Proc Natl Acad Sci U S A*. 106:9477-82.

Taveggia, C., G. Zanazzi, A. Petrylak, H. Yano, J. Rosenbluth, S. Einheber, X. Xu, R.M. Esper, J.A. Loeb, P. Shrager, M.V. Chao, D.L. Falls, L. Role, and J.L. Salzer. 2005. Neuregulin-1 type III determines the ensheathment fate of axons. *Neuron*. 47:681-94.

Topilko, P., S. Schneider-Maunoury, G. Levi, A. Baron-Van Evercooren, A.B. Chennoufi, T. Seitanidou, C. Babinet, and P. Charnay. 1994. Krox-20 controls myelination in the peripheral nervous system. *Nature*. 371:796-9.

Towbin, H., T. Staehelin, and J. Gordon. 1979. Electrophoretic transfer of proteins from polyacrylamide gels to nitrocellulose sheets: procedure and some applications. *Proc Natl Acad Sci U S A*. 76:4350-4.

Traka, M., L. Goutebroze, N. Denisenko, M. Bessa, A. Nifli, S. Havaki, Y. Iwakura, F. Fukamauchi, K. Watanabe, B. Soliven, J.A. Girault, and D. Karagogeos. 2003. Association of TAG-1 with Caspr2 is essential for the molecular organization of juxtaparanodal regions of myelinated fibers. *J Cell Biol*. 162:1161-72.

Trapp, B.D., and K.A. Nave. 2008. Multiple sclerosis: an immune or neurodegenerative disorder? *Annu Rev Neurosci*. 31:247-69.

Trapp, B.D., J. Peterson, R.M. Ransohoff, R. Rudick, S. Mork, and L. Bo. 1998. Axonal transection in the lesions of multiple sclerosis. *N Engl J Med*. 338:278-85.

Turner, P.R., K. O'Connor, W.P. Tate, and W.C. Abraham. 2003. Roles of amyloid precursor protein and its fragments in regulating neural activity, plasticity and memory. *Prog Neurobiol*. 70:1-32.

Vartanian, T., G. Fischbach, and R. Miller. 1999. Failure of spinal cord oligodendrocyte development in mice lacking neuregulin. *Proc Natl Acad Sci U S A*. 96:731-5.

Vartanian, T., A. Goodearl, A. Viehover, and G. Fischbach. 1997. Axonal neuregulin signals cells of the oligodendrocyte lineage through activation of HER4 and Schwann cells through HER2 and HER3. *J Cell Biol*. 137:211-20.

Vassar, R., B.D. Bennett, S. Babu-Khan, S. Kahn, E.A. Mendiaz, P. Denis, D.B. Teplow, S. Ross, P. Amarante, R. Loeloff, Y. Luo, S. Fisher, J. Fuller, S. Edenson, J. Lile, M.A. Jarosinski, A.L. Biere, E. Curran, T. Burgess, J.C. Louis, F. Collins, J. Treanor, G. Rogers, and M. Citron. 1999. Beta-secretase cleavage of Alzheimer's amyloid precursor protein by the transmembrane aspartic protease BACE. *Science*. 286:735-41.

Viehover, A., R.H. Miller, S.K. Park, G. Fischbach, and T. Vartanian. 2001. Neuregulin: an oligodendrocyte growth factor absent in active multiple sclerosis lesions. *Dev Neurosci*. 23:377-86.

von Arnim, C.A., A. Kinoshita, I.D. Peltan, M.M. Tangredi, L. Herl, B.M. Lee, R. Spoelgen, T.T. Hshieh, S. Ranganathan, F.D. Battey, C.X. Liu, B.J. Bacskai, S. Sever, M.C. Irizarry, D.K. Strickland, and B.T. Hyman. 2005. The low density lipoprotein receptor-related protein (LRP) is a novel beta-secretase (BACE1) substrate. *J Biol Chem*. 280:17777-85.

Voyvodic, J.T. 1989. Target size regulates calibre and myelination of sympathetic axons. *Nature*. 342:430-3.

Wakatsuki, S., T. Kurisaki, and A. Sehara-Fujisawa. 2004. Lipid rafts identified as locations of ectodomain shedding mediated by Meltrin beta/ADAM19. *J Neurochem*. 89:119-23.

Wakatsuki, S., N. Yumoto, K. Komatsu, T. Araki, and A. Sehara-Fujisawa. 2009. Roles of meltrin-beta/ADAM19 in progression of Schwann cell differentiation and myelination during sciatic nerve regeneration. *J Biol Chem*. 284:2957-66.

Wang, J.Y., S.J. Miller, and D.L. Falls. 2001. The N-terminal region of neuregulin isoforms determines the accumulation of cell surface and released neuregulin ectodomain. *J Biol Chem*. 276:2841-51.

Warrington, A.E., K. Asakura, A.J. Bieber, B. Ciric, V. Van Keulen, S.V. Kaveri, R.A. Kyle, L.R. Pease, and M. Rodriguez. 2000. Human monoclonal antibodies

reactive to oligodendrocytes promote remyelination in a model of multiple sclerosis. *Proc Natl Acad Sci U S A*. 97:6820-5.

Warrington, A.E., A.J. Bieber, V. Van Keulen, B. Ciric, L.R. Pease, and M. Rodriguez. 2004. Neuron-binding human monoclonal antibodies support central nervous system neurite extension. *J Neuropathol Exp Neurol*. 63:461-73.

Waxman, S.G. 1997. Axon-glia interactions: building a smart nerve fiber. *Curr Biol*. 7:R406-10.

Wehr, M.C., R. Laage, U. Bolz, T.M. Fischer, S. Grunewald, S. Scheek, A. Bach, K.A. Nave, and M.J. Rossner. 2006. Monitoring regulated protein-protein interactions using split TEV. *Nat Methods*. 3:985-93.

Wehr, M.C., L. Reinecke, A. Botvinnik, and M.J. Rossner. 2008. Analysis of transient phosphorylation-dependent protein-protein interactions in living mammalian cells using split-TEV. *BMC Biotechnol*. 8:55.

Weiner, J.A., and J. Chun. 1999. Schwann cell survival mediated by the signaling phospholipid lysophosphatidic acid. *Proc Natl Acad Sci U S A*. 96:5233-8.

Wen, D., E. Peles, R. Cupples, S.V. Suggs, S.S. Bacus, Y. Luo, G. Trail, S. Hu, S.M. Silbiger, R.B. Levy, and et al. 1992. Neu differentiation factor: a transmembrane glycoprotein containing an EGF domain and an immunoglobulin homology unit. *Cell*. 69:559-72.

Wen, D., S.V. Suggs, D. Karunagaran, N. Liu, R.L. Cupples, Y. Luo, A.M. Janssen, N. Ben-Baruch, D.B. Trollinger, V.L. Jacobsen, and et al. 1994. Structural and functional aspects of the multiplicity of Neu differentiation factors. *Mol Cell Biol*. 14:1909-19.

White, J.M. 2003. ADAMs: modulators of cell-cell and cell-matrix interactions. *Curr Opin Cell Biol*. 15:598-606.

Willem, M., I. Dewachter, N. Smyth, T. Van Dooren, P. Borghgraef, C. Haass, and F. Van Leuven. 2004. beta-site amyloid precursor protein cleaving enzyme 1 increases amyloid deposition in brain parenchyma but reduces cerebrovascular amyloid angiopathy in aging BACE x APP[V717I] double-transgenic mice. *Am J Pathol*. 165:1621-31.

Willem, M., A.N. Garratt, B. Novak, M. Citron, S. Kaufmann, A. Rittger, B. DeStrooper, P. Saftig, C. Birchmeier, and C. Haass. 2006. Control of peripheral nerve myelination by the beta-secretase BACE1. *Science*. 314:664-6.

Willem, M., S. Lammich, and C. Haass. 2009. Function, regulation and therapeutic properties of beta-secretase (BACE1). *Semin Cell Dev Biol*. 20:175-82.

Wolpowitz, D., T.B. Mason, P. Dietrich, M. Mendelsohn, D.A. Talmage, and L.W. Role. 2000. Cysteine-rich domain isoforms of the neuregulin-1 gene are required for maintenance of peripheral synapses. *Neuron*. 25:79-91.

Wong, H.K., T. Sakurai, F. Oyama, K. Kaneko, K. Wada, H. Miyazaki, M. Kurosawa, B. De Strooper, P. Saftig, and N. Nukina. 2005. beta Subunits of voltage-gated sodium channels are novel substrates of beta-site amyloid precursor protein-cleaving enzyme (BACE1) and gamma-secretase. *J Biol Chem*. 280:23009-17.

Wullschleger, S., R. Loewith, and M.N. Hall. 2006. TOR signaling in growth and metabolism. *Cell*. 124:471-84.

Yang, P., K.A. Baker, and T. Hagg. 2006. The ADAMs family: coordinators of nervous system development, plasticity and repair. *Prog Neurobiol*. 79:73-94.

Yarden, Y., and M.X. Sliwkowski. 2001. Untangling the ErbB signalling network. *Nat Rev Mol Cell Biol*. 2:127-37.

Yokozeki, T., S. Wakatsuki, K. Hatsuzawa, R.A. Black, I. Wada, and A. Sehara-Fujisawa. 2007. Meltrin beta (ADAM19) mediates ectodomain shedding of Neuregulin beta1 in the Golgi apparatus: fluorescence correlation spectroscopic observation of the dynamics of ectodomain shedding in living cells. *Genes Cells*. 12:329-43.

Zacchetti, D., E. Chieregatti, B. Bettegazzi, M. Mihailovich, V.L. Sousa, F. Grohovaz, and J. Meldolesi. 2007. BACE1 expression and activity: relevance in Alzheimer's disease. *Neurodegener Dis*. 4:117-26.

Zanazzi, G., S. Einheber, R. Westreich, M.J. Hannocks, D. Bedell-Hogan, M.A. Marchionni, and J.L. Salzer. 2001. Glial growth factor/neuregulin inhibits Schwann cell myelination and induces demyelination. *J Cell Biol.* 152:1289-99.

Zhao, J., H. Chen, J.J. Peschon, W. Shi, Y. Zhang, S.J. Frank, and D. Warburton. 2001. Pulmonary hypoplasia in mice lacking tumor necrosis factor-alpha converting enzyme indicates an indispensable role for cell surface protein shedding during embryonic lung branching morphogenesis. *Dev Biol.* 232:204-18.

Zhou, H.M., G. Weskamp, V. Chesneau, U. Sahin, A. Vortkamp, K. Horiuchi, R. Chiusaroli, R. Hahn, D. Wilkes, P. Fisher, R. Baron, K. Manova, C.T. Basson, B. Hempstead, and C.P. Blobel. 2004. Essential role for ADAM19 in cardiovascular morphogenesis. *Mol Cell Biol.* 24:96-104.

List of publications

<u>V.Velanac,</u> T. Unterbarnscheidt, M.N. Gummert, T.M. Fischer, C. Taveggia, M. Willem, M.H. Schwab, and K.A. Nave. Control of peripheral myelination by proteolytic processing and limited axonal transport of Neuregulin1 type III (in preparation).

M. H. Schwab, C. Humml, **<u>V. Velanac</u>**, T. Unterbarnscheidt, S. Wichert, S. Hermann, U. Keyser, M.N. Gummert, G. Michailov, B.G. Brinkmann, M.W. Sereda, L. Role, and K. A. Nave. NRG1 type III signalling promotes glial lipid synthesis and determines the myelination status of peripheral axons (in preparation).

B.G. Brinkmann., A. Agarwal, M.W. Sereda, A.N. Garratt, T. Muller, H. Wende, R.M. Stassart, S. Nawaz, C. Humml, **<u>V. Velanac</u>**, K. Radyushkin, S. Goebbels, T.M. Fischer, R.J. Franklin, C. Lai, H. Ehrenreich, C. Birchmeier, M.H. Schwab, and K.A. Nave. (2008). Neuregulin-1/ErbB signalling serves distinct functions in myelination of the peripheral and central nervous system. Neuron. 59:581-95.

Curriculum Vitae

Viktorija Velanac

Date and place of birth:	04. 06. 1978 in Belgrade
Nationality:	Serbian
Home address:	Hainholzweg 30 37085 Goettingen Germany Tel: +49 551 250 96 94
Work address:	MPI of Experimental Medicine Department of Neurogenetics Hermann-Rein Str. 3 37075, Goettingen, Germany. Tel. +49 551 3899-773 Fax: +49 551 3899-753
E-mail:	velanac@em.mpg.de

Academic background:

1993-1997	Gymnasium "Sveti Sava" in Belgrade
1997-2004	University of Belgrade Faculty of Biology Department of Molecular Biology and Physiology Group of Experimental Biomedicine
2004	Graduated from University and acquired title of Graduate Molecular Biologist and Physiologist Average record obtained 9.57 out of 10 Diploma thesis: Influence of sub-lethal doses of epirubicine hydrochloride on HER-2 receptor expression on cells of mammary carcinoma cell lines MDA-MB-361 and MDA-MB-453"
2005-present	Graduate student at Max Planck Institute of Experimental Medicine (Goettingen) Department of Neurogenetics Thesis: BACE1 dependent NRG1 function in PNS myelination

Fellow of GGNB/NEUREST PhD programme

Research experience:

1/ 2004-8/2004	Diploma thesis project at the "National Cancer Research Center" Department of Experimental Oncology.
3/2005-4/2005	Internship at MPI for Neuroendocrinology, (Hannover)
2005-Present	PhD project at MPI of Experimental Medicine
9/2006-11/2006	Guest researcher at the Mayo Clinic (Rochester) Department of Neurology

Teaching skills:

4/2008	Supervised practicum project Axonal stimulation of Schwann cells by NRG1
6/2009-9/2009	Supervised diploma project Analysis of function, processing and localization of NRG1 type III variants in CNS of transgenic mice
8/2009	Supervised practicum project BACE1 processed NRG1 protein expression and effects on Schwann cell proliferation in sciatic nerve of transgenic mice

Fellowships and awards:

2005-2008	Marie Curie host fellowship for early stage researchers training
2008-present	Graduate fellowship from Max Planck institute of Experimental Medicine

Languages:	Serbian: native English: fluent Russian: basic German: basic
Computer skills:	Word, Excel, Outlook, PowerPoint, Photoshop, Illustrator, Image J.

Oral presentations:

10/2007	Role of NRG1 in myelination Neuron-glia interactions in health and disease FENS summer school, Dubrovnik
4/2008	BACE1 dependent NRG1 function in PNS myelination Annual PhD retreat of NEUREST program
10/2008	BACE1 dependent NRG1 function in PNS myelination Annual PhD retreat of Max-Planck Institute of Experimental Medicine

Poster presentations:

19-24 October 2007	A threshold level of Neuregulin1 induces myelination C. Humml; M.H. Schwab; V. Velanac; G.V. Michailov; B.G. Brinkmann; A. Agrawal; C. Birchmeier; L. Role; M.W. Sereda; K.A. Nave Neuron-glia interactions in health and disease FENS summer school, Dubrovnik